AD-A151 771 FLIGHT CONTROL SYSTEM RECONFIGURATION DESIGN USING QUANTITATIVE FEEDBACK THEORY(U) AIR FORCE INST OF TECH WRIGHT-PATTERSON AFB OH SCHOOL OF ENGI.. P B ARNOLD 1/3

UNCLASSIFIED DEC 84 AFIT/GE/ENG/84D-15 F/G 1/4 NL

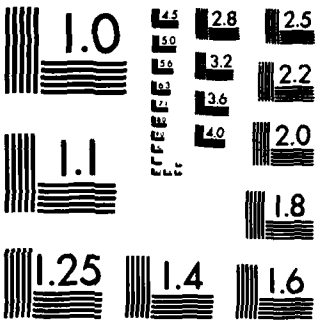

MICROCOPY RESOLUTION TEST CHART
NATIONAL BUREAU OF STANDARDS-1963-A

REPRODUCED AT GOVERNMENT EXPENSE

DTIC
1

AD-A151 771

FLIGHT CONTROL SYSTEM
RECONFIGURATION DESIGN USING
QUANTITATIVE FEEDBACK THEORY

THESIS

AFIT/GE/ENG/84D-15 Phillip B. Arnold
Major USAF

This document has been approved
for public release and sale; its
distribution is unlimited.

DTIC
ELECTE
APR 01 1985
S D
E

DTIC FILE COPY

DEPARTMENT OF THE AIR FORCE
AIR UNIVERSITY
AIR FORCE INSTITUTE OF TECHNOLOGY

Wright-Patterson Air Force Base, Ohio

85 03 13 255

AFIT/GE/ENG/84D-15

FLIGHT CONTROL SYSTEM RECONFIGURATION DESIGN USING QUANTITATIVE FEEDBACK THEORY

THESIS

AFIT/GE/ENG/84D-15 Phillip B. Arnold
Major USAF

Approved for public release; distribution unlimited

DTIC
ELECTE
APR 01 1985
S D
E

AFIT/GE/ENG/84D-15

FLIGHT CONTROL SYSTEM RECONFIGURATION DESIGN USING QUANTITATIVE FEEDBACK THEORY

THESIS

Presented to the Faculty of the School of Engineering
of the Air Force Institute of Technology
Air University
in Partial Fulfillment of the
Requirements for the Degree of
Master of Science

Phillip B. Arnold, B.S.E.E.
Major USAF
Graduate Electrical Engineering
December 1984

Approved for public release; distribution limited

Preface

I extend my sincere thanks to my thesis advisors Professors Constantine H. Houpis, Isaac Horowitz, and John J. D'Azzo for their cooperation and patience throughout this thesis effort. Their help contributed immensely to the successful completion of this thesis. A special acknowledgement is given to Mr. Yin-Kuei Liao of the Chung-Shan Institute of Science, Republic of China. His expert assistance given so freely and tirelessly is greatly appreciated.

My fellow classmates in the flights controls sequence provided many new insights and fresh ideas during countless informal discussions. For their contributions, I extend my sincere gratitude to Major Terry Courtheyn, Captain Harvey Russell of the Canadian Armed Forces, and Lieutenant Robert Eslinger.

My family has been very understanding throughout this demanding ordeal. Their encouragement and enthusiasm sustained me during the long days and nights. To my wife Marybeth, and my daughters Carey and Becky, I give my love.

Table of Contents

		Page
Preface		ii
List of Figures		v
List of Tables		xiii
Abstract		xix
I.	Introduction	1
	I.1 Background	2
	I.2 Problem	3
	I.3 Assumptions	4
	I.4 Approach	6
	I.5 Presentation	7
II.	Aircraft	8
	II.1 Introduction	8
	II.2 Aerodynamic Model	8
	II.3 Summary	15
III.	Reconfiguration Theory	16
	III.1 Introduction	16
	III.2 Reconfiguration Theory and System Model	16
	III.3 Equivalent Plant Development	19
	III.4 Summary	22
IV.	Compensator Designs	23
	IV.1 Introduction	23
	IV.2 Plant Equations	23
	IV.3 Specifications	25
	IV.4 Loop Bound Design, L_{2o}	29
	IV.5 Loop Bound Design, L_{1o}	40
	IV.6 Stability Design for Three Simultaneous Failures	45
	IV.7 Summary	51

Page

V. Results 53

V.1 Introduction 53
V.2 Simulation 53
V.2.1 Pitch Rate Command Response . . 54
V.2.2 Roll Rate Command Response . . . 67
V.3 Saturation 80
V.4 QFT Insights 86
V.5 Control Surface "Hardover" 87
V.6 Summary 92

VI. Conclusions and Recommendations 94

VI.1 Discussion 94
VI.2 Conclusions 95
VI.3 Recommendations 96

Appendix A: Flight Parameters and Aerodynamic Derivatives 97

Appendix B: Reconfiguration Theory 102

Appendix C: Equivalent Plant Transfer Function Matrices 131

Appendix D: Pitch Rate and Roll Rate Response Models 152

Appendix E: Templates of Q_{11} and Q_{22} 156

Appendix F: Simulation Programs 163

Appendix G: Control Surface Deflections 189

Bibliography 208

Vita 209

DTIC COPY INSPECTED 1

Accession For
NTIS GRA&I ☒
DTIC TAB ☐
Unannounced ☐
Justification
By
Distribution/
Availability Codes
Dist | Avail and/or Special
A-1

List of Figures

Figure		Page
1-1	Flight Envelope Design Points	5
3-1	Plant and Compensation Model Signal Flow Diagram	17
4-1	Pitch Rate Tolerances in the Time Domain . .	26
4-2	Pitch Rate Tolerances in the Frequency Domain	27
4-3	Roll Rate Tolerances in the Time Domain . .	28
4-4	Roll Rate Tolerances in the Frequency Domain	28
4-5	Equivalent SISO Systems	30
4-6	Template of Q_{11} at $\omega = 0.1$ Radians/Second .	31
4-7	Template of Q_{22} at $\omega = 0.1$ Radians/Second .	32
4-8	Nichol's Chart Plot of L_{2o} and Bounds . . .	38
4-9	Bode Plot of L_{2o}	39
4-10	Nichol's Chart Plot of L_{1o}, L_{1o}', and Bounds	44
4-11	Bode Plot of L_{1o}	45
4-12	L_{2o_e} and Bounds for Stability Only (One Elevator Only)	49
4-13	L_{1o_e} and Bounds for Stability Only (One Elevator Only)	50
5-1	Bode Plot Comparison of G_1 and the Approximation for G_1	55
5-2(a)	Pitch Rate Responses, Flight Condition One .	56
5-2(b)	Pitch Rate Responses, Flight Condition Two .	56

Figure		Page
5-2(c)	Pitch Rate Responses, Flight Condition Three	57
5-2(d)	Pitch Rate Responses, Flight Condition Four	57
5-3(a)	Roll Rate Cross-Coupling Responses, Flight Condition One	61
5-3(b)	Roll Rate Cross-Coupling Responses, Flight Condition Two	61
5-3(c)	Roll Rate Cross-Coupling Responses, Flight Condition Three	62
5-3(d)	Roll Rate Cross-Coupling Responses, Flight Condition Four	62
5-4(a)	Elevator and Flaperon Deflections for Pitch Rate, CSC Mode One and Flight Condition One	64
5-4(b)	Elevator and Flaperon Deflections for Pitch Rate, CSC Mode Two and Flight Condition One	64
5-4(c)	Elevator and Flaperon Deflections for Pitch Rate, CSC Mode Three and Flight Condition One	65
5-4(d)	Elevator and Flaperon Deflections for Pitch Rate, CSC Mode Four and Flight Condition One	65
5-4(e)	Elevator and Flaperon Deflections for Pitch Rate, CSC Mode Five and Flight Condition One	66
5-4(f)	Elevator and Flaperon Deflections for Pitch Rate, CSC Mode Six and Flight Condition One	66
5-5(a)	Roll Rate Responses, Flight Condition One	68
5-5(b)	Roll Rate Responses, Flight Condition Two	68
5-5(c)	Roll Rate Responses, Flight Condition Three	69
5-5(d)	Roll Rate Responses, Flight Condition Four	69

Figure		Page
5-6	Bode Plot Comparison of G_2 and the Approximation for G_2	72
5-7(a)	Pitch Rate Cross-Coupling Responses, Flight Condition One	74
5-7(b)	Pitch Rate Cross-Coupling Responses, Flight Condition Two	74
5-7(c)	Pitch Rate Cross-Coupling Responses, Flight Condition Three	75
5-7(d)	Pitch Rate Cross-Coupling Responses, Flight Condition Four	75
5-8(a)	Elevator and Flaperon Deflections for Roll Rate, CSC Mode One and Flight Condition One	77
5-8(b)	Elevator and Flaperon Deflections for Roll Rate, CSC Mode Two and Flight Condition One	77
5-8(c)	Elevator and Flaperon Deflections for Roll Rate, CSC Mode Three and Flight Condition One	78
5-8(d)	Elevator and Flaperon Deflections for Roll Rate, CSC Mode Four and Flight Condition One	78
5-8(e)	Elevator and Flaperon Deflections for Roll Rate, CSC Mode Five and Flight Condition One	79
5-8(f)	Elevator and Flaperon Deflections for Roll Rate, CSC Mode Six and Flight Condition One	79
5-9	Elevator and Flaperon Deflections With Saturation, CSC Mode One and Flight Condition One	81
5-10	Roll Rate Response With and Without Saturation, CSC Mode One and Flight Condition One	81
5-11	Roll Rate Response With and Without Saturation, CSC Mode Two and Flight Condition One	82

Figure		Page
5-12(a)	Pitch Rate Cross-coupling Response With and Without Saturation, CSC Mode Two and Flight Condition One	82
5-12(b)	Elevator and Flaperon Deflections for CSC Mode Two and Flight Condition One . . .	83
5-13	Elevator and Flaperon Deflections for Roll Rate with $\mu_{12} = 0.5$, CSC Mode One and Flight Condition One	84
5-14	Elevator and Flaperon Deflections for Pitch Rate with a Ramped Input, 0.5 sec to Peak Value (CSC Mode One and Flight Condition One)	85
5-15	Elevator and Flaperon Deflections for Roll Rate with a Ramped Input, 1 sec to Peak Value (CSC Mode One and Flight Condition One)	85
5-16	Template of Q_{11} at $\omega = 1.0$ r/s, Includes $\delta_1^a = \delta_1^b = 0$	88
5-17	Bounds on L Resulting from τ_{11} Demands . . .	89
5-18(a)	Pitch Rate Response from Elevator Hardover, Flight Condition Two	90
5-18(b)	Roll Rate Response from Elevator Hardover, Flight Condition Two	91
5-19(a)	Pitch Rate Response from Flaperon Hardover, Flight Condition Two	91
5-19(b)	Roll Rate Response from Flaperon Hardover, Flight Condition Two	92
B-1	A 4-input, 2-output, 2-mode structure . . .	128
B-2	A 5-input, 3-output, 2-mode structure . . .	129
B-3	A 10-input, 6-output, 2-mode structure . . .	130
E-1(a)	Template of Q_{11} at $\omega = 0.5$ Rad/Sec	157
E-1(b)	Template of Q_{22} at $\omega = 0.5$ Rad/Sec	157

Figure		Page
E-2(a)	Template at Q_{11} at ω = 4.0 Rad/Sec	158
E-2(b)	Template of Q_{22} at ω = 4.0 Rad/Sec	158
E-3(a)	Template of Q_{11} at ω = 8 Rad/Sec	159
E-3(b)	Template of Q_{22} at ω = 8 Rad/Sec	159
E-4(a)	Template of Q_{11} at ω = 10 Rad/Sec	160
E-4(b)	Template of Q_{22} at ω = 10 Rad/Sec	160
E-5(a)	Template of Q_{11} at ω = 20 Rad/Sec	161
E-5(b)	Template of Q_{22} at ω = 20 Rad/Sec	161
E-6(a)	Template of Q_{11} at ω = 50 Rad/Sec	162
E-6(b)	Template of Q_{22} at ω = 50 Rad/Sec	162
G-1(a)	Control Surface Deflections for Pitch Rate Command, Flight Condition 2-- CSC Mode 1	190
G-1(b)	Control Surface Deflections for Pitch Rate Command, Flight Condition 2-- CSC Mode 2	190
G-1(c)	Control Surface Deflections for Pitch Rate Command, Flight Condition 2-- CSC Mode 3	191
G-1(d)	Control Surface Deflections for Pitch Rate Command, Flight Condition 2-- CSC Mode 4	191
G-1(e)	Control Surface Deflections for Pitch Rate Command, Flight Condition 2-- CSC Mode 5	192
G-1(f)	Control Surface Deflections for Pitch Rate Command, Flight Condition 2-- CSC Mode 6	192
G-2(a)	Control Surface Deflections for Pitch Rate Command, Flight Condition 3-- CSC Mode 1	193
G-2(b)	Control Surface Deflections for Pitch Rate Command, Flight Condition 3-- CSC Mode 2	193

significantly impacts LCC as actuators are 50 percent of FCS LCC. Correspondingly, simpler actuators reduce maintenance actions required (4).

Quantitative feedback theory is ideally suited for the FCS reconfiguration problem. In QFT the design is accomplished a priori so that the system output is in the acceptable set of outputs for all possible members of the plant set. Surface failures simply increase the number of equations in the equivalent plant set, as is seen in Chapter III. The transparency of QFT enables the designer to readily see the extra "cost of feedback" for this enlargement of the plant equation set by including surface failures (5). A QFT design approach also reduces the need for complex fault identification and isolation (FDI) schemes.

I.2 Problem

The main purpose of this thesis effort is to investigate the usefulness of QFT in designing for FCS reconfiguration. The minimum phase plant equations are based upon linearized equations of motion for the AFTI/F-16. Non-minimum phase plant equations are not covered in this thesis. Using QFT, control laws are developed to achieve specified performance tolerances for several flight control surface failures over a large portion of the flight envelope. Pitch rate (q) and roll rate (p) are the two output variables to be controlled. Control surfaces are

In this thesis, QFT is applied to a FCS reconfiguration problem in an attempt to gain insight into its utility as a design tool.

The remainder of the first chapter presents pertinent background information, a statement and scope of the problem, the assumptions used, the approach taken, and the sequence of presentation for the thesis.

I.1 Background

Several promising benefits of inherent reconfiguration have been detailed in Self-Repairing Flight Control System Reliability and Maintainability, Program Plan (4). The primary benefits to be derived from inherent reconfiguration include improvements in reliability and maintainability (R&M), survivability, and reduced life cycle costs (LCC).

Improvements in R&M are expected as a result of fewer and less complex FCS components. Survivability will be improved by taking advantage of existing redundant control surfaces, thereby reducing the dependency on any one set of control surfaces for primary control about an axis. The reduction in criticality of the control surfaces allows a reduction in the redundancy level at the actuator. The actuator no longer becomes the redundancy integrator and the actuator then can be made simple and less complex. Simplex or dual actuators can be contemplated which

FLIGHT CONTROL SYSTEM RECONFIGURATION DESIGN
USING QUANTITATIVE FEEDBACK THEORY

I. Introduction

Design planning for the next generation fighter aircraft is presently in progress. The aircraft, known as the Advanced Tactical Fighter (ATF), will have a flight control system (FCS) capable of taking advantage of the inherent redundancy existing in redundant flight control surfaces. This means that no single loss or failure of a FCS component will result in loss of aircraft control. A digital flight control system will redistribute control authority to the remaining components to generate the necessary aerodynamic forces and moments. This reconfiguration of control authority by an aircraft with inherent redundancy gives rise to the term "inherent reconfiguration."

Methods of developing reconfiguration schemes are now being investigated by the Flight Dynamics Laboratory (1). One promising approach is quantitative feedback theory (QFT) as developed and successfully applied to a number of difficult problems by Dr. Isaac Horowitz (2; 3). Quantitative feedback theory is ideally suited to develop robust control laws for systems with highly uncertain parameters.

Fixed-compensators and prefilters are synthesized for the pitch rate and roll rate channels, and a digital simulation is conducted at four points in the flight envelope with up to two simultaneous surface failures, as well as, for the unimpaired aircraft. Results of the simulation show that the compensators provide robust control for each control surface configuration at each flight condition. Compensator designs are also synthesized to provide only stability when three of the four surfaces are failed.

The theory developed by Dr. Horowitz is found to be effective in designing for robustness despite large uncertainty arising from control surface failures, and plant parameter variation. Flight control research using quantitative feedback theory should be continued. The fixed-compensator design approach has potential to significantly reduce the complexity of a reconfigurable flight control system. A computer-aided design package for quantitative feedback theory should be developed to facilitate design work.

Abstract

Quantitative theory developed by Dr. Isaac Horowitz of the Weizmann Institute of Science, Israel is used to develop control laws for the AFTI/F-16 with a reconfigurable flight control system. Compensators are synthesized to control pitch rate and roll rate through individually controlled elevators and flaperons. Robust control of these variables is required over a large portion of the flight envelope despite flight control surface failures.

Linearized aerodynamic data are used to develop the aircraft model in state-variable format. The longitudinal and lateral-directional equations are coupled in the control matrix. Individual control of the elevators and flaperons is obtained by dividing the dimensionalized control derivatives for a control surface pair in half and assigning each surface of the pair one-half of the total derivative value. The system with individually controlled surfaces represents a four input-two output system which is transformed into an equivalent two input-two output system for each control surface configuration and flight condition. Quantitative feedback theory is then applied to the equivalent systems.

θ -- Pitch angle

ϕ -- Roll angle

μ_{ij} -- Control surface constants

ω -- Frequency

w -- Weight

$\underline{x}$ -- State vector

X_θ -- Dimensional variation of x-force with pitch angle

X_u -- Dimensional variation of x-force with forward velocity

X_α -- Dimensional variation of x-force with angle-of-attack

X_q -- Dimensional variation of x-force with pitch rate

X_δ -- Dimensional variation of x-force with elevator (δ_1) and flaperon (δ_2)

Y_ϕ -- Dimensional variation of y-force with roll angle

Y_β -- Dimensional variation of y-force with sideslip angle

Y_p -- Dimensional variation of y-force with roll rate

Y_r -- Dimensional variation of y-force with yaw rate

Y_δ -- Dimensional variation of y-force with elevator (δ_1) or flaperon (δ_2)

Z_θ -- Dimensional variation of z-force with pitch angle

Z_u -- Dimensional variation of z-force with forward velocity

Z_α -- Dimensional variation of z-force with angle-of-attack

Z_q -- Dimensional variation of z-force with pitch rate

Z_δ -- Dimensional variation of z-force with elevator (δ_1) or flaperon (δ_2)

δ_1 -- Elevator input

δ_2 -- Flaperon input

δ_r -- Rudder input

δ_c -- Canard input

M_p -- Peak value

M_θ -- Dimensional variation of pitching moment with pitch angle

M_u -- Dimensional variation of pitching moment with forward velocity

M_α -- Dimensional variation of pitching moment with angle-of-attack

M_q -- Dimensional variation of pitching moment with pitch rate

M_δ -- Dimensional variation of pitching moment with elevator (δ_1) or flaperon (δ_2)

N_β -- Dimensional variation of yawing moment with side-slip angle

N_p -- Dimensional variation of yawing moment with roll rate

N_r -- Dimensional variation of yawing moment with yaw rate

N_δ -- Dimensional variation of yawing moment with elevator (δ_1) or flaperon (δ_2)

p -- Roll rate

$\underline{P}_e$ -- Equivalent plant matrix

P_{ij} -- Basic plant equations

q -- Pitch rate

Q_{ij} -- Plant equations for equivalent single input-single output systems

r -- Yaw rate

s -- Wing reference area

$\underline{T}$ -- System transfer function matrix (t_{ij})

t_s -- Settling time

t_r -- Rise time

u -- Forward velocity

List of Symbols

α -- Angle-of-attack

$\underline{A}$ -- Plant matrix

$\underline{B}$ -- Control matrix

b_{ij} -- Performance specification bounds

b -- Wing span

β -- Sideslip angle

$\bar{C}$ -- Wing aerodynamic chord

Ft -- Feet

lbs -- Pounds

g_1 -- Pitch rate compensator transfer function

g_2 -- Roll rate compensator transfer function

f_{ij} -- Prefilter

I_{xx} -- Moment of inertia about x-axis

I_{yy} -- Moment of inertia about y-axis

I_{zz} -- Moment of inertia about z-axis

I_{xz} -- Product of inertia in xyz system

L_β -- Dimensional variation of rolling moment with sideslip angle

L_p -- Dimensional variation of rolling moment with roll rate

L_r -- Dimensional variation of rolling moment with yaw rate

L_δ -- Dimensional variation of rolling moment with elevator (δ_1) or flaperon (δ_2)

L_{1o} -- Pitch rate nominal loop transmission

L_{2o} -- Roll rate nominal loop transmission

Table		Page
C-6	Equivalent Plant Equations for the Single Input-Single Output Systems for Flight Condition Two	143
C-7	Equivalent Plant Equations for the Single Input-Single Output Systems for Flight Condition Three	146
C-8	Equivalent Plant Equations for the Single Input-Single Output Systems for Flight Condition Four	149

List of Tables

Table		Page
2-1	AFTI/F-16 Aircraft Data	9
5-1	Figure of Merit Tolerances for Pitch Rate . .	58
5-2	Pitch Rate Response Figures of Merit	59
5-3	Estimated Roll Angles with Pitch Rate Commanded	63
5-4	Surface Position and Rate Limits	67
5-5	Figure of Merit Tolerances for Roll Rate . . .	70
5-6	Roll Rate Response Figures of Merit	71
5-7	Estimated Pitch Angle with Roll Rate Commanded	73
A-1	Aircraft Data for Flight Condition One	98
A-2	Aircraft Data for Flight Condition Two	99
A-3	Aircraft Data for Flight Condition Three . . .	100
A-4	Aircraft Data for Flight Condition Four . . .	101
C-1	Equivalent Plant Matrices for Flight Condition One	132
C-2	Equivalent Plant Matrices for Flight Condition Two	134
C-3	Equivalent Plant Matrices for Flight Condition Three	136
C-4	Equivalent Plant Matrices for Flight Condition Four	138
C-5	Equivalent Plant Equations for the Single Input-Single Output Systems for Flight Condition One	140

Figure		Page
G-6(d)	Control Surface Deflections for Roll Rate Command, Flight Condition 4--CSC Mode 4	206
G-6(e)	Control Surface Deflections for Roll Rate Command, Flight Condition 4--CSC Mode 5	207
G-6(f)	Control Surface Deflections for Roll Rate Command, Flight Condition 4--CSC Mode 6	207

Figure		Page
G-4(d)	Control Surface Deflections for Roll Rate Command, Flight Condition 2--CSC Mode 4	200
G-4(e)	Control Surface Deflections for Roll Rate Command, Flight Condition 2--CSC Mode 5	201
G-4(f)	Control Surface Deflections for Roll Rate Command, Flight Condition 2--CSC Mode 6	201
G-5(a)	Control Surface Deflections for Roll Rate Command, Flight Condition 3--CSC Mode 1	202
G-5(b)	Control Surface Deflections for Roll Rate Command, Flight Condition 3--CSC Mode 2	202
G-5(c)	Control Surface Deflections for Roll Rate Command, Flight Condition 3--CSC Mode 3	203
G-5(d)	Control Surface Deflections for Roll Rate Command, Flight Condition 3--CSC Mode 4	203
G-5(e)	Control Surface Deflections for Roll Rate Command, Flight Condition 3--CSC Mode 5	204
G-5(f)	Control Surface Deflections for Roll Rate Command, Flight Condition 3--CSC Mode 6	204
G-6(a)	Control Surface Deflections for Roll Rate Command, Flight Condition 4--CSC Mode 1	205
G-6(b)	Control Surface Deflections for Roll Rate Command, Flight Condition 4--CSC Mode 2	205
G-6(c)	Control Surface Deflections for Roll Rate Command, Flight Condition 4--CSC Mode 3	206

Figure		Page
G-2(c)	Control Surface Deflections for Pitch Rate Command, Flight Condition 3--CSC Mode 3	194
G-2(d)	Control Surface Deflections for Pitch Rate Command, Flight Condition 3--CSC Mode 4	194
G-2(e)	Control Surface Deflections for Pitch Rate Command, Flight Condition 3--CSC Mode 5	195
G-2(f)	Control Surface Deflections for Pitch Rate Command, Flight Condition 3--CSC Mode 6	195
G-3(a)	Control Surface Deflections for Pitch Rate Command, Flight Condition 4--CSC Mode 1	196
G-3(b)	Control Surface Deflections for Pitch Rate Command, Flight Condition 4--CSC Mode 2	196
G-3(c)	Control Surface Deflections for Pitch Rate Command, Flight Condition 4--CSC Mode 3	197
G-3(d)	Control Surface Deflections for Pitch Rate Command, Flight Condition 4--CSC Mode 4	197
G-3(e)	Control Surface Deflections for Pitch Rate Command, Flight Condition 4--CSC Mode 5	198
G-3(f)	Control Surface Deflections for Pitch Rate Command, Flight Condition 4--CSC Mode 6	198
G-4(a)	Control Surface Deflections for Roll Rate Command, Flight Condition 2--CSC Mode 1	199
G-4(b)	Control Surface Deflections for Roll Rate Command, Flight Condition 2--CSC Mode 2	199
G-4(c)	Control Surface Deflections for Roll Rate Command, Flight Condition 2--CSC Mode 3	200

two flaperons and two horizontal tails each one individually controlled. Control surface configurations are as follows:

Mode 1 - All four surfaces are operating normally.

Mode 2 - One horizontal tail is failed.

Mode 3 - One flaperon is failed.

Mode 4 - One horizontal tail and one flaperon are failed (same side).

Mode 5 - One horizontal tail and one flaperon are failed (opposite sides).

Mode 6 - Both flaperons are failed.

Throughout this thesis, modes 1 through 6 are referred to as control surface configuration (CSC) modes, and a case refers to a particular flight condition and CSC mode. Also, for the purposes of this study, a failed surface is defined to be fixed in the neutral reference position.

A large degree of parameter uncertainty is incorporated into the design by choosing four design points representing a large portion of the flight envelope. These design points are seen in Figure 1-1.

I.3 Assumptions

The aircraft equations of motion were developed by Mr. Finley Barfield using the assumptions listed below (6).

1. The aircraft is a rigid body, and mass is constant.

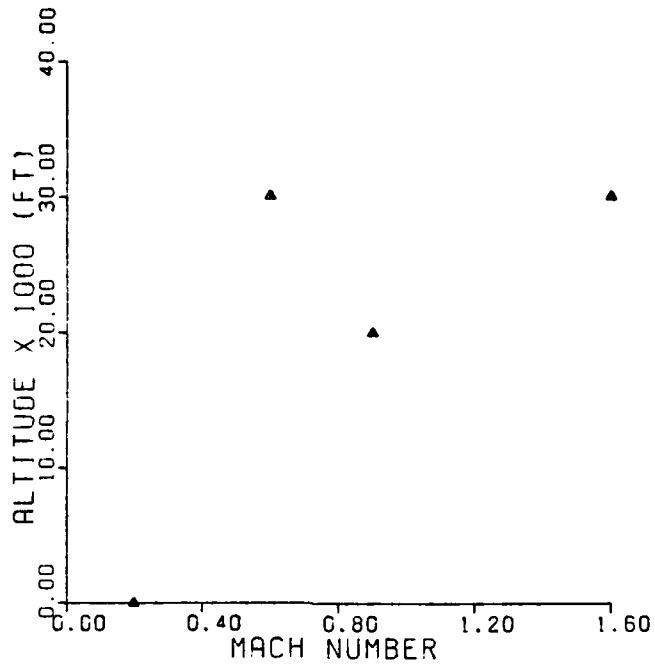

Fig. 1-1. Flight Envelope Design Points

2. *Thrust is not changing.*

3. The earth's surface is an inertial reference frame.

4. The atmosphere is assumed fixed with respect to the earth.

5. The equations of motion can be decoupled into a longitudinal and a lateral-directional set.

6. Linearization about an operating condition is acceptable for point designs.

7. Aerodynamics are fixed for Mach number and altitude.

A detailed explanation of each of the above assumptions is presented in Reference 6.

In addition to the above assumptions, the lateral and longitudinal control derivatives for the elevators and flaperons are halved in order to obtain control coefficients for the individual control surfaces. This approach is assumed suitably accurate for a preliminary design study of this nature.

I.4 Approach

The first step in the design process is to derive the basic plant transfer functions. These are obtained from the aircraft equations in state-variable form, with the longitudinal and lateral control elements coupled in the input matrix. From the system block diagram, equivalent plant equations are derived for each of the previously described surface configurations. As described in Chapter III, the four input-two output system is transformed into an equivalent two-by-two system. The resulting two-by-two equivalent plant transfer function matrices, $\underline{P}_e$, are then inverted to yield reciprocal expressions, $\underline{P}_e^{-1} = (1/Q_{ij})$, for equivalent single input-single output (SISO) systems. Next, output specifications are formulated.

The pitch rate and roll rate specifications are first developed in the time domain, and then transformed into the frequency domain via the Laplace transformation. Designing in the frequency domain avoids the more difficult convolution operations of time functions. The design specifications serve mainly to demonstrate the application of

the technique. They are based upon what the author feels are reasonable from his personal experience gained from flying fighter aircraft, and serve primarily as a basis for demonstrating QFT. Next, the compensators are synthesized according to the techniques of Reference 3.

The longitudinal and lateral controller designs are incorporated into the complete system, and the design is verified by simulations at each flight condition for each control surface configuration. Control surface deflections are also examined for position and rate saturation.

I.5 Presentation

This thesis consists of six chapters. Chapter II contains the aircraft equations of motion in state variable format that are used to derive the basic plant transfer function equations. Chapter III presents the system model used in the simulation and the quantitative feedback synthesis theory applied to the reconfiguration problem. The actual design of the control laws is presented in Chapter IV. Chapter V displays the output and control surface responses, and evaluations of such. Chapter VI contains the conclusions and recommendations.

II. Aircraft

II.1 Introduction

In this chapter the decoupled longitudinal and lateral aircraft equations of motion in state-variable format are coupled together in the input matrix allowing control of individual elevators and flaperons. From these coupled aircraft equations, the basic plant transfer functions of interest are computed. The linearized, aerodynamic coefficients used to develop the equations of motion are developed by the General Dynamics Corporation, and are taken from Reference 6. A description of the AFTI/F-16 and its flight control system is also given in Reference 6. The aerodynamic coefficients used in the equations are listed in Appendix A for four flight conditions. Table 2-1 presents pertinent aircraft data for the AFTI/F-16.

II.2 Aerodynamic Model

The equations of motion are written in state-space form, $\dot{\underline{x}} = \underline{Ax} + \underline{Bu}$. They are a set of first-order differential equations which represent the aircraft dynamics. The elements of the $\underline{A}$ and $\underline{B}$ matrices are dimensionalized body axis coefficients. Coefficients in the stability axis system are converted to the body axis system using a computer program called Conversion and Transformation (6).

TABLE 2-1

AFTI/F-16 AIRCRAFT DATA

Aircraft Parameters	
Wing Mean Aerodynamic Chord, c(ft)	= 11.32
Wing Reference Area, s(ft^2)	= 300.0
Wing Span, b(ft)	= 30.0
Weight, w(lbs)	= 21,018.0
Moment of Inertias	
I_{xx}(slug-ft^2)	= 10,033.4
I_{yy}(slug-ft^2)	= 53,876.3
I_{zz}(slug-ft^2)	= 61,278.4
I_{xz}(slug-ft^2)	= 282.132

The body axis is chosen as the design axis for two primary reasons. First, the sensors providing feedback signals actually measure body accelerations and rates. Secondly, the pilot desires to control accelerations and rates that he actually feels which are body accelerations and rates (6).

Using the assumptions of Chapter I, and assuming that coupling can be ignored between the longitudinal and lateral axes, two sets of linear, first-order differential equations result. The longitudinal set of equations has the following form:

$$\begin{bmatrix} \dot{\theta} \\ \dot{u} \\ \dot{\alpha} \\ \dot{q} \end{bmatrix} = \begin{bmatrix} 0 & 0 & 0 & 1 \\ X_\theta' & X_u' & X_\alpha' & X_q' \\ Z_\theta' & Z_u' & Z_\alpha' & Z_q' \\ M_\theta' & M_u' & M_\alpha' & M_q' \end{bmatrix} \begin{bmatrix} \theta \\ u \\ \alpha \\ q \end{bmatrix} + \begin{bmatrix} 0 & 0 \\ X_{\delta_e}' & X_{\delta_f}' \\ Z_{\delta_e}' & Z_{\delta_f}' \\ M_{\delta_e}' & M_{\delta_f}' \end{bmatrix} \begin{bmatrix} \delta_e \\ \delta_f \end{bmatrix} \qquad (2\text{-}1)$$

where

θ = pitch angle (deg)

u = forward velocity (ft/sec)

α = angle-of-attack (deg/sec)

q = pitch rate (deg/sec)

The lateral set of equations has the following form:

$$\begin{bmatrix} \dot{\phi} \\ \dot{\beta} \\ \dot{p} \\ \dot{r} \end{bmatrix} = \begin{bmatrix} 0 & 0 & 1 & 0 \\ Y_\phi' & Y_\beta' & Y_p' & Y_r' \\ 0 & L_\beta' & L_p' & L_r' \\ 0 & N_\beta' & N_p' & N_r' \end{bmatrix} \begin{bmatrix} \phi \\ \beta \\ p \\ r \end{bmatrix} + \begin{bmatrix} 0 & 0 & 0 \\ Y_{\delta_a}' & Y_{\delta_r}' & Y_{\delta_c}' \\ L_{\delta_a}' & L_{\delta_r}' & L_{\delta_c}' \\ N_{\delta_a}' & N_{\delta_r}' & N_{\delta_c}' \end{bmatrix} \begin{bmatrix} \delta_a \\ \delta_r \\ \delta_c \end{bmatrix}$$

(2-2)

where

ϕ = bank angle (deg)

β = sideslip angle (deg)

p = roll rate (deg/sec)

r = yaw rate (deg/sec)

Using the computer program Total, transfer function expressions for the desired output-to-input relationships are computed (7). These transfer functions are referred to as the basic plant equations. They are identified by a two-digit subscript, and a superscript (a or b). The first digit in the subscript denotes the output while the second digit denotes the control surface input that generates the output. Pitch and roll rates are identified by a 1 or a 2, respectively. Likewise, the elevators and flaperons are identified by a 1 or a 2, respectively. A superscript "a" or "b" denotes a right or left control surface, respectively. For example, $P_{12}{}^{a}$ identifies the basic plant equation whose output is pitch rate generated by the right flaperon. Combining the longitudinal and lateral matrices, and dividing control between individual elevator and flaperon surfaces results in a set of equations with coupling between the longitudinal and lateral axes in the control matrix (Eq. 2-3).

$$
\begin{bmatrix} \dot{\theta} \\ \dot{u} \\ \dot{\alpha} \\ \dot{q} \\ \dot{\phi} \\ \dot{\beta} \\ \dot{p} \\ \dot{r} \end{bmatrix}
=
\begin{bmatrix}
0 & 0 & 0 & 1 & 0 & 0 & 0 & 0 \\
X_\theta' & X_u' & X_\alpha' & X_q' & 0 & 0 & 0 & 0 \\
Z_\theta' & Z_u' & Z_\alpha' & Z_q' & 0 & 0 & 0 & 0 \\
M_\theta' & M_u' & M_\alpha' & M_q' & 0 & 0 & 0 & 0 \\
0 & 0 & 0 & 0 & 0 & 0 & 1 & 0 \\
0 & 0 & 0 & 0 & Y_\phi' & Y_\beta' & Y_p' & Y_r' \\
0 & 0 & 0 & 0 & 0 & L_\beta' & L_p' & L_r' \\
0 & 0 & 0 & 0 & 0 & N_\beta' & N_p' & N_r'
\end{bmatrix}
\begin{bmatrix} \theta \\ u \\ \alpha \\ q \\ \phi \\ \beta \\ p \\ r \end{bmatrix}
$$

$$
+
\begin{bmatrix}
0 & 0 & 0 & 0 & 0 & 0 \\
\tfrac{1}{2}X_{\delta_e}' & \tfrac{1}{2}X_{\delta_e}' & \tfrac{1}{2}Y_{\delta_f}' & \tfrac{1}{2}Y_{\delta_f}' & 0 & 0 \\
\tfrac{1}{2}Z_{\delta_e}' & \tfrac{1}{2}Z_{\delta_e}' & \tfrac{1}{2}Z_{\delta_f}' & \tfrac{1}{2}Z_{\delta_f}' & 0 & 0 \\
\tfrac{1}{2}M_{\delta_e}' & \tfrac{1}{2}M_{\delta_e}' & \tfrac{1}{2}M_{\delta_f}' & \tfrac{1}{2}M_{\delta_f}' & 0 & 0 \\
0 & 0 & 0 & 0 & 0 & 0 \\
\tfrac{1}{2}Y_{\delta_e}' & -\tfrac{1}{2}Y_{\delta_e}' & \tfrac{1}{2}Y_{\delta_a}' & -\tfrac{1}{2}Y_{\delta_a}' & Y_{\delta_r}' & Y_{\delta_c}' \\
\tfrac{1}{2}L_{\delta_e}' & -\tfrac{1}{2}L_{\delta_e}' & \tfrac{1}{2}L_{\delta_a}' & -\tfrac{1}{2}L_{\delta_a}' & L_{\delta_r}' & Y_{\delta_c}' \\
\tfrac{1}{2}N_{\delta_e}' & -\tfrac{1}{2}N_{\delta_e}' & \tfrac{1}{2}N_{\delta_a}' & -\tfrac{1}{2}N_{\delta_a}' & N_{\delta_r}' & N_{\delta_c}'
\end{bmatrix}
\cdot
\begin{bmatrix} \delta_1^a \\ \delta_1^b \\ \delta_2^a \\ \delta_2^b \\ \delta_r \\ \delta_c \end{bmatrix}
\qquad (2\text{-}3)
$$

where

δ_1^a = right elevator surface

δ_1^b = left elevator surface

δ_2^a = right flaperon surface

δ_2^b = left flaperon surface

δ_r = rudder surface

δ_c = canard surface

Plant expressions are computed for each of the flight conditions, and are listed next. Due to symmetry, $P_{ij}^{a} = P_{ij}^{b}$.

Flight Condition 1 (Mach = 0.2 at 30 ft)

$$P_{11}^{a} = \frac{q}{\delta_1^{a}} = \frac{-1.118s(s+0.01822)(s+0.4568)}{(s-0.3633)(s+1.3)(s+0.07683\pm j0.2065)} \tag{2-4}$$

$$P_{12}^{a} = \frac{q}{\delta_2^{a}} = \frac{.1209s(s+0.06537)(s+0.2589)}{(s-0.3633)(s+1.3)(s+0.07683\pm j0.2065)} \tag{2-5}$$

$$P_{22}^{a} = \frac{p}{\delta_2^{a}} = \frac{-2.239s(s+0.205\pm j0.853)}{(s+0.1041)(s+0.6835)(s+0.2741\pm j1.909)} \tag{2-6}$$

$$P_{21}^{a} = \frac{p}{\delta_1^{a}} = \frac{-2.142s(s+0.3017\pm j1.562)}{(s+0.1041)(s+0.6835)(s+0.2741\pm j1.909)} \tag{2-7}$$

Flight Condition 2 (Mach = 0.6 at 30,000 ft)

$$P_{11}^{a} = \frac{-2.931s(s+0.01004)(s+0.5502)}{(s-1.167)(s+2.028)(s+0.006472\pm j0.07803)} \tag{2-8}$$

$$P_{12}^{a} = \frac{-0.1059s(s+0.006697)(s+1.861)}{(s-1.167)(s+2.028)(s+0.006472\pm j0.07803)} \tag{2-9}$$

$$P_{22}^{a} = \frac{-8.723s(s+0.219\pm j1.607)}{(s+0.07795)(s+0.8265)(s+0.211\pm j1.953)} \tag{2-10}$$

$$P_{21}^{a} = \frac{-6.792s(s+0.2442\pm j2.101)}{(s+0.07795)(s+0.8265)(s+0.211\pm j1.953)} \tag{2-11}$$

Flight Condition 3 (Mach = 0.9 at 20,000 ft)

$$P_{11}^{a} = \frac{-12.03s(s+0.01262)(s+1.51)}{(s-0.9645)(s+3.223)(s+0.007553\pm j0.05384)} \tag{2-12}$$

$$P_{12}^{a} = \frac{-3.236s(s+0.01254)(s+1.646)}{(s-0.9645)(s+3.223)(s+0.007553\pm j0.05384)} \tag{2-13}$$

$$P_{22}^{a} = \frac{-25.53s(s+0.3541\pm j2.927)}{(s+0.02719)(s+2.697)(s+0.391\pm j2.962)} \tag{2-14}$$

$$P_{21}^{a} = \frac{-25.36s(s+0.3749\pm j3.578)}{(s+0.02719)(s+2.697)(s+0.391\pm j2.962)} \tag{2-15}$$

Flight Condition 4 (Mach = 1.6 at 30,000 ft)

$$P_{11}^{a} = \frac{-16.45s(s+0.02996)(s+1.097)}{(s+0.01516\pm j0.02343)(s+0.8012\pm j6.592)} \tag{2-16}$$

$$P_{12}^{a} = \frac{-2.925s(s+0.03459)(s+0.6861)}{(s+0.01516\pm j0.02343)(s+0.8012\pm j6.592)} \tag{2-17}$$

$$P_{22}^{a} = \frac{-7.084s(s+0.4083\pm 4.916)}{(s+0.03448)(s+2.171)(s+0.4996\pm j3.129)} \tag{2-18}$$

$$P_{21}^{a} = \frac{-23.3s(s+0.3774\pm j3.848)}{(s+0.03448)(s+2.171)(s+0.4996\pm j3.129)} \tag{2-19}$$

II.3 Summary

The aircraft equations of motion in state-variable format are presented in this chapter. The longitudinal and lateral axes are coupled within the control matrix allowing control of individual elevators and flaperons. Also presented are the basic plant transfer functions of interest computed from the coupled aircraft equations of motion for each of the four flight conditions.

The next chapter presents the reconfiguration system model, and quantitative feedback theory as applied to the reconfiguration.

III. Reconfiguration Theory

III.1 Introduction

The concepts of QFT can be used to design fixed compensators to achieve tolerance specifications (2; 3). The specifications are to be satisfied despite highly uncertain parameters which can arise from aircraft control surface failures (partial or total), and from widely varying flight conditions. The specifications must also be satisfied for the normal system (no failures). The advantage of a fixed compensator design is that fast identification of failures is not necessary. A more optimum compensator can be switched in later, if required, after the failure state has been explicitly identified. This chapter presents the MIMO system model, and develops an equivalent plant matrix for which QFT is applicable.

III.2 Reconfiguration Theory and System Model

The structure of the system model is seen in Figure 3-1, and represents a four input-two output system. A two-elevator, two-flaperon system is represented with each individual surface separately controllable. The elevators and flaperons are capable of moving individually, and symmetrically or differentially in pairs. The right

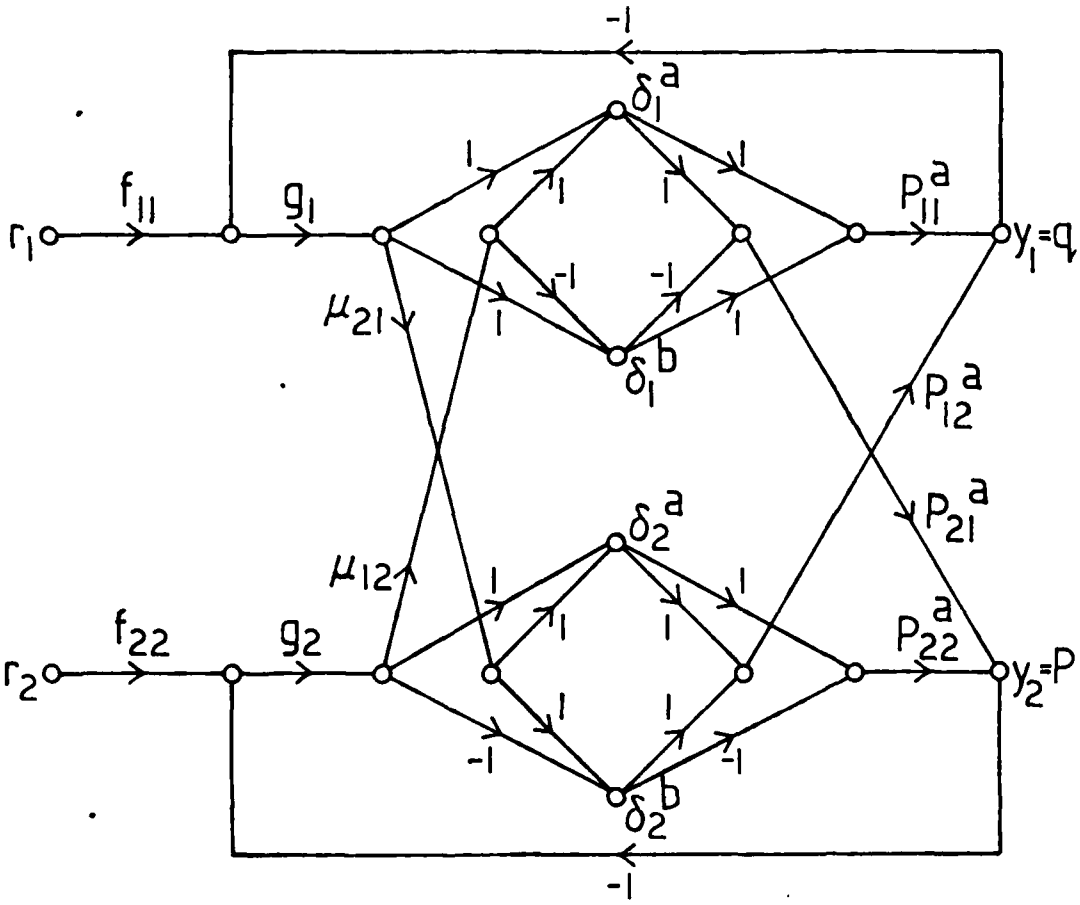

Fig. 3-1. Plant and Compensation Model Signal Flow Diagram

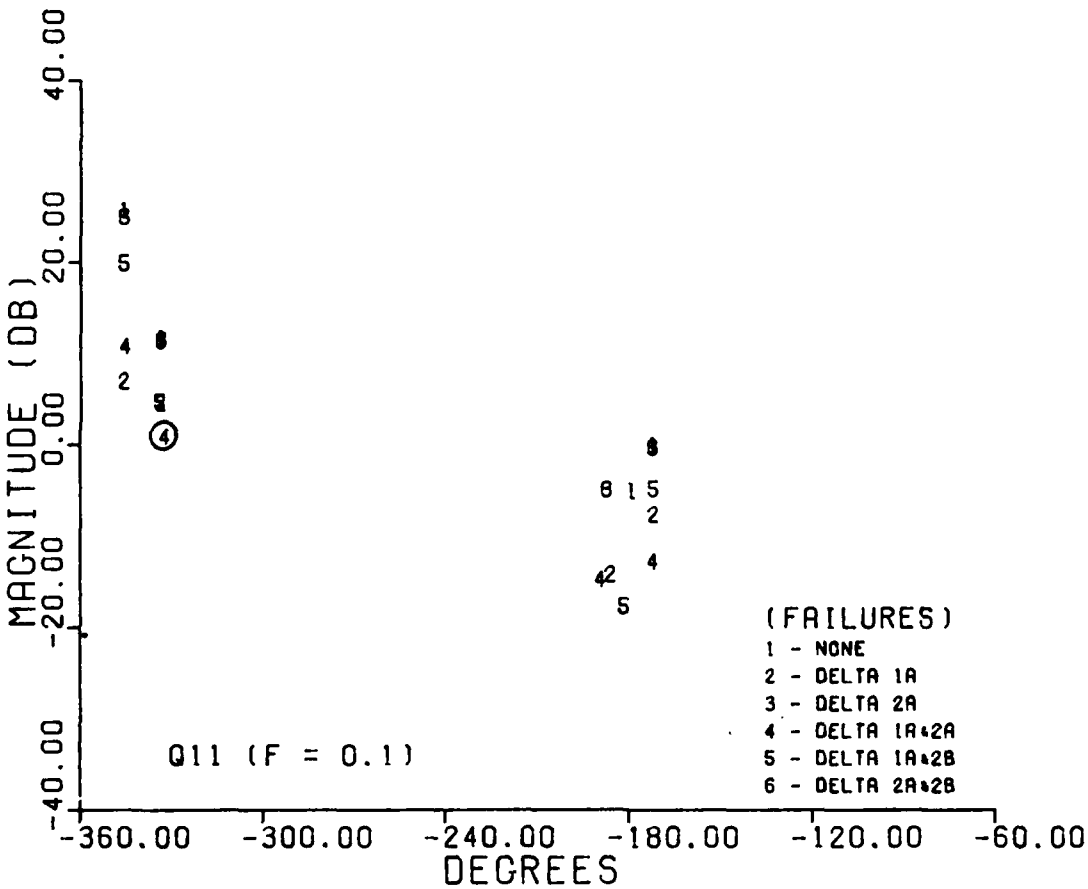

Fig. 4-6. Template of Q_{11} at ω = 0.1 Radians/Second

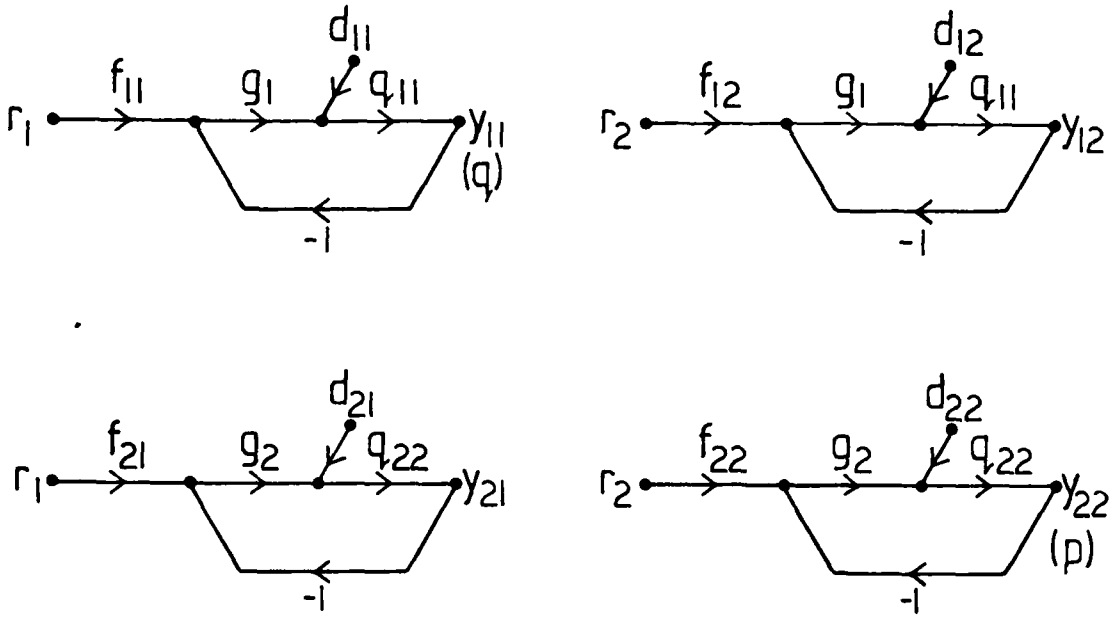

Fig. 4-5. Equivalent SISO Systems

at ω = 0.1 rad/sec are seen in Figures 4-6 and 4-7, respectively. The q channel is represented by Q_{11}, and the p channel by Q_{22}. Each template represents the variable uncertainty at a particular frequency for the six CSC modes and four flight conditions. Thus, each template has 24 points; the modes are numbered 1 through 6 as indicated on the template figures. Each CSC mode is repeated four times at a particular frequency corresponding to the four flight conditions. A nominal condition is chosen and indicated by circling that condition on each template. The nominal condition for Q_{11} is flight condition 2, CSC mode 4 (Mach = 0.6; δ_1^a and δ_2^a failed), while flight condition 4, CSC mode 4 (Mach = 1.6) is selected as the nominal condition

TABLE 4-1

FIGURE OF MERIT TOLERANCES FOR PITCH RATE

Settling Time t_s (sec)	Rise Time t_r (sec)	Peak Value M_p (deg/sec)
1.5 - 3.0	0.33 - 1.63	$\leq$ 11

TABLE 4-2

FIGURE OF MERIT TOLERANCES FOR ROLL RATE

Settling Time t_s (sec)	Rise Time t_r (sec)	Peak Value M_p (deg/sec)
3.0 - 6.0	0.65 - 3.23	$\leq$ 55

Transfer function models for roll rate are also listed in Appendix D. Once acceptable tolerances are established, bounds on the loop transmissions are formed.

IV.4 Loop Bound Design, L_{2o}

The decision must be made on which loop transmission (L) is to be designed first. Since the equivalent system is a two-by-two structure with two inputs to consider, both the command and the BNIC elements must be analyzed for each L to define the loop bounds. The equivalent SISO single-loop systems are seen in Figure 4-5.

As to which L to design first, both loops require the same analysis, so neither is less complicated than the other. For this problem, the L for the p channel is designed first because of the smaller uncertainty associated with this variable. This is seen by comparing the plant templates for p and q. Templates of Q_{11} and Q_{22}

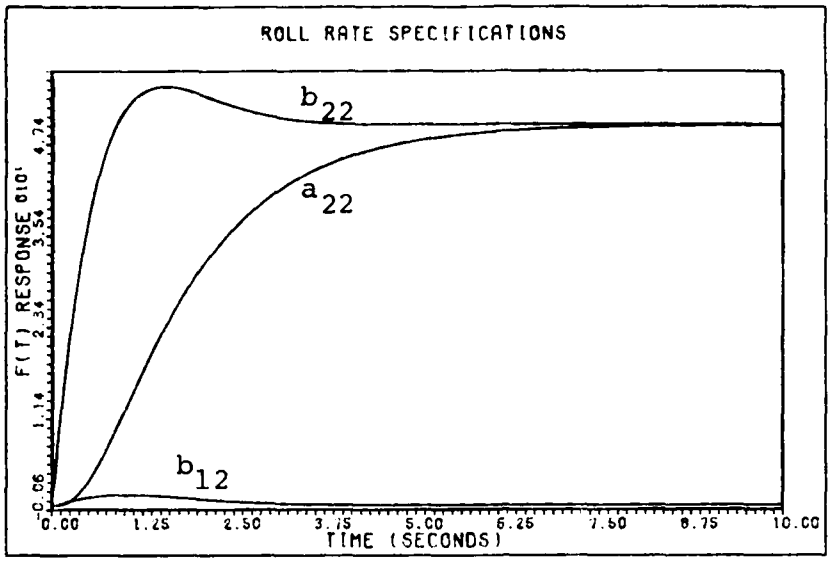

Fig. 4-3. Roll Rate Tolerances
in the Time Domain

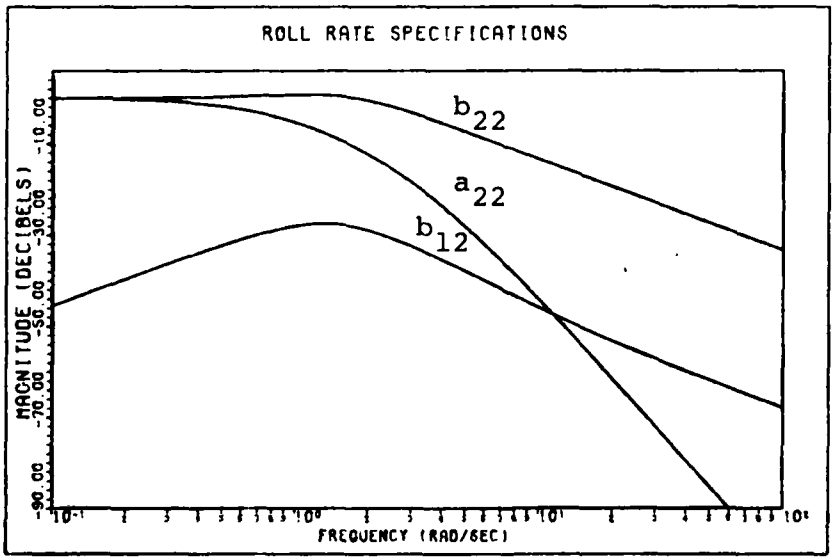

Fig. 4-4. Roll Rate Tolerances
in the Frequency Domain

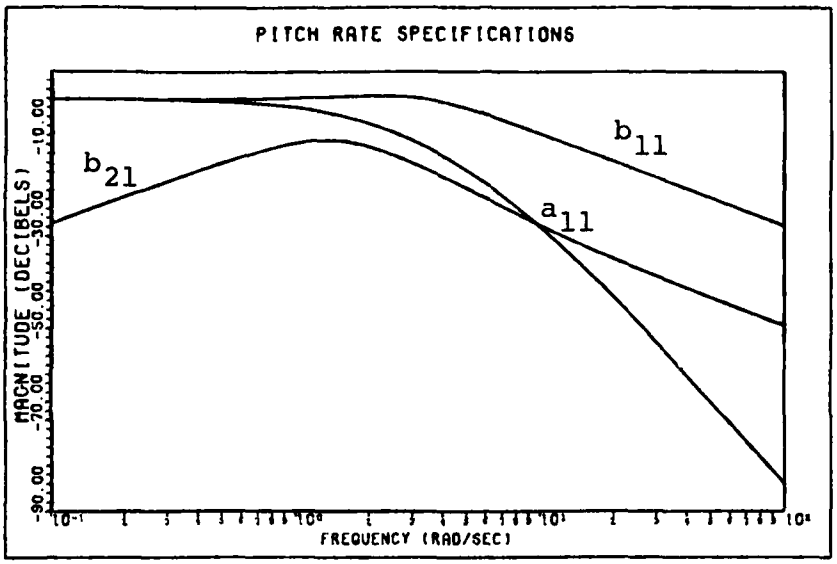

Fig. 4-2. Pitch Rate Tolerances in the Frequency Domain

merit are given in Reference 10. Tolerances for these figures of merit are seen in Table 4-1. The p tolerance b_{21} is modeled for a total roll angle of approximately five degrees. This specification is established with severe failure situations in mind, such as one elevator and one flaperon failed on the same side. Five degrees of roll angle seems quite reasonable for situations such as this. Tolerances are also established for the p command responses.

Roll rate tolerances b_{22}, a_{22}, and b_{12} are also established as is done for the q tolerances. It is desired that the p commanded be 50 deg/sec with small q resulting. The q tolerance b_{12} is modeled for a total pitch angle of approximately three degrees. Figures 4-3 and 4-4 illustrate the time and frequency domain tolerances for p, and Table 4-2 lists the figure of merit tolerances for p.

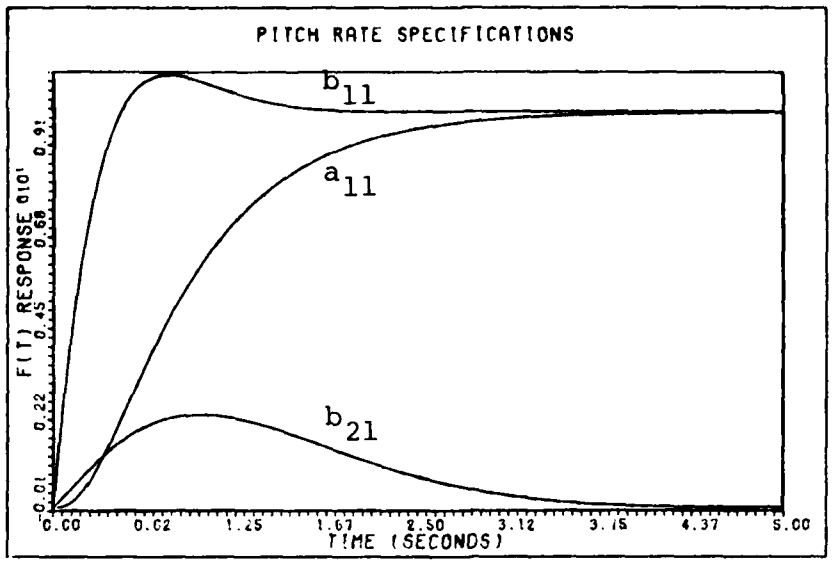

Fig. 4-1. Pitch Rate Tolerances in the Time Domain

The p response is a result of loop interaction, and is denoted by b_{21}. The time response tolerances transformed into the frequency domain are seen in Figure 4-2. As discussed earlier, all design work is accomplished in the frequency domain. Transfer function models for the response tolerances are listed in Appendix D. Figures of merit are established for the response tolerances.

Figures of merit for the outputs of interest are established primarily on what the author feels are reasonable from his personal experience gained from flying fighter aircraft. The main concern is to demonstrate the efficacy of QFT when applied to a reconfiguration problem. Settling time t_s, rise time t_r, and peak value M_p are chosen as the design figures of merit. Definitions for the figures of

realizable for that specific $\underline{P}_e$. The second condition, also derived in Reference 8, requires that

$$\left|\frac{Q_{11}Q_{22}}{Q_{12}Q_{21}}\right| < 1 \quad \text{as } s \to \infty \tag{4-1}$$

This must be so for all $\underline{P}_e \in P$, and all $\omega >$ some ω_h, where $|1+L| < 1$. This second condition is an inherent constraint. Both of the above conditions for this thesis are found to be satisfied for every $\underline{P}_e$, so design can proceed.

IV.3 Specifications

In general, a control problem exists because a set of performance criteria are specified (10). Acceptable tolerances for the closed-loop responses are established, and the goal is to find compensation which guarantees that these tolerances are satisfied over the range of plant uncertainty. In QFT it is guaranteed that the amount of feedback designed into the system is such that the desired responses are obtained despite highly uncertain plant parameters (2). Compensation is synthesized so that the specifications are satisfied for all design flight conditions and CSC modes.

The tolerances for the q and p responses of Figure 3-1, when q is commanded, are illustrated in Figure 4-1. It is desired that the q commanded be ten degrees per second (deg/sec) with small p resulting. The upper bound for the q response is denoted by b_{11} and the lower bound by a_{11}.

and CSC mode. For this study the equivalent plant set has as members the matrices for each flight condition and CSC mode, giving a total of 24 matrices (4 flight conditions times 6 CSC modes). The elements of each $\underline{P}_e$ are listed in Appendix C. After developing the $\underline{P}_e$, $\underline{P}_e^{-1}$ is computed using the computer program Total, obtaining $\underline{P}_e^{-1} = (1/Q_{ij})$. The Q_{ij} become the plant elements for the equivalent SISO systems (2; 3). Appendix C also lists the individual Q_{ij} for each flight condition and CSC mode. Notice in Appendix C that some of the Q's have unstable poles. This does not present an obstacle for this technique. This is addressed later in this chapter. Zeros in the right-half-plane, however, represent a non-minimum phase system, and, as a result, the design is more difficult. Dr. Horowitz has developed QFT to design for non-minimum phase plants (9). Since this thesis does not involve non-minimum phase plants, they are not addressed. Before proceeding with the design, certain conditions must first be satisfied for the MIMO synthesis technique to be applicable.

Two conditions must be satisfied before proceeding (8). First, $\underline{P}_e^{-1}$ must exist in order to obtain the Q_{ij} elements for the single-loop systems. This is the "controllability" condition and must be true for each flight condition and CSC mode. If the determinant of $\underline{P}_e$ equals zero it means that the plant outputs are not independently

IV. Compensator Designs

IV.1 Introduction

This chapter presents the steps used in the design of the compensators g_1, g_2 in Figure 3-1. The procedure is started by inverting the elements of the equivalent plant transfer function matrices for the various CSC modes to yield the Q_{ij} plant equations for the single-loop systems (see Figure 4-5, Section IV.4). These Q_{ij} plant equations are used in the detailed design execution. The p channel compensator is designed first due to a smaller amount of uncertainty associated with this variable. Using data derived in the design of this loop, the q channel compensator is then derived using the "improved method" (8). Simple, first-order prefilters are designed for both channels. The synthesis begins with the plant equations.

IV.2 Plant Equations

The design process begins by obtaining the basic plant transfer function equations from Eq. (2-3) for each design flight condition. These equations are listed in Chapter II. The equivalent plant transfer function matrices ($\underline{P}_e$) are developed as described in Chapter III from these basic plant equations. Equivalent plant transfer function matrices are developed for each flight condition

III.4 Summary

Presented in this chapter is the multiple input-multiple output system model and reconfiguration theory. An equivalent square plant matrix is also developed from a non-square plant matrix so that quantitative feedback theory QFT can be applied. In the next chapter, the compensator design procedures and the results are presented.

Substitutions are made into Eq. (3-7) for the various control surface configurations producing closed-loop transfer functions for each command and cross coupling response. For example, consider the case in which the right elevator has failed ($\delta_1{}^a = 0$); this implies that $P_{11}{}^a$ and $P_{21}{}^a$ are equal to zero. With these substitutions, the equivalent plant matrix becomes

$$\underline{P}_e = \begin{bmatrix} P_{11}{}^b + \mu P_{12} & \Delta P_{12} + \mu P_{11}{}^b \\ -P_{21}{}^b + \mu \Delta P_{22} & P_{22} + \mu P_{21}{}^b \end{bmatrix} \tag{3-8}$$

This new equivalent plant matrix is used to determine the four t_{ij} transfer functions. Each control surface failure situation can be treated in this manner to obtain the resulting plant transfer function. The various failures give different equivalent plant matrices for each flight condition. Quantitative feedback theory is applied to the entire set. The number of elements in the set $\underline{P}_e$ is the product of the number of CSC modes considered by the number of flight conditions. Appendix C lists the entire $\underline{P}_e$ set used in this thesis. QFT is well suited for this type of problem since the surface failures merely enlarge the plant set. The extra "cost of feedback" can readily be seen by the designer.

$$\underline{\delta} = \begin{bmatrix} f_1g_1 & \mu f_2g_2 \\ f_1g_1 & -\mu f_2g_2 \\ \mu f_1g_1 & f_2g_2 \\ \mu f_1g_1 & -f_2g_2 \end{bmatrix} \begin{bmatrix} r_1 \\ r_2 \end{bmatrix} - \begin{bmatrix} g_1 & \mu g_2 \\ g_1 & -\mu g_2 \\ \mu g_1 & g_2 \\ \mu g_1 & -g_2 \end{bmatrix} \begin{bmatrix} y_1 \\ y_2 \end{bmatrix} \tag{3-5}$$

From Eqs. (3-1) to (3-5), and by letting $P_{ij} = P_{ij}^{a} + P_{ij}^{b}$, and $\Delta P_{ij} = P_{ij}^{a} - P_{ij}^{b}$, an equivalent plant matrix P_e, emerges as follows:

$$\underline{P}_e = \begin{bmatrix} P_{11}+\mu P_{12} & \Delta P_{12}+\mu\Delta P_{11} \\ \Delta P_{21}+\mu\Delta P_{22} & P_{22}+\mu P_{21} \end{bmatrix} = \begin{bmatrix} P_{11_e} & P_{12_e} \\ P_{21_e} & P_{22_e} \end{bmatrix} \tag{3-6}$$

Now the plant matrix is square, and QFT is directly applicable. This two-by-two MIMO system can be reduced to four SISO single-loop systems for the design synthesis (2; 3).

After completing all the matrix operations the final expression for $\underline{T}$ becomes

$$\underline{T} = \{t_{ij}\}$$

$$= \frac{\begin{bmatrix} \{f_1g_1P_{11_e}(g_2P_{22_e}+1)-f_1g_1g_2P_{12_e}P_{21_e}\} & \{f_2g_2P_{1\cdot}\} \\ \{f_1g_1P_{21_e}\} & \{f_2g_2P_{22_e}(g_1P_{11_e}+1)-f_2g_1g_2P_{12_e}P_{21_e}\} \end{bmatrix}}{(g_1P_{11_e}+1)(g_2P_{22_e}+1)-f_1f_2g_1g_2P_{12_e}P_{21_e}} \tag{3-7}$$

failure. In Figure 3-1, μ_{12} and μ_{21} are constants which determine the division of control effort between the flaperons and elevators. For this preliminary study, optimization of these constants is not addressed, and both μ's are set equal to 0.25 for the majority of the simulations. Henceforth, the subscripts are dropped on these two constants. Preliminary theory has been developed to enable the designer to specify the optimum division of control effort. Appendix B contains this work along with a detailed explanation of reconfiguration theory for larger, more complex systems. The next section presents the development of an equivalent plant for which QFT is applicable.

III.3 Equivalent Plant Development

In Figure 3-1, $\underline{Y} = \underline{P\delta} = \underline{P}\{\underline{GFr} - \underline{GY}\}$ (3-1)

Thus,

$$\underline{T} = \{t_{ij}\} = \{\underline{I} + \underline{PG}\}^{-1}\ \underline{PGF} \tag{3-2}$$

where $t_{ij} = \underline{(I} + \underline{PG})^{-1}$.

$$\underline{P} = \begin{bmatrix} P_{11}{}^{a} & P_{11}{}^{b} & P_{12}{}^{a} & P_{12}{}^{b} \\ P_{21}{}^{a} & -P_{21}{}^{b} & P_{22}{}^{a} & -P_{22}{}^{b} \end{bmatrix} \tag{3-3}$$

$$\underline{\delta} = [\delta_1{}^{a},\ \delta_1{}^{b},\ \delta_2{}^{a},\ \delta_2{}^{b}] \tag{3-4}$$

and left elevators are designated by $\delta_1{}^a$ and $\delta_1{}^b$, respectively; the flaperons are designated similarly by $\delta_2{}^a$ and $\delta_2{}^b$. The longitudinally controlled output variable is pitch rate (q), while the laterally controlled output variable is roll rate (p). As stated in Chapter II, the plant transfer function designator, P_{ij}, relates the ith output to the jth input (control surface). A superscript "a" or "b" denotes the right or left control surface. For example, $P_{21}{}^a$ denotes the effect of the right elevator ($\delta_1{}^a$) on roll rate (output y_2). For a normally operating system, $P_{ij}{}^a = P_{ij}{}^b$. Minus signs are associated with P_{21} and P_{22} so that the two pairs of surfaces move differentially to generate roll rate. In the no fail case, surfaces move an equal amount in either direction to generate the commanded rates. No interaction is desired between the longitudinal and lateral modes under normal operating conditions.

Normally, the elevators move together in the same direction to excite only the longitudinal mode, and the flaperons move opposite each other to excite only the lateral mode. Separate control of the surfaces increases the flexibility of a system by exciting both aerodynamic modes when a single surface is actuated. For instance, using the structure of Figure 3-1, the surfaces can continue to act in pairs under normal operation, but act separately, as necessary, to offset parameter changes resulting from single or multiple control system component

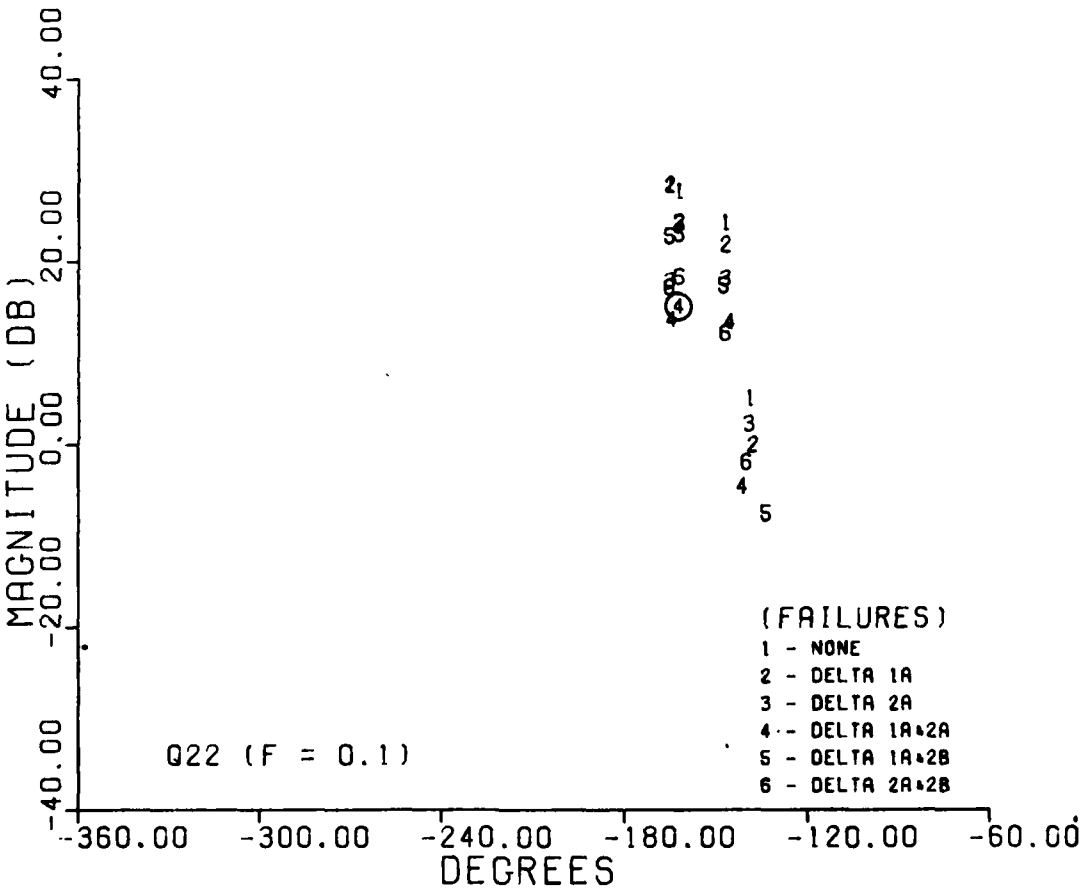

Fig. 4-7. Template of Q_{22} at ω = 0.1 Radians/Second

for Q_{22}. Dr. Horowitz recommends using the same nominal condition for each loop design. This eliminates any confusion as to the nominal condition when solving for the compensator explicitly. Templates are made for frequencies approximately one octave apart until the locus of points is essentially a vertical line. Appendix E contains templates of Q_{11} and Q_{22} at several frequencies. An analysis of the p channel is accomplished next.

The BNIC system whose output is y_{21} is analyzed first since only the input due to loop interaction is considered. A response due to r_1 does not exist for this single-loop system since the prefilter f_{21} is chosen to be zero. Consider the expression for y_{21}

$$y_{21} = \frac{d_{21}Q_{21}}{1+g_2Q_{22}} \tag{4-2}$$

where

$$d_{21} = t_{11}/Q_{21}(2), \text{ and } L_2 = g_2Q_{22} \tag{4-3a,b}$$

Rewriting Eq. (4-2)

$$y_{21} = \frac{(t_{11}/Q_{21})Q_{22}}{1+L_2} \leq b_{21} \tag{4-4}$$

with b_{21} being the specification bound for p due to the q command. To ensure total compliance for all acceptable t_{11}, the upper bound of t_{11} for the q response becomes b_{11}. Upon rearranging terms, Eq. (4-4) becomes

$$\left|\frac{1}{1+L_2}\right| \leq \left|\frac{b_{21}Q_{21}}{b_{11}Q_{22}}\right| \tag{4-5}$$

In order to determine the most demanding bound, use the minimum value of Q_{21} for all flight conditions and CSC modes at the frequency in question. Also, use the nominal value for Q_{22}, Q_{22o}. This procedure results in overdesign unless $|L_2| >> 1$. If $|L_2| >> 1$ is not a valid assumption, then Q_{21} and Q_{22} in Eq. (4-5) should correspond to the same flight condition and CSC mode. This takes into account the correlation between Q_{21} and Q_{22}. The bound on L_{2o} is then formed from the most demanding of all the bounds from Eq. (4-5) at each phase angle. For this particular problem, the demands on L_{2o} are high in the low frequency region making $|L_2| >> 1$ a valid assumption. Equation (4-6) is used to locate bounds on L_{2o} up to $\omega = 2$ r/s. At higher frequencies another technique, described later, is used. Equation (4-5) now becomes

$$\left|\frac{1}{1+L_{2o}}\right| \leq \left|\frac{b_{21}Q_{21_{min}}}{b_{11}Q_{22o}}\right| \tag{4-6}$$

The resulting bound is the bound for the nominal L_2, L_{2o}. The terms on the right hand side of Eq. (4-6) are constants obtained from the Bode plots of their transfer functions. In the region where $|1+L_{2o}| \simeq |L_{2o}|$, Eq. (4-6) becomes

$$|L_{2o}| \geq \left| \frac{b_{11}Q_{22o}}{b_{21}Q_{21_{min}}} \right| \tag{4-7}$$

and the demand on L_{2o} is obtained explicitly. Equation (4-7) results in a contour on the modified Nichol's Chart (MNC), also referred to as the inverted Nichol's Chart, and is compared with an analysis of the y_{22} loop of Figure 4-5 to produce the most demanding bound on L_{2o}. A detailed explanation of the MNC is presented in Reference 2. Using Eq. (4-7), at $\omega = 0.1$ r/s L_{2o} is calculated as follows:

$$|L_{2o}| \geq 0.172+27-(-26.9-22.5) \simeq 76 \text{ decibels (dB)}$$

Parallel vertical lines are used to indicate the log magnitude (LM) operation. The bound on L_{2o} at $\omega = 0.1$ r/s coincides with the horizontal line for L_{2o} because the $(1+L_{2o})^{-1}$ contour at -76 dB is also a horizontal line.

The y_{22} loop in Figure 4-5 has two inputs to consider, r_2 and d_{22}, and therefore two transfer function expressions must be analyzed. The expression for t_{22} is

$$t_{22} = \tau_{22} + \tau_{d_{22}} \tag{4-8}$$

where

$$\tau_{22} = \frac{f_{22}q_2Q_{22}}{1+g_2Q_{22}} = \frac{f_{22}L_2}{1+L_2} \tag{4-9}$$

$$\tau_{d_{22}} = \frac{d_{22}Q_{22}}{1+L_2} = \frac{(b_{12}/Q_{21})Q_{22}}{1+L_2} \tag{4-10}$$

Using the value of L_{2o} found in the analysis of y_{21}, $\tau_{d_{22_{max}}}$ is determined from the expression

$$\left|\tau_{d_{22_{max}}}\right| = \left|\frac{b_{12}Q_{22o}}{L_{2o}Q_{21_{min}}}\right| \tag{4-11}$$

Next, the template of q_{22} for the frequency in question is taken and placed on the Nichol's Chart to determine $|\tau_{22_{max}}/\tau_{22_{min}}|$. If Eq. (4-12), below, is satisfied, then the bound found in the first analysis satisfies both loops and is used as the bound on L_{2o} for that one frequency.

$$|2\tau_{d_{22_{max}}}| + |\tau_{22_{max}}| - |\tau_{22_{min}}| \leq \left|\frac{(b_{22}-a_{22})}{2}\right| \tag{4-12}$$

If Eq. (4-12) is not satisfied, then the template of Q_{22} is translated vertically until it is satisfied. The contour through the Q_{22o} point becomes the new bound on L_{2o}. For this thesis it is found that the demands from y_{21} are the most demanding and, as a result, determine the bounds on L_{2o} for ω_i such that $|1+L_{2o}| \simeq |L_{2o}|$. At higher frequencies this approximation is not valid, and another method is used to locate the bounds on L_{2o}.

The lower specification bound a_{22} is less than -12 dB for $\omega > 2$ r/s. The LMf_{22} is also relatively small in the region since it is sloping down at approximately the same rate as a_{22}. In Eq. (4-8) the small magnitude of f_{22} makes τ_{22} negligible in comparison to $\tau_{d_{22}}$. This

leaves $\tau_{d_{22}}$ and $\tau_{d_{21}}$ to determine the bounds on L_{2o} for $\omega > 2$ r/s. It is found that the -4 dB contour satisfies the constraints imposed by both $\tau_{d_{22}}$ and $\tau_{d_{21}}$ in this region. This greatly simplifies the task of determining bounds. The template of Q_{22} is translated down and horizontally as necessary on the Nichol's Chart so that the template remains outside, but as close as possible to the -4 dB contour. The trace of the nominal point during this procedure becomes the bound on L_{2o}. This procedure is repeated for several frequencies until the universal high frequency bound is formed (2). Figure 4-8 shows L_{2o} and its bounds plotted on the Nichol's Chart, and the transfer function expression for L_{2o} is

$$L_{2o} = \frac{5.95(10^6)(s+0.3)(s+12.9)(s+120)}{s(s+0.2)(s+3.46)(s+48)(s^2+900s+562,500)} \qquad (4\text{-}13)$$

Inspection of Figure 4-8 shows that L_{2o} is close to its bounds for the lower frequencies, and avoids the -4 dB contours at high frequency. If L_{2o} were optimally designed, it would lie exactly on its bound at each frequency, and the loop transmission bandwidth would be minimum. The bandwidth of the loop transmission is an important consideration, and if too large, the system can be susceptible to noise. Using Total, the bandwidth of L_{2o} is found to be 34 r/s. No attempt to analyze the system for susceptibility

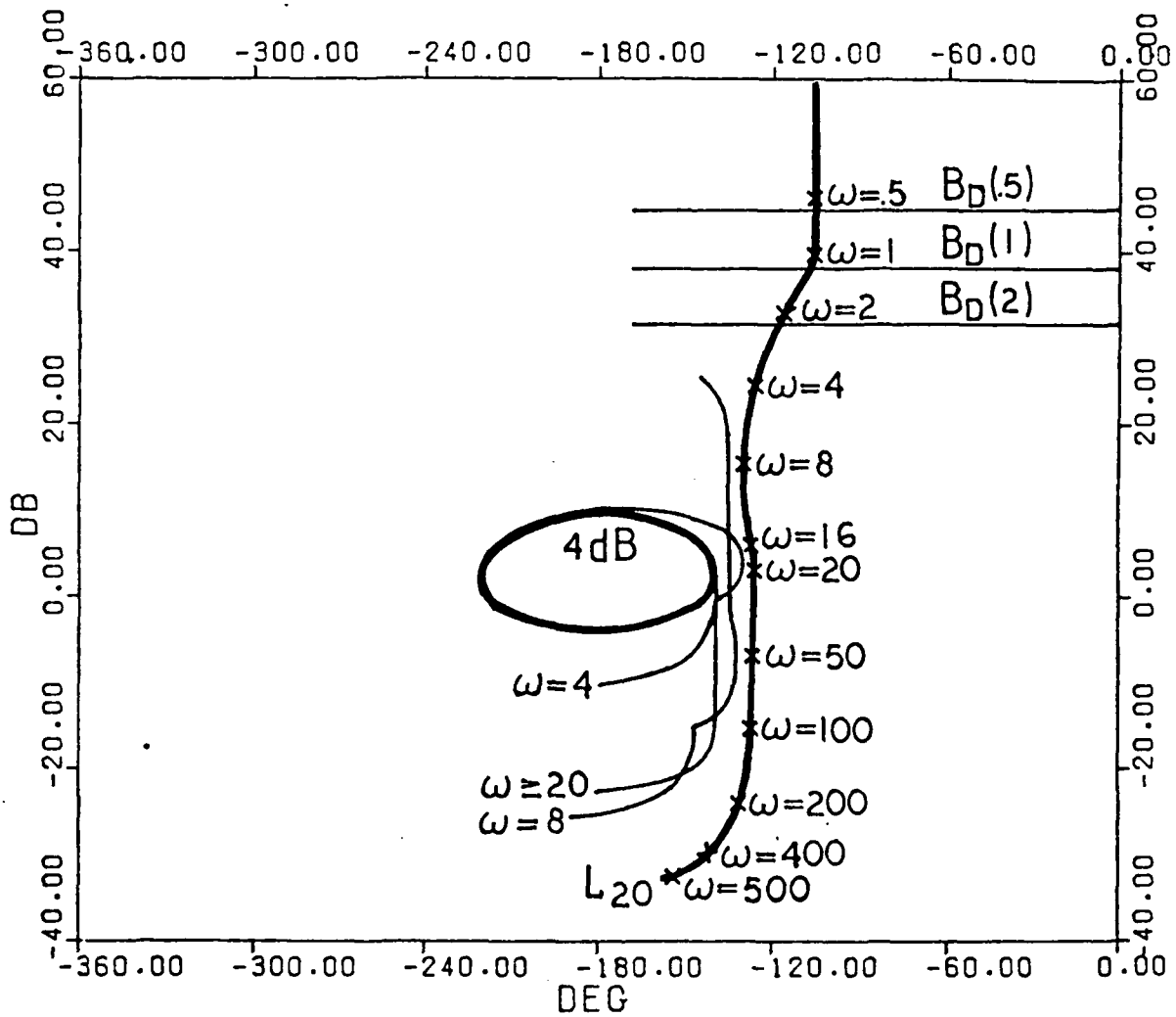

Fig. 4-8. Nichol's Chart Plot of L_{2o} and Bounds

to noise is made in this thesis. The Bode plot of L_{2o} is seen in Figure 4-9, and the compensator g_2 is derived from L_{2o}.

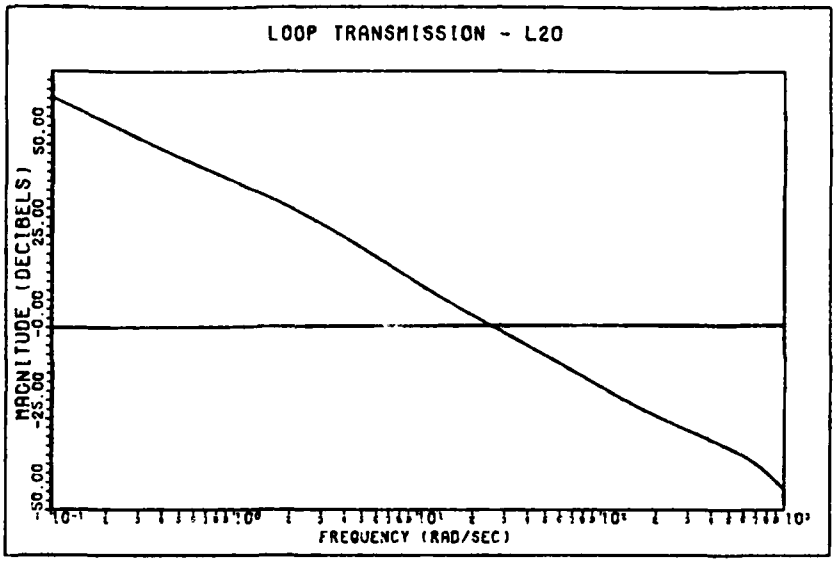

Fig. 4-9. Bode Plot of L_{2o}

The compensator g_2 is obtained from the following equation

$$g_2 = L_{2o}/Q_{22o} \tag{4-14}$$

where

$$Q_{22o} = \left[\frac{-2.64s(s^2+1.2412s+37.33)}{(s+0.03448)(s+2.171)(s^2+0.9992s+10.04)}\right] \tag{4-15}$$

and

$$g_2 = \left[\frac{-2.25(10^6)(s+.03448)(s+.3)(s+2.171)(s+12.9)(s+120)(s^2+.9992s+10.04)}{s^2(s+.2)(s+3.46)(s+48)(s^2+1.24s+37.3)(s^2+900s+562,500)}\right] \tag{4-16}$$

After L_{2o} is determined, the prefilter f_{22} is derived.

Using the methods of Reference 2, f_{22} is derived to be

$$f_{22} = \frac{2.78}{(s^2+2.668s+2.78)} \tag{4-17}$$

Due to a limitation on the number of equations that the simulation program can accommodate, f_{22} is simplified to

$$f_{22} = \frac{2}{(s+2)} \tag{4-18}$$

Equation (4-18) is a good approximation of Eq. (4-17) in the important low frequency region, and satisfies the prefilter design criteria of Reference 2. The compensator g_2 is not guaranteed to be without some overdesign, but a method to reduce some of the overdesign has been developed. This method is known as the "improved method," and is applied in the design of compensator g_1 in Section IV.5 (8).

IV.5 Loop Bound Design, L_{1o}

The exact equations for t_{22} and t_{21} are substituted into t_{11} and t_{12} to yield the following equations

$$t_{11} = \frac{f_{11}L_{1_e}}{1+L_{1_e}} \tag{4-19}$$

where

$$L_{1_e} = q_1 Q_{11_e} = \frac{q_1 Q_{11}(1+L_2)}{(1-\gamma_{12}+L_2)} \tag{4-20a}$$

and

$$\gamma = \frac{Q_{11}Q_{22}}{Q_{12}Q_{21}} \tag{4-20b}$$

It is found that in this problem $\gamma << 1$ for all cases. Simplifying Eq. (4-20a) to $L_{1_e} = L_1$, then Eq. (4-19) becomes

$$t_{11} = \frac{f_{11}L_1}{L+L_1} \tag{4-21}$$

The y_{12} equation becomes

$$t_{12} = \frac{f_{22}L_2}{Q_{12}\{(1+L_1)(1+L_2)-\gamma\}} \tag{4-22}$$

For ω_i such that $1+L_2 \simeq L_2$, Eq. (4-22) reduces to

$$t_{12} = \frac{f_{22}}{Q_{12}(1+L_1)} \tag{4-23}$$

Equations (4-21) and (4-23) are used to derive the bounds on L_{1o}. The procedure is similar to that used for L_{2o}, except t_{11} consists only of the term due to the command input. The loop interaction term disappears since this is a BNIC problem. In the low frequency region where $|1+L_1| \simeq |L_1|$, the t_{12} expression creates the greatest demands on L_{1o}, and the following inequality is used to derive the bounds in this region.

$$t_{12} = \frac{f_{22}}{Q_{12}(1+L_1)} \leq b_{12} \tag{4-24}$$

$$\left|\frac{1}{1+L_1}\right| \leq \left|\frac{b_{12}Q_{12}}{f_{22}}\right| \tag{4-25}$$

for $|1+L_1| \simeq |L_1|$

$$|L_{1o}| \geq \left|\frac{f_{22}}{b_{12}Q_{12_{min}}}\right| \tag{4-26}$$

As an example, at $\omega = 0.1$ r/s, using Eq. (4-26) L_{1o} is calculated to be

$$|L_{1o}| \geq 0 - (-45.5 + 1.34) \simeq 44 \text{ dB}$$

This becomes the bound for L_{1o} at $\omega = 0.1$ r/s since the contour of $(1+L_{1o})^{-1}$ is essentially a horizontal line on the MNC for this value of L_{1o}. Bounds in the medium and high frequency regions are obtained as is done for the L_{2o} bounds in the same regions. The loop transmission L_{1o} is shaped next.

The nominal q_{11} selected for L_{1o} is

$$q_{11o} = \frac{-2.235s(s+.0107)(s+.4845)}{(s-1.167)(s+2.028)(s^2+.012944s+.006131)} \tag{4-27}$$

Notice that Eq. (4-27) has an unstable pole at $s = 1.167$. To avoid trying to achieve exact cancellation, L_{1o} must be shaped with this unstable pole as a factor. One technique is to shape L_{1o} to include the pole and zero combination, $\frac{(s+1.167)}{(s-1.167)}$. This expression has a magnitude of one, and

a phase angle that decreases with increasing frequency. Each bound on L_{1o} as derived above is shifted by the arg $\left[\frac{s+1.167}{s-1.167}\right]$, and L_{1o}' is shaped using the new bounds. The desired L_{1o} is then obtained by shifting L_{1o}' back in the direction of the original bounds by the same number of degrees. The relationship between L_{1o} and L_{1o}' is

$$L_{1o} = L_{1o}' \frac{(s+1.167)}{(s-1.167)} \tag{4-28}$$

For ease of loop shaping, this method is found to be preferable to including only the unstable pole. The Nichol's Chart plots of L_{1o} and L_{1o}' are seen in Figure 4-10, and the Bode plot of L_{1o} is seen in Figure 4-11. Figure 4-10 shows that there is overdesign in L_{1o}. The bandwidth of L_{1o} is found to be 24 r/s. Dividing L_{1o} by Q_{11o}, g_1 is found to be

$$g_1' = \frac{-2.39(10^6)(s+.3)(s+1.1)(s+1.167)(s+2.028)(s+20)(s+430)(s^2+.012944s+.00613)}{s^2(s+.0107)(s+.4845)(s+.5)^2(s+35)(s+87)(s^2+1272s+1,123,600)} \tag{4-29}$$

Notice that (s-1.167) does not appear as a factor in the denominator of g_1, and exact cancellation is not a problem.

A simple design is found to suffice for f_{11}. The expression for f_{11} is

$$f_{11} = 2/(s+2) \tag{4-30}$$

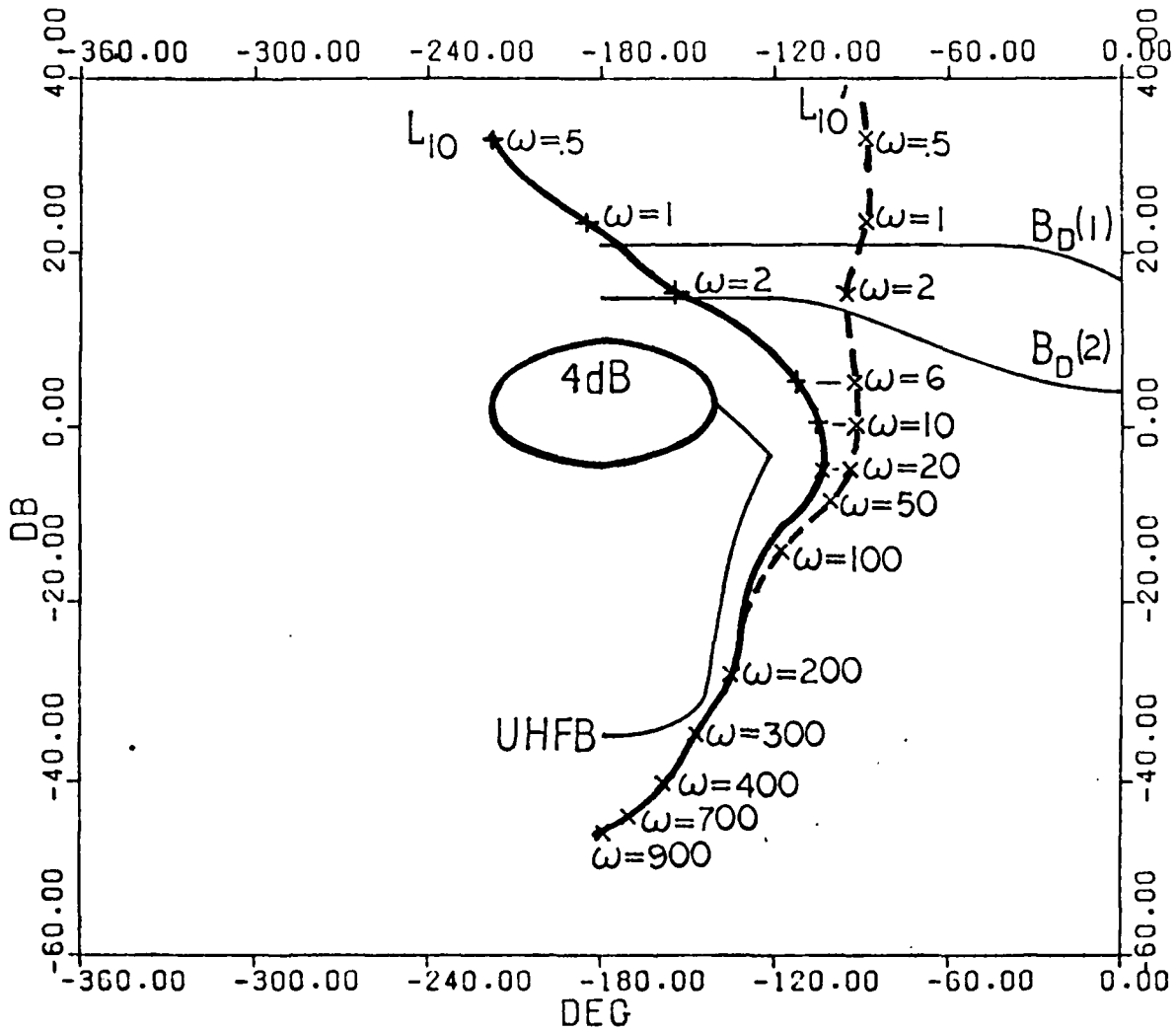

Fig. 4-10. Nichol's Chart Plot of L_{1o}, L_{1o}', and Bounds

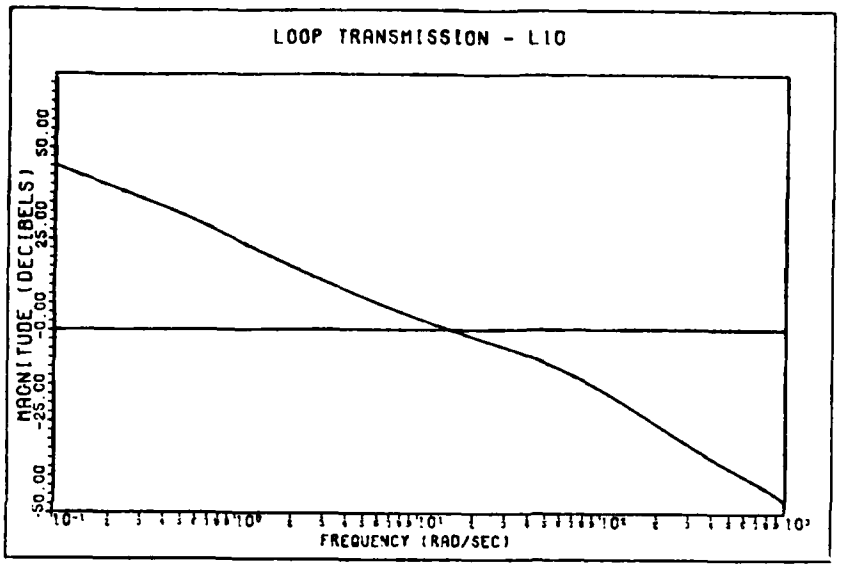

Fig. 4-11. Bode Plot of L_{1o}

IV.6 Stability Design for Three Simultaneous Failures

In this section the characteristic polynomials are derived for two configurations with three of the four control surfaces failed. For this study, it is desired to achieve only a stable system. No attempt is made to meet performance specifications. Bounds for stability are formed using templates that include all six CSC modes previously analyzed plus the configuration of interest for which only one surface is controllable. As before, a nominal condition is chosen and the stability bounds are drawn on the Nichol's Chart. The 3 dB contour is used for gain and phase margins. The nominal loop transmission is then shaped as is done for L_{2o} in Chapter IV. By examining the zeros of the characteristic polynomial, which is a function

TABLE 5-2

PITCH RATE RESPONSE FIGURES OF MERIT

Flight Condition	CSC Mode	Settling Time t_s (sec)	Rise Time t_r (sec)	Peak Value M_p (deg/sec)
1	1	2.16	1.15	9.96
	2	3.12	1.22	9.91
	3	2.20	1.14	9.97
	4	3.24	1.22	9.90
	5	3.84	1.28	9.91
	6	2.16	1.14	9.96
2	1	2.84	1.30	10.40
	2	3.60	1.50	10.80
	3	2.80	1.25	10.40
	4	3.68	1.75	11.00
	5	3.54	1.50	10.80
	6	2.80	1.29	10.40
3	1	1.90	1.10	10.00
	2	1.87	1.10	10.10
	3	1.90	1.10	10.00
	4	2.22	1.19	10.20
	5	1.88	1.10	10.10
	6	1.90	1.10	10.00
4	1	1.86	1.07	9.87
	2	1.70	1.05	9.67
	3	1.88	1.00	9.87
	4	1.64	0.98	9.36
	5	1.72	1.03	9.68
	6	1.86	1.06	9.86

compliance with the performance tolerances listed in Table 4-1, repeated here as Table 5-1. Settling time, rise time, and peak value are calculated for each response and listed in Table 5-2.

TABLE 5-1

FIGURE OF MERIT TOLERANCES
FOR PITCH RATE

Settling Time t_s (sec)	Rise Time t_r (sec)	Peak Value M_p (deg/sec)
1.5 - 3.0	0.33 - 1.63	$\leq$ 11

From Table 5-2 it is seen that design tolerances for t_s are not satisfied in all instances. The t_s calculated for modes 2, 4, and 5 of flight conditions 1 and 2 is found to exceed the maximum allowed t_s of 3 seconds. An explanation for the increased settling times at flight conditions 1 and 2 may lie in the relative locations of the poles and zeros of the basic plant equations $P_{11}{}^a$ and $P_{12}{}^a$, Sec. II.2. The poles of these basic plant equations for q at flight conditions 3 and 4 tend to be located farther to the left in relation to their zeros than are corresponding poles of the same plant equations for flight conditions 1 and 2. Therefore, system closed-loop roots are probably more negative at flight conditions 3 and 4 and the resulting settling times will be greater at flight conditions 1 and 2. The t_s is easily reduced by decreasing the

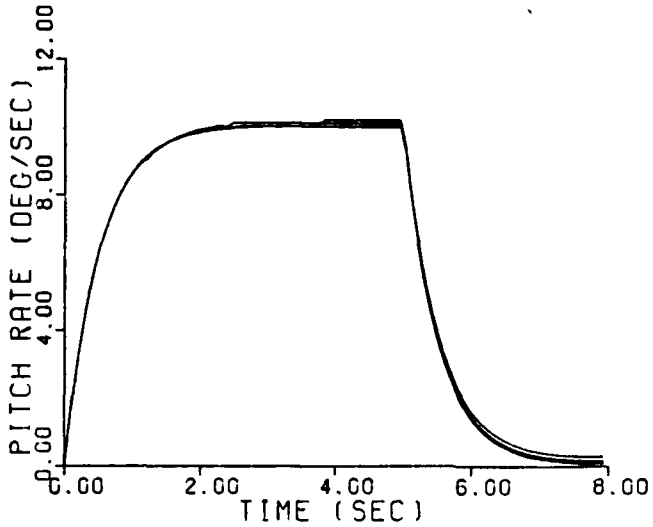

Fig. 5-2(c). Pitch Rate Responses, Flight Condition Three

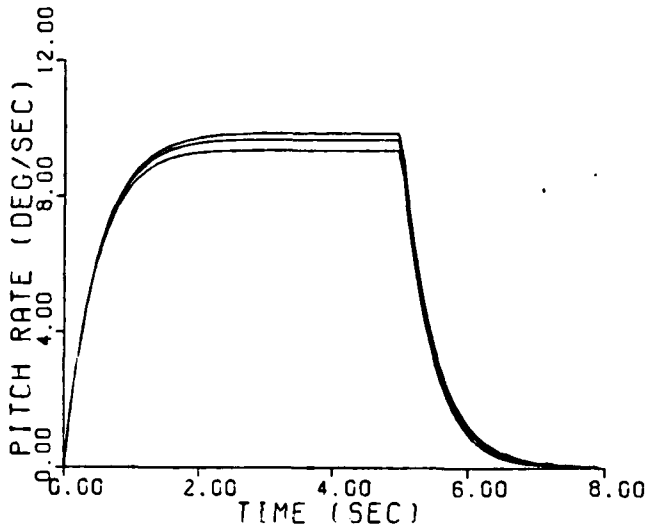

Fig. 5-2(d). Pitch Rate Responses, Flight Condition Four

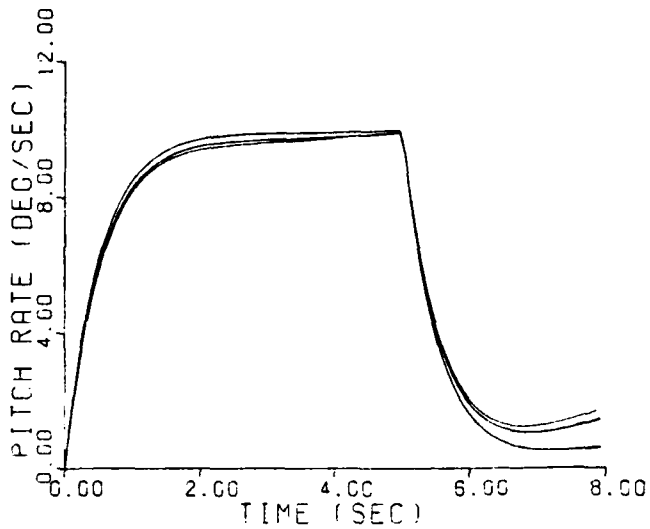

Fig. 5-2(a). Pitch Rate Responses, Flight Condition One

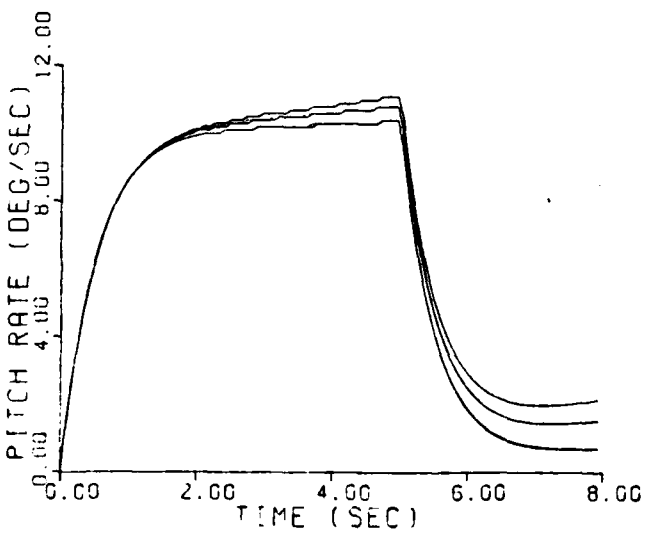

Fig. 5-2(b). Pitch Rate Responses, Flight Condition Two

is necessary due to a limitation on the number of equations that the simulation program can accommodate. Figure 5-1 shows a Bode plot comparison of Eqs. (4-28) and (5-1). Reducing the order to g_1 by one-half is certain to make the implementation of the controller more practical.

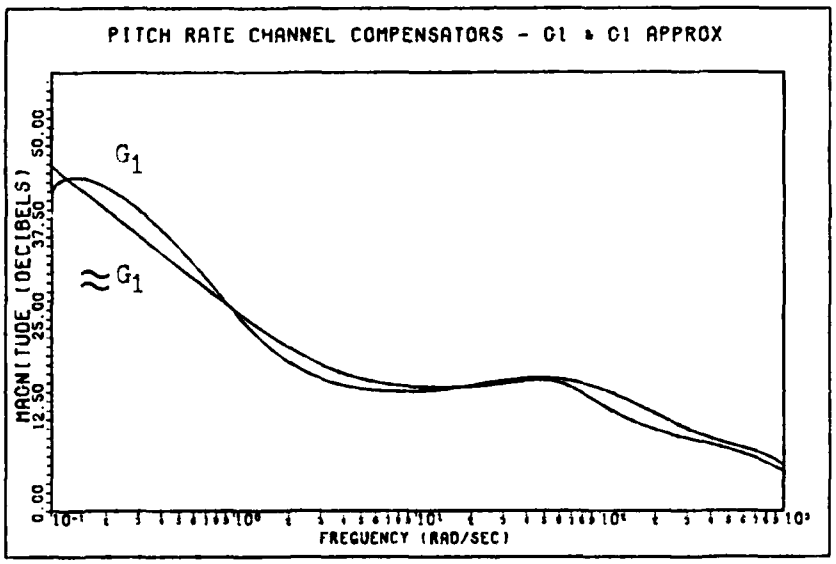

Fig. 5-1. Bode Plot Comparison of G_1 and the Approximation for G_1

The q responses for the four flight conditions and six CSC modes are seen in Figures 5-2a to 5-2d. Each figure represents the responses for one flight condition and the six CSC modes. The responses are examined for

are explained for compliance with the performance tolerances detailed in Chapter IV. Surface deflections are examined for saturation, and a more efficient division of control effort is investigated to reduce or eliminate saturation. Control surface initial rates are found to saturate for more cases when the input is a pulse, but representative examples with ramped inputs are also presented showing rates that are not saturated. Mr. Yin-Kuei Liao of the Chung-Shan Institute of Science and Technology, Republic of China, developed the computer program used to simulate the system of Figure 2-1. It is recommended that follow-on thesis efforts in QFT concentrate on developing a computer-aided design (CAD) package adaptable to higher-order systems. A listing of the computer programs used in the simulation is presented in Appendix F. Compliance with the specifications for q are investigated first.

V.2.1. Pitch Rate Command Response

Before proceeding with the q responses, it is noted that the compensator g_1, Eq. (4-28), is approximated as follows:

$$g_1 = \frac{-6.6(10^5)(s+4)(s+100)(s^2+0.013s+0.006)}{s(s+0.0223)(s+25)(s+630)^2} \qquad (5\text{-}1)$$

Thus, the order of g_1 is reduced from tenth to fifth-order. Equation (5-1) is obtained from a straight-line approximation of the Bode plot for Eq. (4-28). The approximation

V. Results

V.1 Introduction

The results of the computer simulation are presented in this chapter. The digital simulation program integrates the system equations in state-variable form to yield the desired outputs. The q and p command and cross-coupling responses are examined for compliance with performance tolerances. Control surfaces are examined for proper sense of movement and saturation. The insights that QFT affords a designer are investigated, and the results of control surface "hardover" simulations are illustrated. A brief description of the simulation program follows.

V.2 Simulation

The system represented in Figure 2-1 is simulated with the plant, prefilter, and compensator equations in state-variable form. A digital integration routine is applied to the system over a desired time interval to yield a nonlinear, real-time simulation which includes control surface position saturation. The outputs of the simulation are p, q, and the four control surface positions (right/left elevators and right/left flaperons). Outputs are obtained for each design flight condition and control surface configuration (CSC) mode, and the q and p responses

transmissions are then shaped on the Nichol's Chart. Simple expressions for the prefilters are derived completing the designs. Lastly, stability only designs for configurations with three simultaneous surface failures are synthesized, and further illustrates the potential of quantitative feedback theory. Chapter V presents the system simulations.

$$(1+L_{2o_e}) = \frac{(s+1.56)(s+32.5\pm j46.9)(s+424.6\pm j567)}{s(s+22.9)(s+34.6)(s+429.2\pm j572.2)} \qquad (4\text{-}39)$$

and

$$(1+L_{1o_e}) = \frac{(s+1.996)(s+1388\pm j1838)(s+1426\pm j1914)}{s(s+1408\pm j1877)^2} \qquad (4\text{-}40)$$

The characteristic polynomial is formed by the product of Eqs. (4-39) and (4-40). Again, the system is stable as all the zeros of Eq. (4-37) lie in the left-half-plane.

These designs for stability further illustrate the power of QFT. Loss of aircraft control is the probable result if time is required to identify and switch in compensation for the two failure cases examined in this section. No identification and switching in of compensation is required for the fixed compensators designed using QFT. This buys the aircrew valuable time; for example, time to maneuver the aircraft into more favorable ejection parameters.

IV.7 Summary

This chapter presents a complete description of the procedure used in the compensator designs. First, the equivalent plant expressions are derived, and the equivalent single-loop plant equations (Q_{ij}) are obtained. Specifications are derived for the command and cross-coupling responses. Based on these specifications, bounds on the loop transmissions are obtained, and the loop

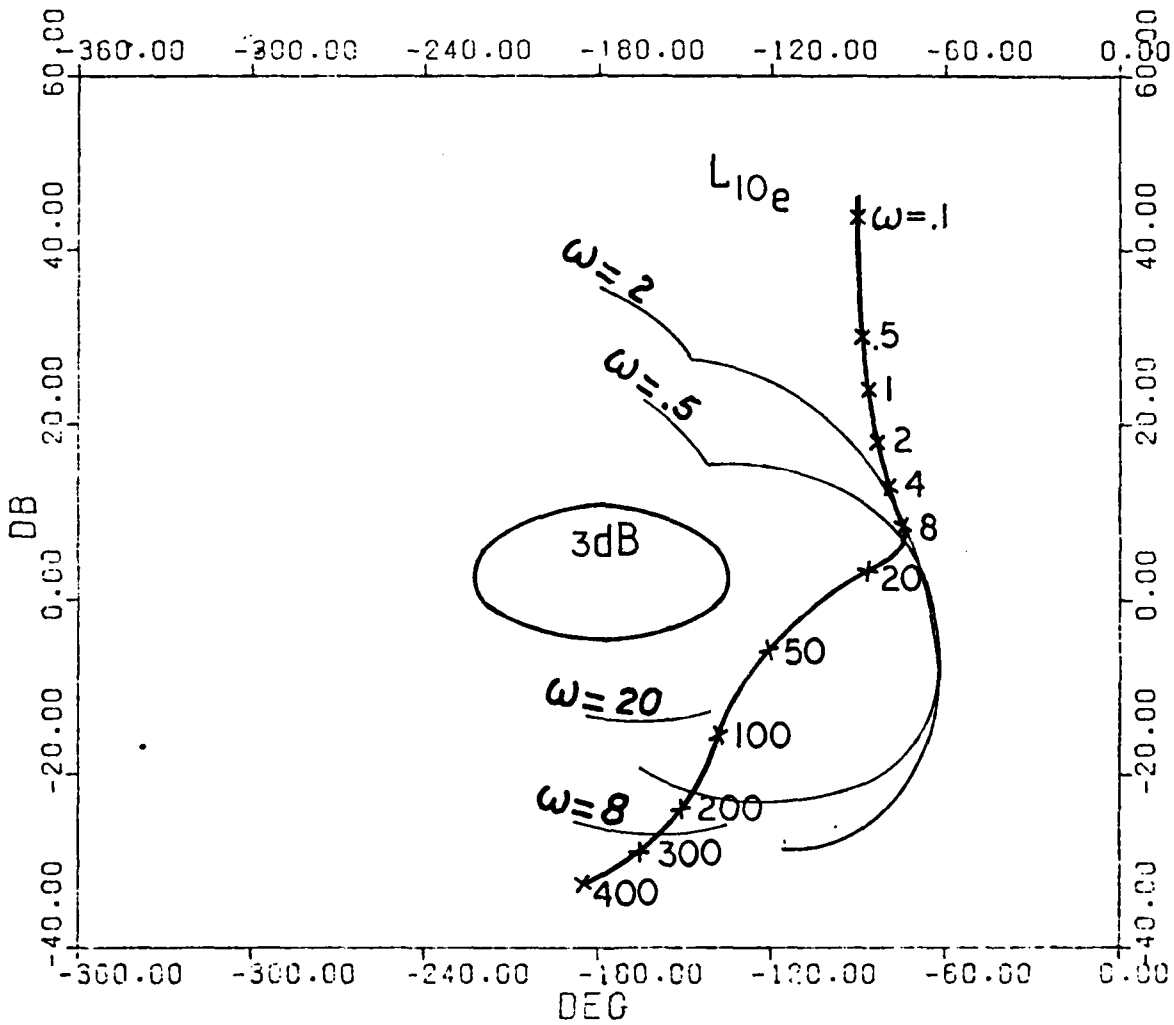

Fig. 4-13. L_{10_e} and Bounds for Stability Only (One Elevator Only)

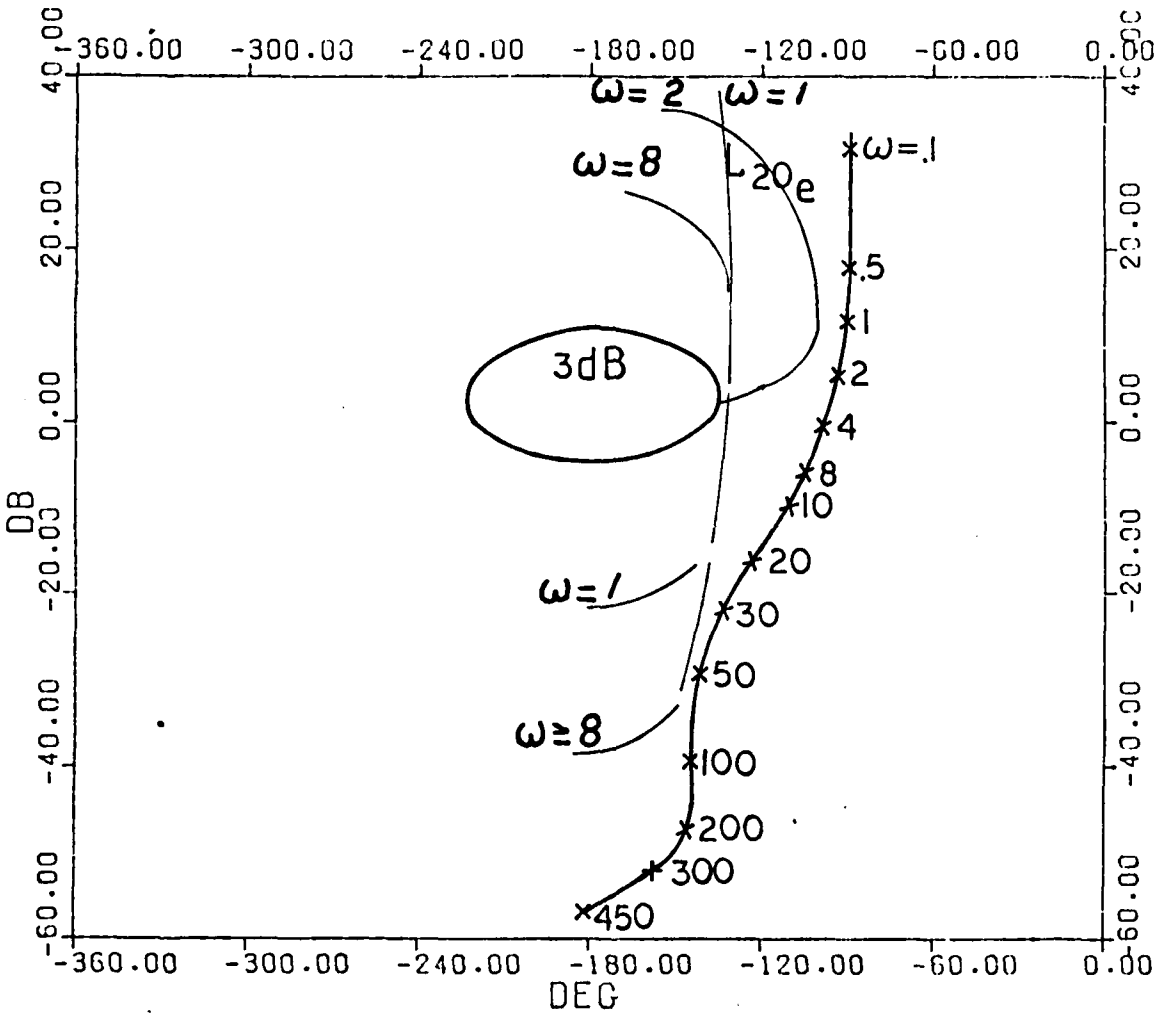

Fig. 4-12. L_{2o_e} and Bounds for Stability Only (One Elevator Only)

and

$$(1+L_{1o_e}) = \frac{(s+5.7)(s+28.7\pm j37.3)(s+278.5\pm j371.1)}{s(s+22.7)(s+34.6)(s+281.4\pm j375.2)} \quad (4\text{-}36)$$

The characteristic polynomial is the product of Eqs. (4-35) and (4-36), and as can be seen, all zeros are in the left-half-plane, indicating a stable system. Figures 4-12 and 4-13 show L_{2o_e} and L_{1o_e}, respectively, and the bounds on each.

The same procedure as above is used to design for stability when only one flaperon is controllable. In this case only $P_{22}{}^a$ and $P_{12}{}^a$ exist ($P_{11}{}^a = P_{21}{}^a = P_{11}{}^b = P_{21}{}^b = P_{22}{}^b = P_{12}{}^b = 0$). When these substitutions are made into Eq. (3-7), the characteristic polynomial is

$$(1 + \mu P_{12}{}^a g_1 + P_{22}{}^a g_2) \quad (4\text{-}37)$$

Equation (4-37) may be factored as follows

$$(1+P_{22}{}^a g_2)\ \frac{(1+\mu P_{12}{}^a g_1)}{1+P_{22}{}^a g_2} = (1+L_{2o_e})(1+L_{1o_e}) \quad (4\text{-}38)$$

where,

$$L_{2o_e} = P_{22}{}^a g_2, \text{ and } L_{1o_e} = \frac{\mu P_{12}{}^a g_1}{1+P_{22}{}^a g_2}$$

The factors in Eq. (4-38) are derived in a manner similar to that used to derive the factors in Eq. (4-34). The design process yields

$$\underline{T} = \frac{\begin{bmatrix} \mu g_1 P_{12}{}^a & g_2 P_{12}{}^a \\ \mu g_1 P_{22}{}^a & g_2 P_{22}{}^a \end{bmatrix}}{1 + \mu P_{12}{}^a g_1 + P_{22}{}^a g_2} \tag{4-32}$$

The characteristic polynomial for this configuration is

$$1 + \mu P_{12}{}^a g_1 + P_{22}{}^a g_2 \tag{4-33}$$

Equation (4-33) is factored as follows:

$$(1+P_{22}{}^a g_2) \cdot \frac{(1+\mu P_{12}{}^a g_1)}{1+P_{22}{}^a g_2} = (1+L_{2o_e})(1+L_{1o_e}) \tag{4-34}$$

Where,

$$L_{2o_e} = P_{22}{}^a{}_o g_2, \text{ and } L_{1o_e} = \frac{\mu P_{12}{}^a{}_o g_1}{1+P_{22}{}^a{}_o g_2}$$

Prefilters f_1 and f_2 in Eq. (3-7) are made equal to unity for the convenience of this analysis.

Loop transmissions are shaped separately on the Nichol's Chart for each factor in Eq. 4-34. The L_{2o_e} loop is shaped first so that the factor $(1+L_{2o_e})$ can be used in forming the bounds for the L_{1o_e} loop. From Total, the factors of Eq. (4-34) are

$$(1+L_{2o_e}) = \frac{(s+4.9)(s+18.4)(s+299.7\pm j399.7)}{s(s+22.9)(s+300\pm j400)} \tag{4-35}$$

of L_{1o} and L_{2o}, the stability of the system is determined. Configurations for which only one elevator, and only one flaperon are controllable are examined separately.

The first configuration analyzed is the system for which only one elevator surface remains controllable. The remaining elevator and the two flaperons are failed to their neutral reference positions. The design begins by determining $\underline{P}_e$. Only $P_{11}{}^a$ and $P_{22}{}^a$ exist for this configuration ($P_{11}{}^b = P_{21}{}^b = P_{22}{}^a = P_{12}{}^a = P_{22}{}^b = P_{12}{}^b = 0$). These substitutions are made into Eq. (3-6) to yield

$$\underline{P}_e = \begin{bmatrix} P_{11}{}^a & \mu P_{11}{}^a \\ P_{21}{}^a & \mu P_{21}{}^a \end{bmatrix} \tag{4-31}$$

As before, in order to determine the equivalent single-loop plant equations Q_{ij}, $\underline{P}_e{}^{-1}$ must be computed. From Eq. (4-31) $|\underline{P}_e| = 0$, and $\underline{P}_e{}^{-1}$ does not exist. In this case the system effectively becomes a SISO system with only one output independently achievable. The P_{ije} (i=j) plant equations are now used in the detailed design procedure.

When the elements of Eq. (4-31) are substituted into the system transfer function matrix Eq. (3-7), the system matrix for one controllable elevator becomes

time constant of f_{11}. Scheduling of f_{11} may need to be employed if the t_s is too small for some flight conditions. Close examination of the data in Table 5-2 also reveals that the difference between the maximum and minimum t_s is 2.14 sec. This exceeds the t_s tolerance of 1.5 sec by 0.64 sec. Quantitative feedback theory guarantees that the original performance tolerances will be satisfied despite the uncertainty (2). An exact reason why this has occurred is not known, but one possible explanation is that the approximation for g_1 may not be adequate to satisfy the tolerances in all cases. Despite this fact, q is found to be controllable for each flight condition and CSC mode. A roll angle tolerance when q is commanded must also be satisfied.

As stated earlier in Section IV.3, it is desired that the roll angle be less than five degrees when q is commanded. The roll angle is estimated by graphically calculating the area under the p response curves resulting from cross-coupling. The cross-coupling responses are seen in Figures 5-3a to 5-3d. Only four responses are seen per figure as cross-coupling does not occur for CSC modes one and six due to the symmetry of the control surfaces for these two modes. The estimated worse case total roll angle at each flight condition is seen in Table 5-3. Inspection of this data reveals that the roll angle specification is satisfied for all cases. Control surface deflections when q is commanded are examined next.

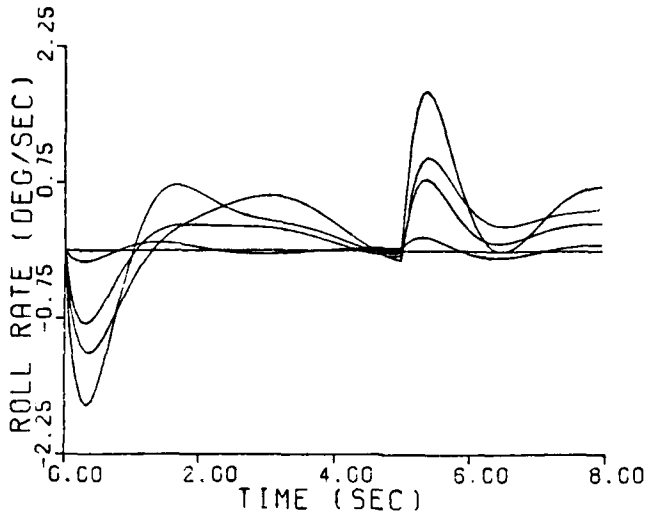

Fig. 5-3(a). Roll Rate Cross-Coupling Responses, Flight Condition One

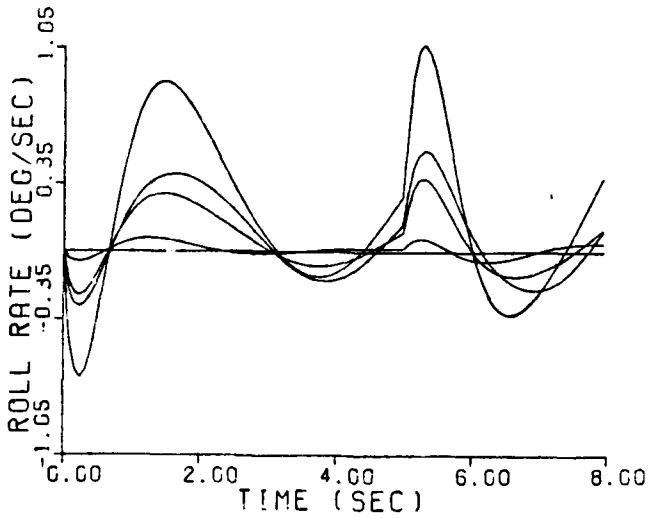

Fig. 5-3(b). Roll Rate Cross-Coupling Responses, Flight Condition Two

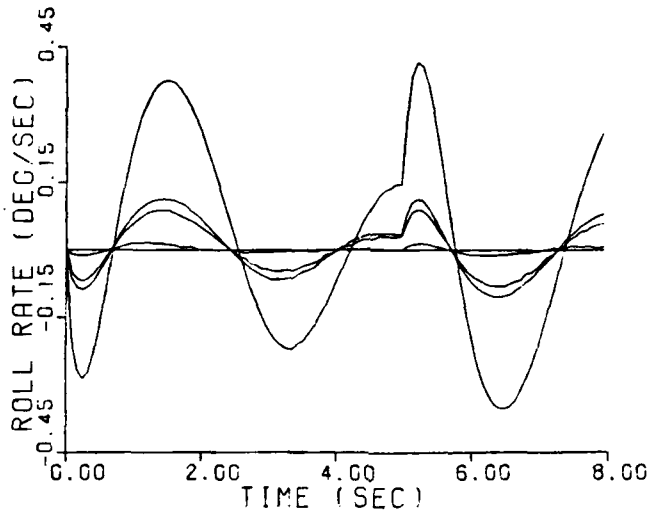

Fig. 5-3(c). Roll Rate Cross-Coupling Responses, Flight Condition Three

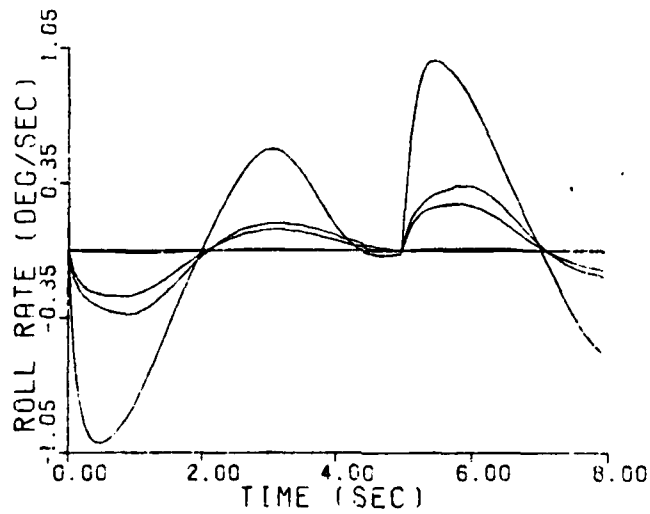

Fig. 5-4(d). Roll Rate Cross-Coupling Responses, Flight Condition Four

TABLE 5-3

ESTIMATED ROLL ANGLES WITH
PITCH RATE COMMANDED

Flight Condition	CSC Mode	Roll Angle (deg)
1	4	2.16
2	4	1.85
3	4	0.74
4	4	2.74

Elevator and flaperon deflections are seen in Figures 5-4a to 5-4f. Due to the large number of figures for the surface deflections, only those figures for flight condition one are presented in the main body of this thesis. The remaining figures are displayed in Appendix G. Negative deflection angles indicate that lift is being generated in the negative direction (down), and vice versa for positive deflection angles. The sign convention used is detailed in Reference 6. Figure 5-4a (CSC mode 1) shows that surfaces are moving in the proper directions to generate positive q. The negative deflections generate negative lift at the elevator and flaperon stations causing the nose of the aircraft to rotate up (positive q). Although not as obvious in some of the figures, surface movements appear to be in the proper sense to generate positive q. Control surface position and rate limit data

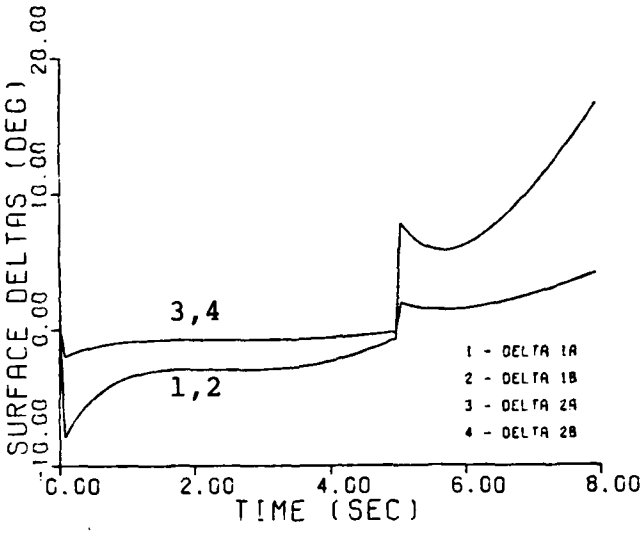

Fig. 5-4(a). Elevator and Flaperon Deflections for Pitch Rate, CSC Mode One and Flight Condition One

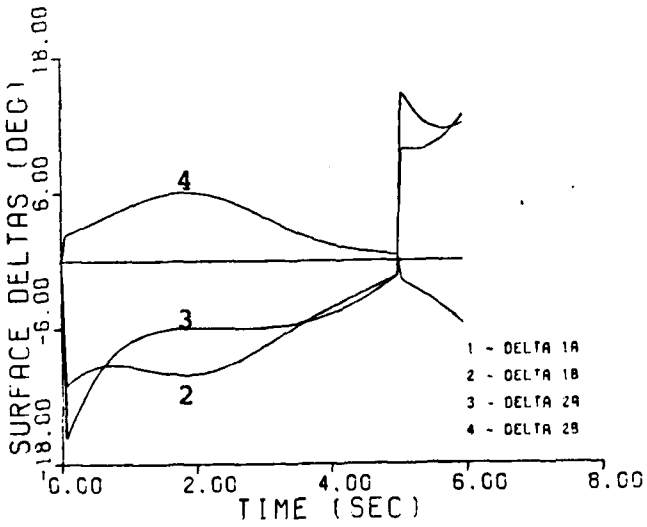

Fig. 5-4(b). Elevator and Flaperon Deflections for Pitch Rate, CSC Mode Two and Flight Condition One

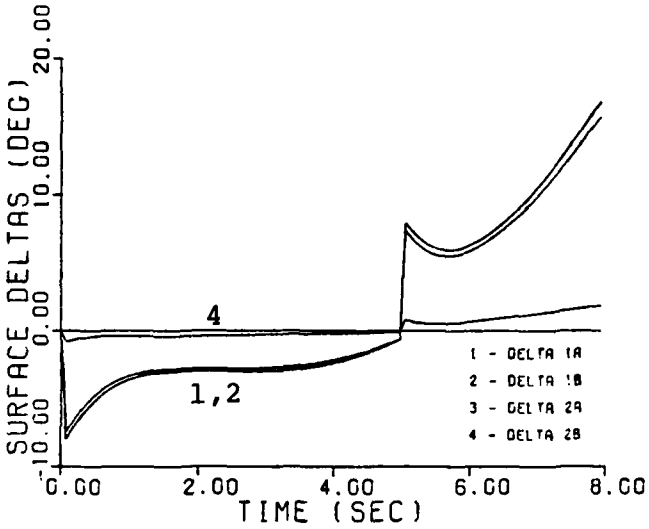

Fig. 5-4(c). Elevator and Flaperon Deflections for Pitch Rate, CSC Mode Three and Flight Condition One

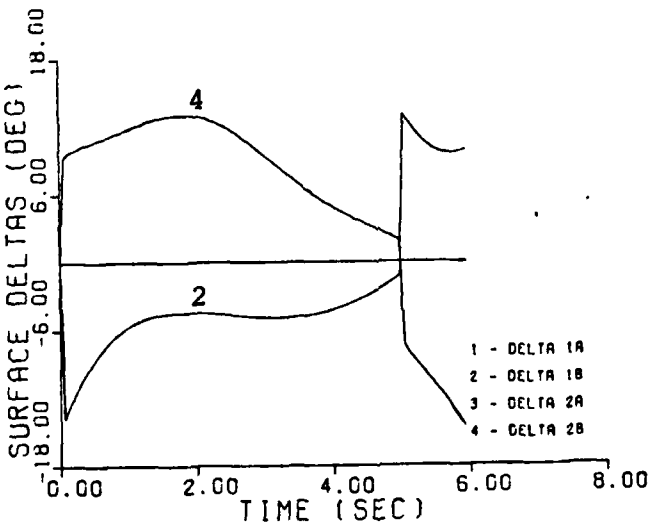

Fig. 5-4(d). Elevator and Flaperon Deflections for Pitch Rate, CSC Mode Four and Flight Condition One

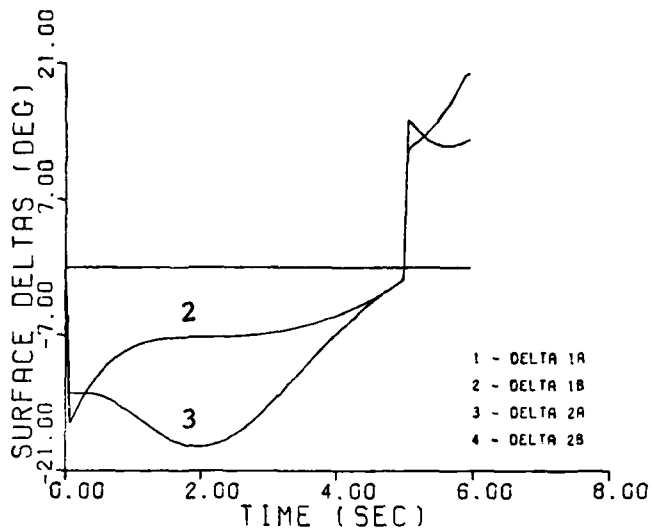

Fig. 5-4(e). Elevator and Flaperon Deflections for Pitch Rate, CSC Mode Five and Flight Condition One

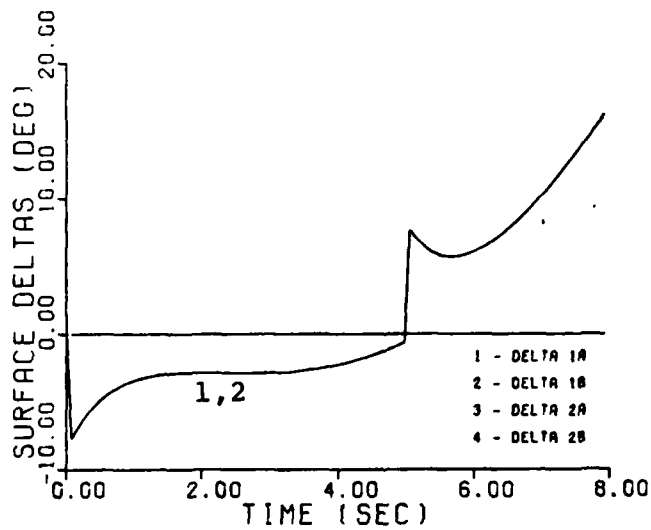

Fig. 5-4(f). Elevator and Flaperon Deflections for Pitch Rate, CSC Mode Six and and Flight Condition One

are taken from Reference 6, and repeated in Table 5-4. Inspection of Figures 5-4a to 5-4f show that surface position saturation does not occur for the q command at flight condition one. Initial surface rates are seen to be quite high, and are estimated to saturate or nearly saturate for the pulse input. Saturation is further addressed in a later section of this chapter. In summary, control surface movements appear to be in the proper sense to generate positive q for all flight conditions and CSC modes.

TABLE 5-4

SURFACE POSITION AND RATE LIMITS

Surface	Position Limit (deg)	Rate Limit (deg/sec)
Elevators	±25	60
Flaperons	±20	52

V.2.2 Roll Rate Command Response

The p responses for the four flight conditions and CSC modes are seen in Figures 5-5a to 5-5d. Each response is examined for compliance with the tolerances listed in Table 4-2, repeated here as Table 5-5.

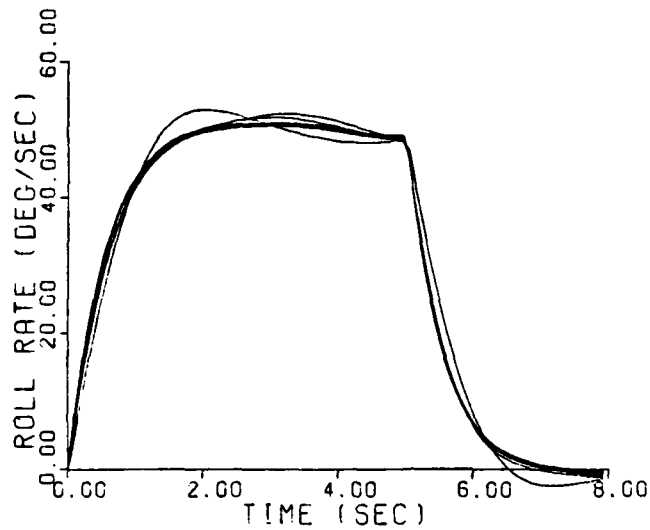

Fig. 5-5(a). Roll Rate Responses, Flight Condition One

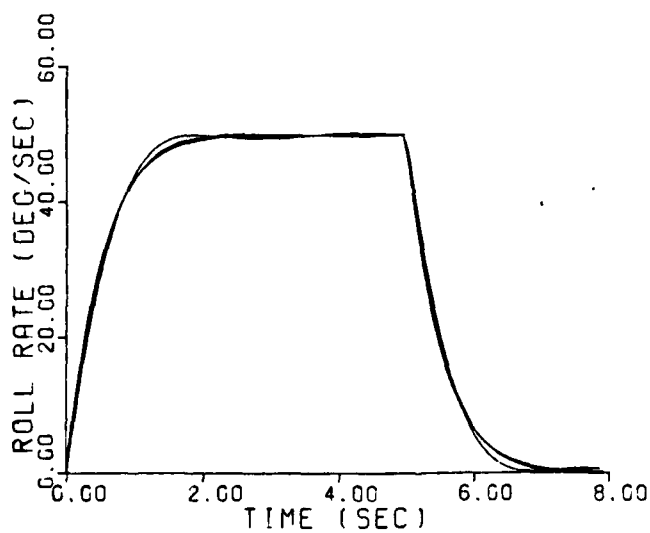

Fig. 5-5(b). Roll Rate Responses, Flight Condition Two

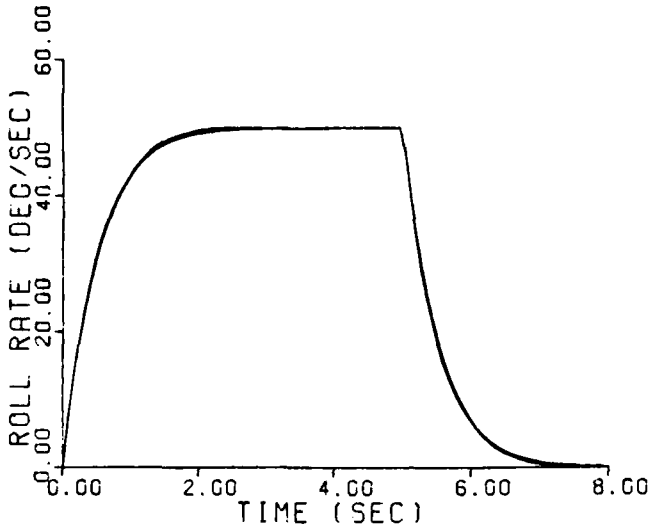

Fig. 5-5(c). Roll Rate Responses, Flight Condition Three

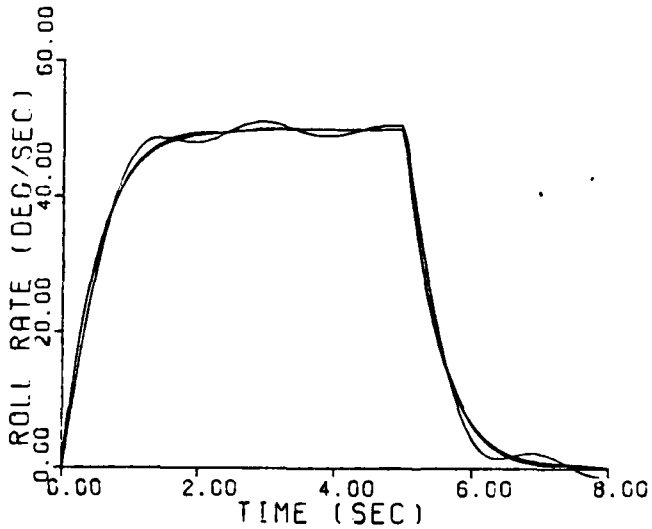

Fig. 5-5(d). Roll Rate Responses, Flight Condition Four

TABLE 5-5

FIGURE OF MERIT TOLERANCES
FOR ROLL RATE

Settling Time t_s (sec)	Rise Time t_r (sec)	Peak Value M_p (deg/sec)
3.0 - 6.0	0.65 - 3.23	$\leq$ 55

The figures of merit calculated for each p response are listed in Table 5-6. As is necessary for g_1, the compensator g_2, Eq. (4-16), is approximated in the same manner as g_1. The approximation for g_2 is

$$g_2 = \frac{-3.68(10^4)(s+3)(s+900)(s^2+2s+4)}{s(s+0.25)(s+50)(s+158)(s+3750)} \qquad (5\text{-}2)$$

The original ninth-order equation for g_2 is reduced to an effective fifth-order equation. Figure 5-6 shows a Bode plot comparison of Eqs. (4-16) and (5-2). The data in Table 5-6 is examined for compliance with performance tolerances.

The data in Table 5-6 indicates that performance tolerances for t_s, t_r, and M_p are satisfied for all but, possibly, one case. The t_s for CSC mode 6 and flight condition one is greater than five seconds due to the oscillatory nature of the response. Also, most of the responses have settling times that are faster than desired. These responses may be slowed by using a larger time constant

TABLE 5-6

ROLL RATE RESPONSE FIGURES OF MERIT

Flight Condition	CSC Mode	Settling Time t_s (sec)	Rise Time t_r (sec)	Peak Value M_p (deg/sec)
1	1	4.25	1.15	50.7
	2	4.16	1.22	51.1
	3	3.84	1.17	51.0
	4	3.84	1.30	51.9
	5	4.00	1.42	52.4
	6	5.00+	1.14	53.0
2	1	1.85	1.06	50.1
	2	4.16	1.21	51.1
	3	1.80	1.10	50.0
	4	1.76	1.10	50.0
	5	1.70	1.02	49.9
	6	1.50	1.00	50.1
3	1	1.92	1.10	50.0
	2	1.88	1.09	50.0
	3	1.86	1.10	50.0
	4	1.76	1.16	50.0
	5	1.84	1.10	50.0
	6	1.76	1.03	50.0
4	1	1.92	1.00	50.0
	2	1.98	1.04	50.1
	3	1.88	1.07	50.0
	4	4.48	0.95	51.1
	5	1.94	1.05	50.1
	6	1.76	1.06	50.1

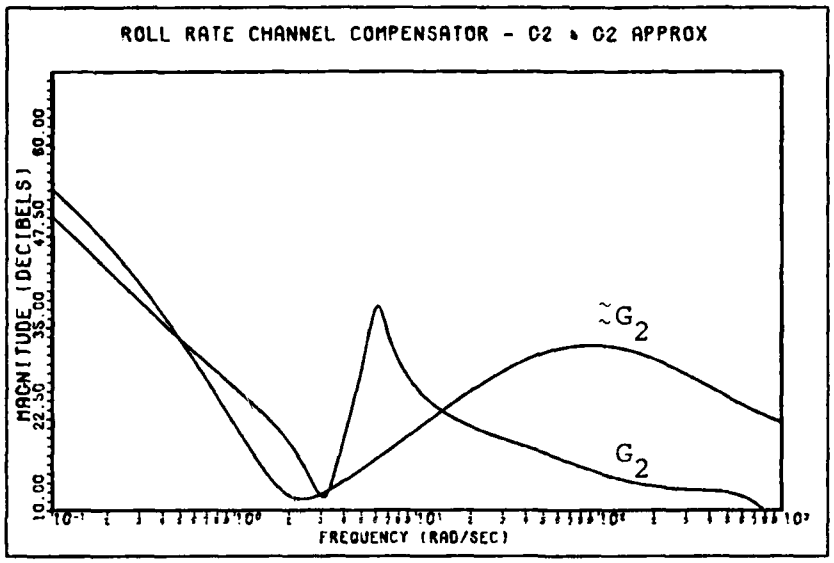

Fig. 5-6. Bode Plot Comparison of G_2 and the Approximation for G_2

in the prefilter f_{22}. A higher-order prefilter can be used to shape the responses to obtain more desirable figures or merit. This is not attempted in this study due to a restriction on the number of equations that the simulation program can accommodate. The q resulting from the p command is examined for compliance with performance specifications.

The pitch angle due to cross-coupling is estimated in the same way that roll angle due to cross-coupling is estimated. It is desired that the pitch angle remain less than three degrees during the p command. The q

cross-coupling responses are shown in Figures 5-7a to 5-7d, and Table 5-7 lists the worse case pitch angle estimated at each flight condition.

TABLE 5-7

ESTIMATED PITCH ANGLE WITH ROLL RATE COMMANDED

Flight Condition	CSC Mode	Pitch Angle (deg)
1	5	-3.10
2	4	-0.70
3	4	-1.00
4	4	-1.25

The magnitude of the pitch angle for CSC mode 5 and flight condition 1 is seen to slightly exceed 3 degrees. If the accuracy of the pitch angle estimations is conservatively estimated at 5 percent, the performance specification for pitch angle is satisfied. Control surface deflections due to the p command are estimated for proper sense of movement and saturation.

AD-A151 771 FLIGHT CONTROL SYSTEM RECONFIGURATION DESIGN USING QUANTITATIVE FEEDBACK THEORY(U) AIR FORCE INST OF TECH WRIGHT-PATTERSON AFB OH SCHOOL OF ENGI.. P B ARNOLD 2/3

UNCLASSIFIED DEC 84 AFIT/GE/ENG/84D-15 F/G 1/4 NL

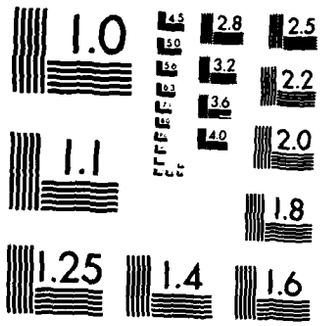

MICROCOPY RESOLUTION TEST CHART
NATIONAL BUREAU OF STANDARDS-1963-A

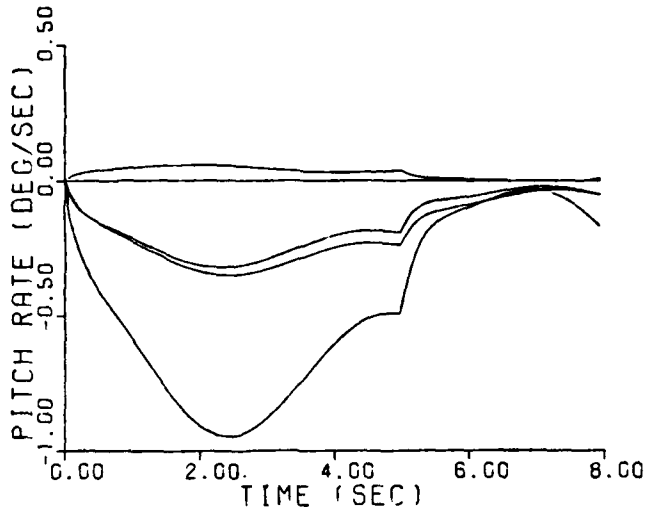

Fig. 5-7(a). Pitch Rate Cross-Coupling Responses, Flight Condition One

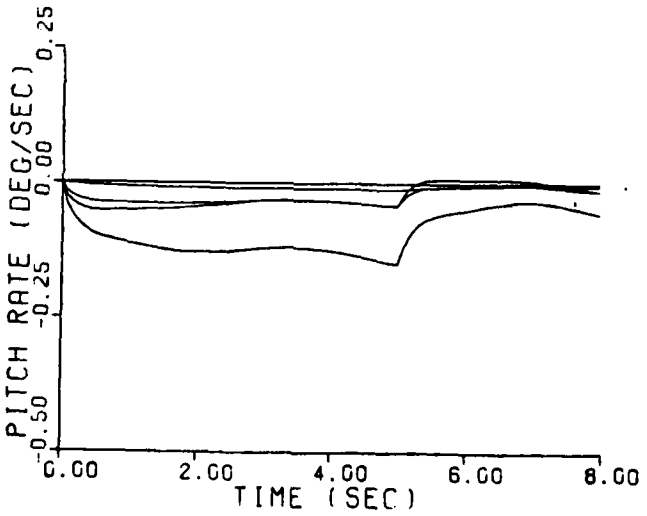

Fig. 5-7(b). Pitch Rate Cross-Coupling Responses, Flight Condition Two

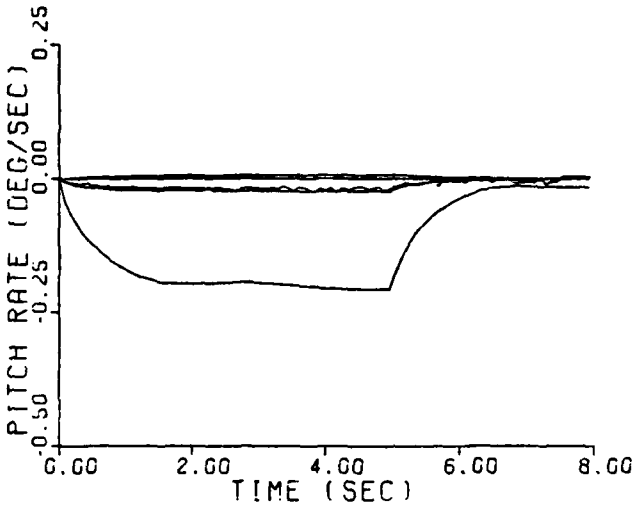

Fig. 5-7(c). Pitch Rate Cross-Coupling Responses, Flight Condition Three

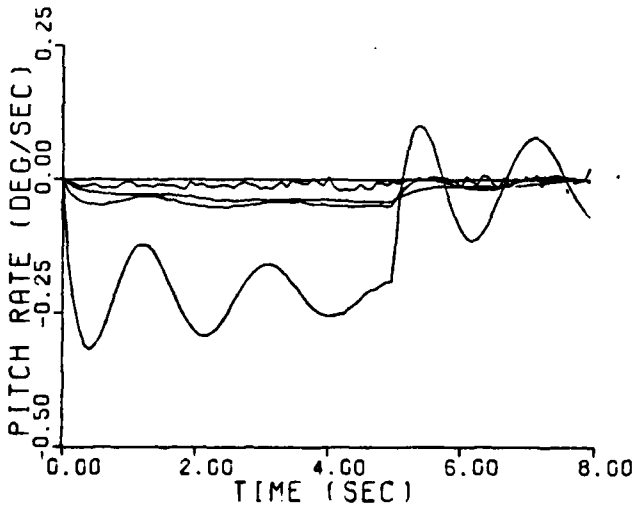

Fig. 5-7(d). Pitch Rate Cross-Coupling Responses, Flight Condition Four

Elevator and flaperon deflections for the p command at flight condition one are seen in Figures 5-8a to 5-8f. As is seen in Figure 5-8a, the surface pairs are moving differentially in the proper sense to generate positive roll rate. The flaperons are also commanded in excess of their 20 degree limit, while the elevators are well below their limit of 25 degrees. This is essentially the case for the remaining figures in this sequence. It is obvious from Figures 5-8 that more of the control effort needs to be shared by the elevators to reduce flaperon movement. This point is addressed later when saturation is discussed. Initial surface rates for all surfaces are near or at saturation for the pulse input; these rates are greatly reduced when the input is ramped, as is seen later. The surface deflection figures for p at flight conditions two, three, and four are displayed in Appendix G.

It is concluded from the pitch rate and roll rate results that the compensators g_1 and g_2 provide robust control for all flight conditions and CSC modes for which the system is designed despite minor qualifications for the pitch rate results. It is also reasonable to conclude that the system provides robust control for all points encompassed by the design flight conditions. Saturation is the next topic of discussion.

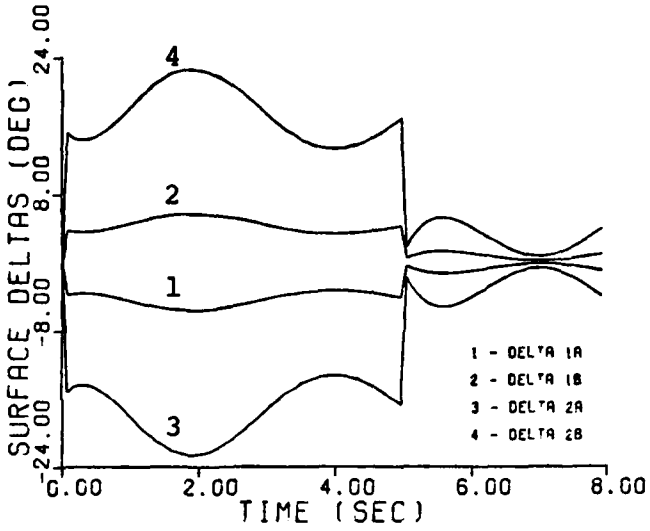

Fig. 5-8(a). Elevator and Flaperon Deflections for Roll Rate, CSC Mode One and Flight Condition One

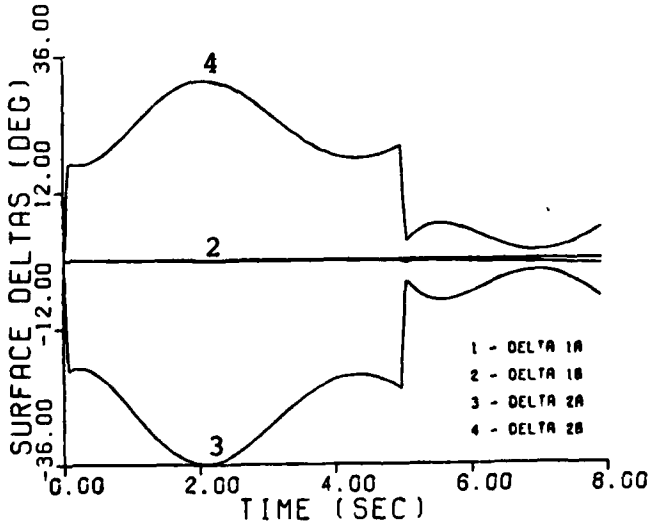

Fig. 5-8(b). Elevator and Flaperon Deflections for Roll Rate, CSC Mode Two and Flight Condition One

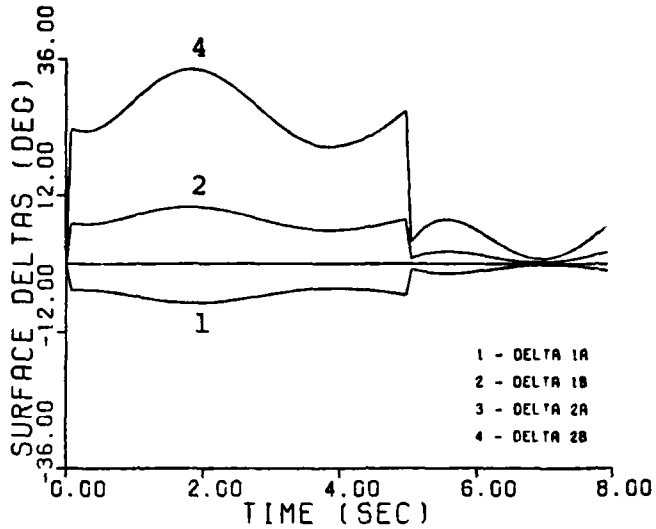

Fig. 5-8(c). Elevator and Flaperon Deflections for Roll Rate, CSC Mode Three and Flight Condition One

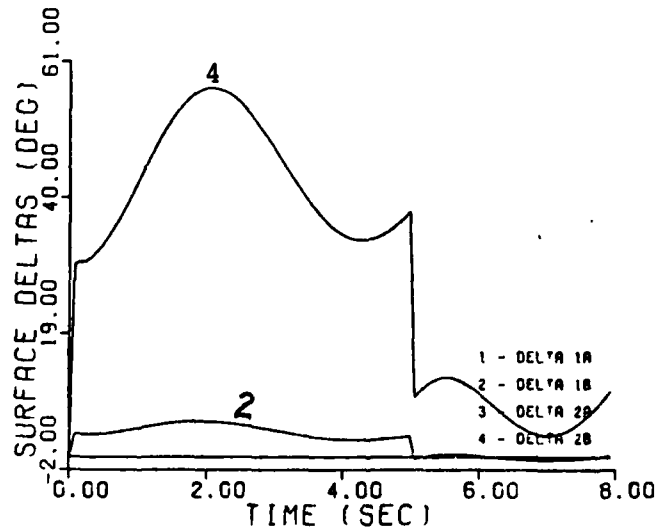

Fig. 5-8(d). Elevator and Flaperon Deflections for Roll Rate, CSC Mode Four and Flight Condition One

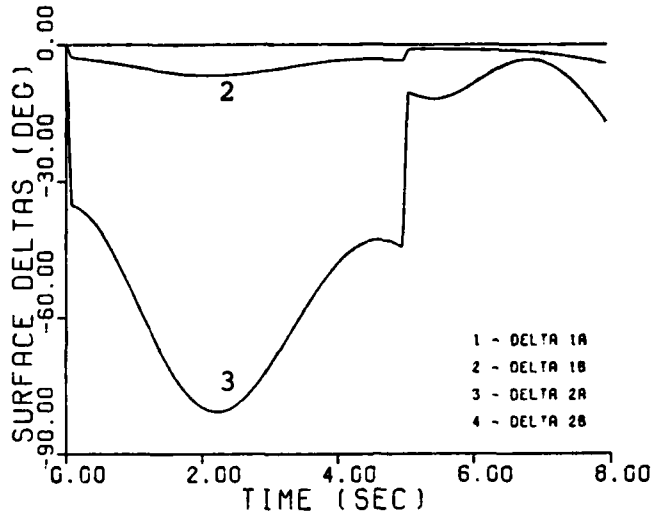

Fig. 5-8(e). Elevator and Flaperon Deflections for Roll Rate, CSC Mode Five and Flight Condition One

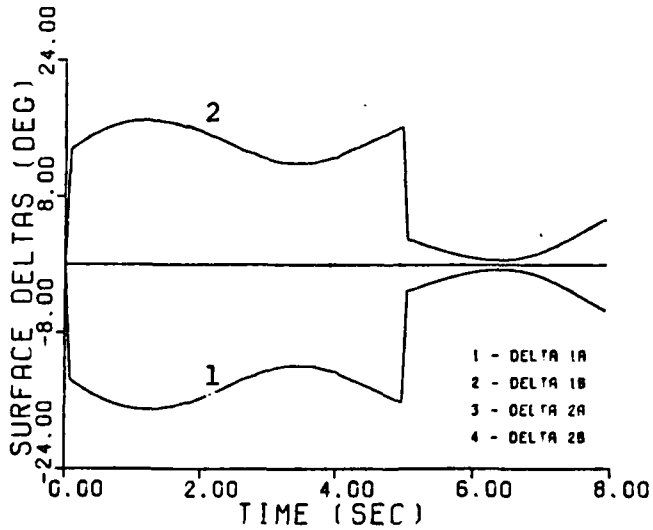

Fig. 5-8(f). Elevator and Flaperon Deflections for Roll Rate, CSC Mode Six and Flight Condition One

V.3 Saturation

Different results are obtained for several of the cases when the provision for position saturation is included in the simulation program. Flight condition one, CSC modes one and two are taken as cases in point. The surface deflections when p is commanded for CSC mode one without saturation are presented in Figure 5-8a, and it is evident that the flaperons show deflections in excess of their limit. The same simulation is run with position saturation included, and the results are seen in Figure 5-9. The flaperons are seen to saturate, and the elevator deflections increase to generate the commanded roll rate. The p responses with and without saturation are seen in Figure 5-10. Note the more oscillatory nature of the response with saturation. The result is much more dramatic for CSC mode two; Figure 5-11 displays the responses for this CSC mode with and without saturation. Cross-coupling is found to increase significantly when surfaces saturate, as is seen in Figure 5-12a. Surface deflections corresponding to Figure 5-12a are seen in Figure 5-12b. It is obvious from these illustrations that position saturation reduces the stability of the system. Saturation can be reduced or eliminated by better distribution of the control effort.

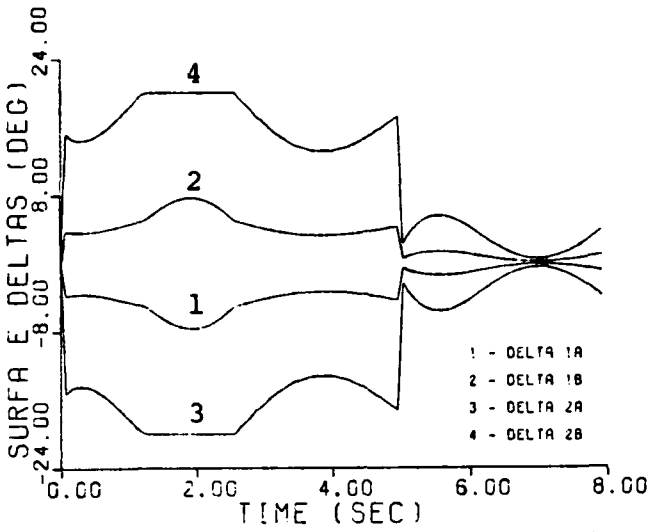

Fig. 5-9. Elevator and Flaperon Deflections With Saturation, CSC Mode One and Flight Condition One

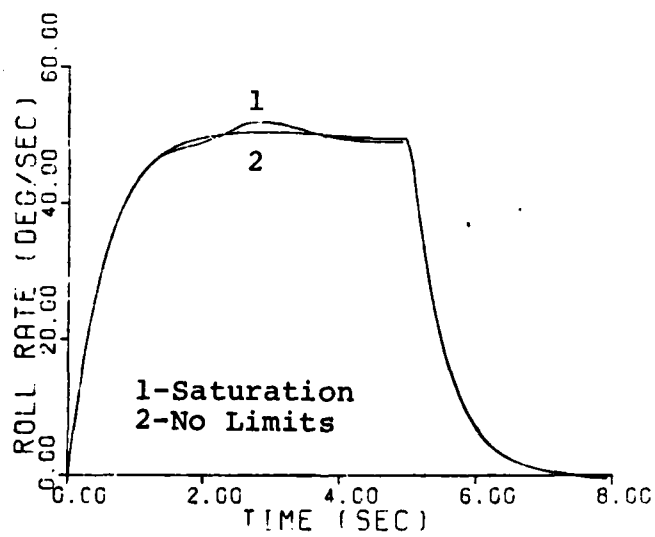

Fig. 5-10. Roll Rate Response With and Without Saturation, CSC Mode One and Flight Condition One

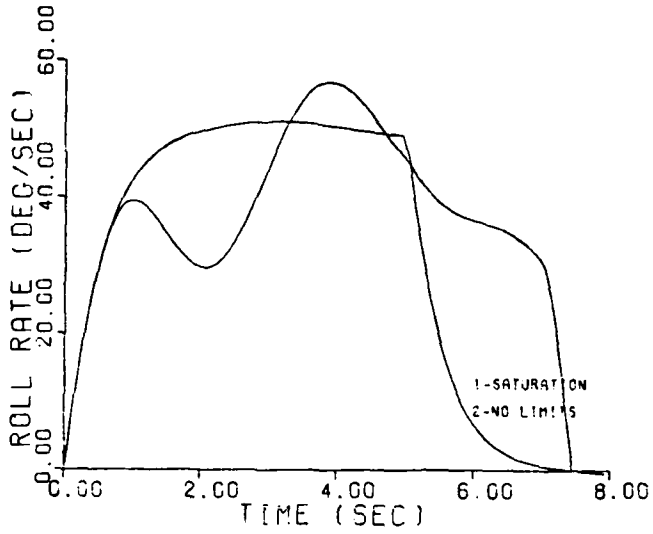

Fig. 5-11. Roll Rate Response With and Without Saturation, CSC Mode Two and Flight Condition One

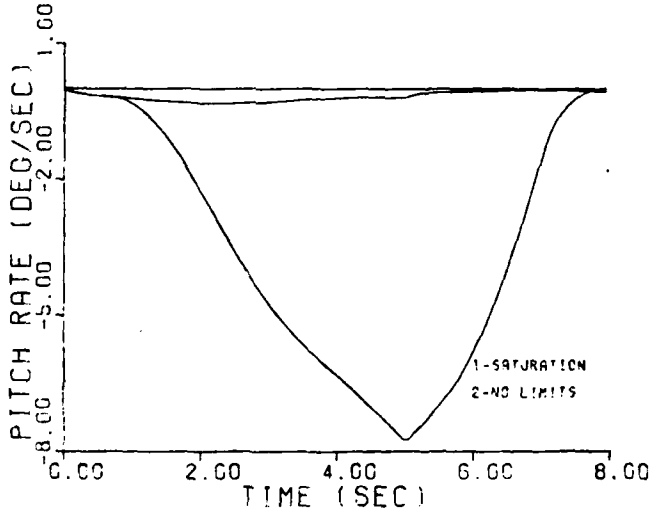

Fig. 5-12(a). Pitch Rate Cross-coupling Response With and Without Saturation, CSC Mode Two and Flight Condition One

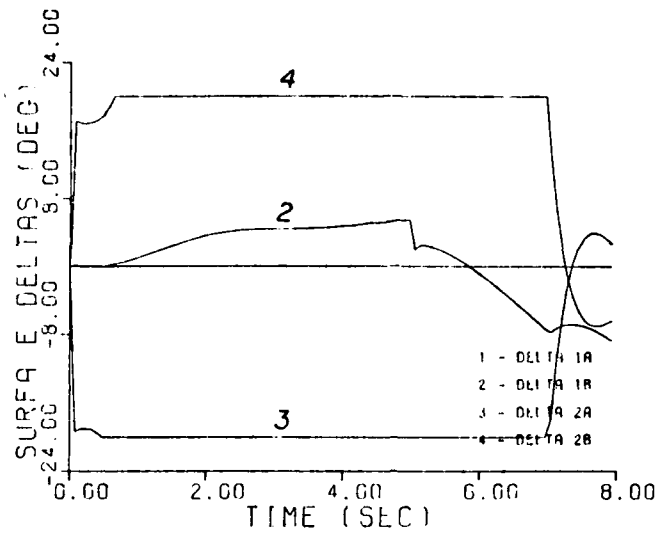

Fig. 5-12(b). Elevator and Flaperon Deflections for CSC Mode Two and Flight Condition One

The division of control effort between the elevators and flaperons may be varied by changing the constants μ_{12} and μ_{21} in Figure 2-1. As discussed in Section III.2, these constants are arbitrarily set at 0.25. Increasing μ_{12} causes the elevators to share more of the effort in generating p. This is seen in Figure 5-13 where μ_{12} is increased to 0.5. By comparing Figure 5-13 with Figure 5-9, it is seen that the flaperons no longer saturate, as more of the command is being generated by the elevators. For a reconfiguration strategy to be effective, some sort of scheme to optimize the division of control surface effort is essential. It is recommended that

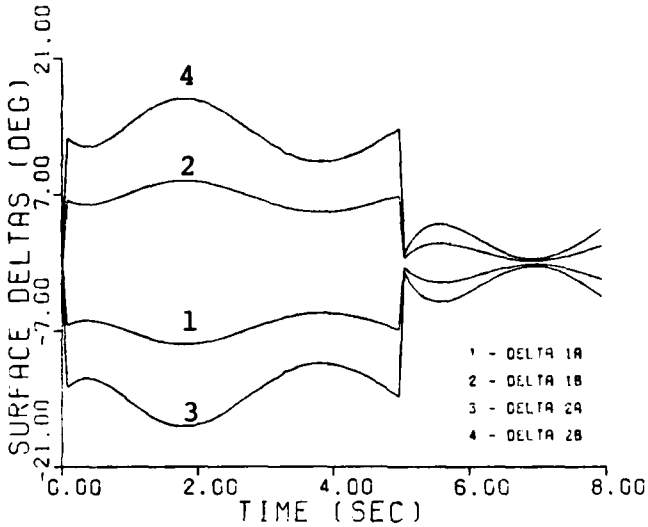

Fig. 5-13. Elevator and Flaperon Deflections for Roll Rate with $\mu_{12} = 0.5$, CSC Mode One and Flight Condition One

follow-on thesis efforts in flight control system reconfiguration investigate strategies to optimize the division of control effort. Appendix B contains theory developed by Dr. Horowitz to optimize the division of control effort. Initial surface rates are noted earlier to be high.

So far, all inputs have been pulse commands. Figures 5-14 and 5-15 illustrate the effect on surface rates when the inputs are ramped. In Figure 5-14 the input is a clipped ramp with a slope of 20 deg/sec^2 (0.5 sec to peak value). The elevator and flaperon initial rates are found to be well below saturation levels. The same is

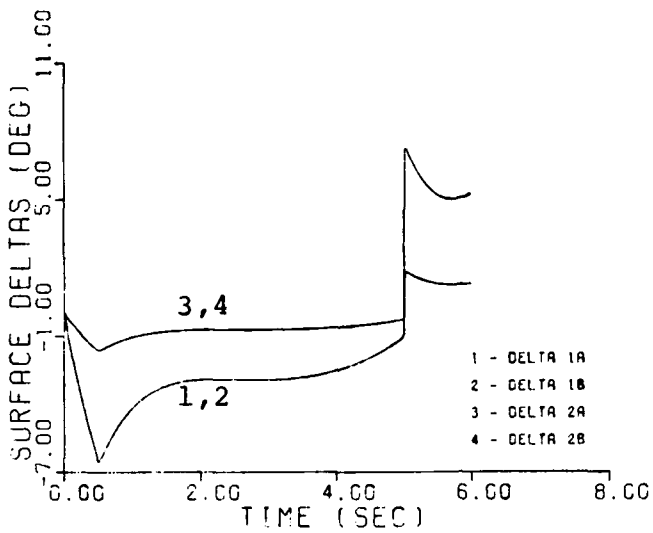

Fig. 5-14. Elevator and Flaperon Deflections for Pitch Rate with a Ramped Input, 0.5 sec to Peak Value (CSC Mode One and Flight Condition One)

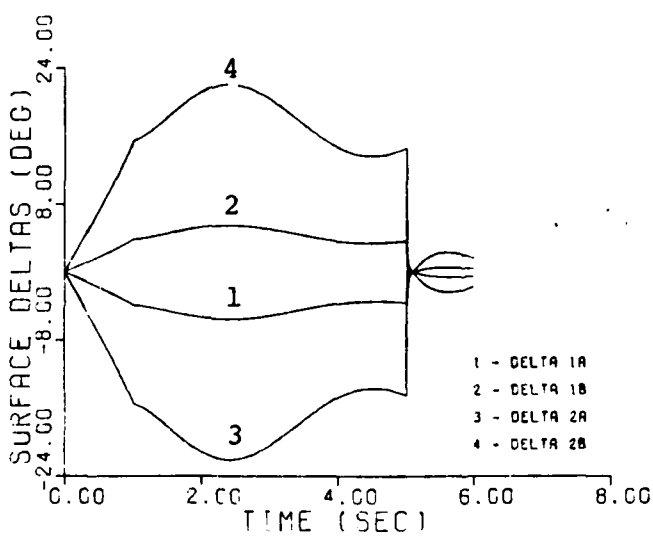

Fig. 5-15. Elevator and Flaperon Deflections for Roll Rate with a Ramped Input, 1 sec to Peak Value (CSC Mode One and Flight Condition One)

TABLE A-2

AIRCRAFT DATA FOR FLIGHT CONDITION TWO
(Mach = 0.6 and 30,000 feet)

$\bar{q}$ (dynamic pressure--lbs/ft^2) = 158.91

V_T (trim velocity--ft/sec) = 596.91

α_T (trim angle-of-attack--deg) = 4.705

Longitudinal Body Axis Primed Dimensional Derivatives		
$Z_\alpha' = -0.526422$	$M_\alpha' = 2.52708$	$X_\alpha' = 23.0402$
$Z_{\delta_e}' = -0.066156$	$M_{\delta_e}' = -5.86214$	$X_{\delta_e}' = 3.17035$
$Z_{\delta_f}' = -0.111711$	$M_{\delta_f}' = -0.211773$	$X_{\delta_f}' = -2.09855$
$Z_q' = 0.997184$	$M_q' = -0.341902$	$X_q' = -48.8785$
$Z_u' = -0.000109$	$M_u' = -0.000337$	$X_u' = -0.005142$
$Z_\theta' = -0.004425$	$M_\theta' = 0.000313$	$X_\theta' = -32.0915$

Lateral-Directional Body Axis Primed Dimensional Derivatives		
$N_\beta' = 2.29583$	$L_\beta' = -19.2246$	$Y_\beta' = -0.154099$
$N_p' = -0.000888$	$L_p' = -0.893601$	$Y_p' = 0.082387$
$N_r' = -0.278676$	$L_r' = 0.318845$	$Y_r' = -0.998322$
$N_{\delta_r}' = -1.96651$	$L_{\delta_r}' = 3.92325$	$Y_{\delta_r}' = 0.021165$
$N_{\delta_a}' = -0.268403$	$L_{\delta_a}' = -17.4468$	$Y_{\delta_a}' = 0.000357$
$N_{\delta_{DT}}' = -1.50547$	$L_{\delta_{DT}}' = -13.5832$	$Y_{\delta_{DT}}' = 0.014398$
$N_{\delta_c}' = 1.51008$	$L_{\delta_c}' = 0.414519$	$Y_{\delta_c}' = 0.007335$

TABLE A-1

AIRCRAFT DATA FOR FLIGHT CONDITION ONE
(Mach = 0.2 and 30 feet)

$\bar{q}$ (dynamic pressure--lbs/ft^2) = 59.18

V_T (trim velocity--ft/sec) = 223.26

α_T (trim angle-of-attack--deg) = 14.98

Longitudinal Body Axis Primed Dimensional Derivatives		
$Z_\alpha' = -0.459802$	$M_\alpha' = 0.542375$	$X_\alpha' = 12.5375$
$Z_{\delta_e}' = -0.074045$	$M_{\delta_e}' = -2.23634$	$X_{\delta_e}' = 0.357830$
$Z_{\delta_f}' = -0.061526$	$M_{\delta_f}' = 0.241866$	$X_{\delta_f}' = -1.97404$
$Z_q' = 0.995737$	$M_q' = -0.633651$	$X_q' = -58.0974$
$Z_u' = -0.000786$	$M_u' = -0.000651$	$X_u' = 0.002886$
$Z_\theta' = -0.037268$	$M_\theta' = -0.000058$	$X_\theta' = -31.1064$

Lateral-Directional Body Axis Primed Dimensional Derivatives		
$N_\beta' = 0.919806$	$L_\beta' = -11.0532$	$Y_\beta' = -0.143895$
$N_p' \quad -0.003864$	$L_p' = -0.934188$	$Y_p' = 0.261703$
$N_r' = -0.257624$	$L_r' = 1.03044$	$Y_r' = -0.994485$
$N_{\delta_r}' = -0.814818$	$L_{\delta_r}' = 1.42280$	$Y_{\delta_r}' = 0.021662$
$N_{\delta_a}' = 0.075009$	$L_{\delta_a}' = -4.47725$	$Y_{\delta_a}' = 0.010422$
$N_{\delta_{DT}}' = -0.603086$	$L_{\delta_{DT}}' = -4.28449$	$Y_{\delta_{DT}}' = 0.022018$
$N_{\delta_c}' = 0.328110$	$L_{\delta_c}' = -0.296006$	$Y_{\delta_c}' = 0.006234$

Appendix A: Flight Parameters and Aerodynamic Derivatives

Flight parameters and aerodynamic derivatives are presented in this appendix for the four design flight conditions. These data are taken directly from Reference 6, and repeated here for the convenience of the reader. An extensive aerodynamic package was developed by the General Dynamics Corporation for the AFTI/F-16. Derivatives are formulated in the body axis system, and have the units of radians, radians/sec, or ft/sec; i.e., X_θ' (radians), X_q' (radians/sec), X_u' (ft/sec), etc.

VI.3 Recommendations

The following recommendations follow directly from the preceding conclusions:

1. Research using quantitative feedback theory for the design of multivariable flight control laws should continue, particularly, for reconfigurable flight control systems. Future investigations should be for systems of third or higher-order. Optimizing the division of control effort and digital control are fundamental prerequisites for a practical reconfigurable flight control system, and should be included in future research efforts. Also, a more accurate aircraft model should be developed to include coupling in the plant matrix.

2. A computer-aided design package should be developed for quantitative feedback theory. This package should include, but not be limited to the following capabilities: Bode plot, Nichol's Chart, plant template formulation, loop transmission boundary derivation, loop transmission shaping, curve fitting, and system simulation. In addition to allowing more difficult design problems to be solved, these capabilities would greatly speed up the design process and result in more precise control laws.

systems may be significant. A fixed-compensator design has the potential to significantly minimize the complexity of fault identification schemes that may be required for a reconfigurable flight control system. The next section presents some of the conclusions that may be drawn from this thesis.

VI.2 Conclusions

1. Procedures developed from quantitative feedback theory are effective in the design of multivariable control laws for normal or impaired flight control systems. The technique reveals important insights to the designer about compensation requirements. This fixed-compensator design approach may significantly reduce the anticipated complexity of reconfigurable flight control systems.

2. The application of quantitative feedback theory in the design of multivariable control laws is a reasonably straightforward process. The technique is relatively simple once the basic theory is understood, and the designer has some practice in its use.

3. The controllers developed in this thesis provide robust control for all flight control surface configurations and flight conditions for which the design is synthesized.

4. An interactive computer-aided design package should be developed for quantitative feedback theory so that design problems of larger scope can be attempted.

VI. Conclusions and Recommendations

VI.1 Discussion

The primary purpose of this thesis is to demonstrate the effectiveness of quantitative feedback theory as applied to flight control system reconfiguration. Compensators are synthesized to be robust for an unimpaired flight control system as well as for several different cases in which the flight control system is severely impaired. The compensators are also to be robust for a large portion of the aircraft flight envelope. Quantitative feedback theory is applied to the linearized, small perturbation equations of motion for a longitudinally unstable aircraft (AFTI/F-16). The application of quantitative feedback theory is found to be relatively straightforward for this difficult multiple input-multiple output problem. The transparency of the technique provides important insights into the compensator requirements from the initial stages of the design process. The results of this thesis demonstrate that quantitative feedback theory is well suited for flight control system reconfiguration design. The fixed-compensator designs are seen to provide satisfactory control at all design points. The importance of fixed-compensator designs in reconfigurable flight control

compensator. Control surface "hardover" is also investigated, and simulation results for this condition further illustrate the utility of quantitative feedback theory. Recommendations and conclusions are presented in the following chapter.

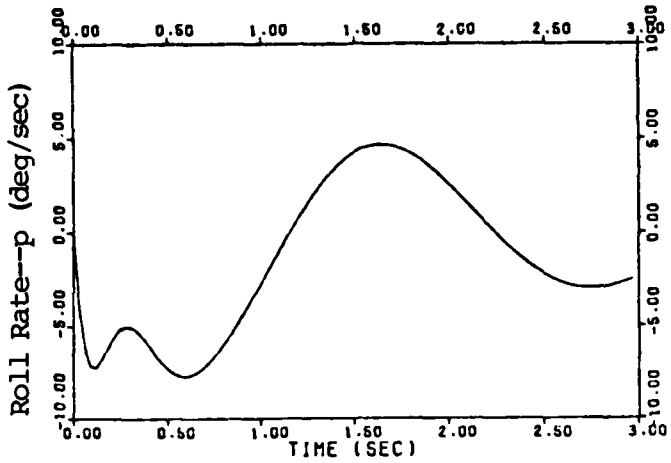

Fig. 5-19(b). Roll Rate Response from Flaperon Hardover, Flight Condition Two

V.6 Summary

This chapter presents a description of the simulation program and the results for the pitch rate and roll rate commands. From an examination of the command and cross-coupling responses it is determined that the compensators g_1 and g_2 provide reasonably robust control over the design flight conditions and control surface configuration modes. Saturation is examined, and the necessity to optimize the division of control effort is evident. Quantitative feedback theory is seen to provide the designer with valuable insights prior to the actual synthesis of the

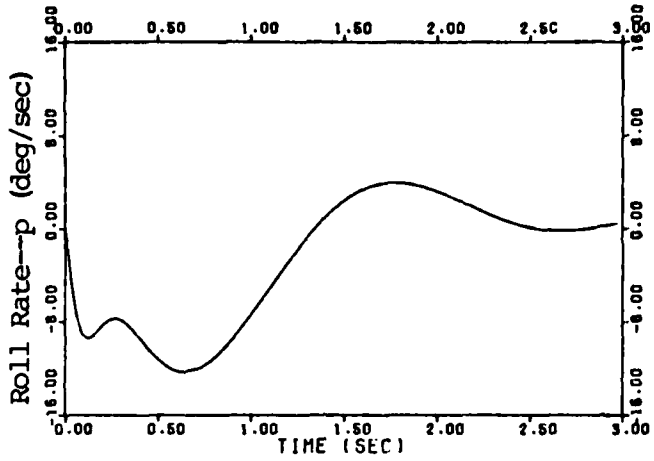

Fig. 5-18(b). Roll Rate Response from Elevator Hardover, Flight Condition Two

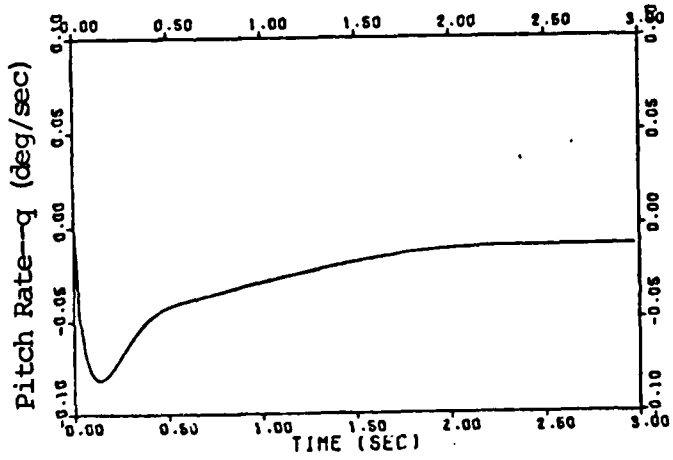

Fig. 5-19(a). Pitch Rate Response from Flaperon Hardover, Flight Condition Two

example, let δ_1^a fail to the hardover position, the result-output vector ($P_{11}^a\delta_{1\,max}^a$, $P_{21}^a\delta_{1\,max}^a$) is treated as a disturbance to be attenuated. The equivalent plant transfer function matrix $\underline{P}_e$ for this condition then becomes identical to $\underline{P}_e$ for $\delta_1^a = 0$ (CSC mode 2) since δ_1^a is no longer controllable. Mr. Yin-Kuei Liao has simulated separate elevator and flaperon hardovers using the compensators derived in Chapter IV. Simulation results are seen in Figures 5-18 to 5-19. The system is seen to effectively attenuate the hardover surface's outputs. The results of this section further demonstrate the utility of QFT for the challenge of FCS reconfiguration. See Appendix B for Dr. Horowitz's explanation of the hardover surface problem.

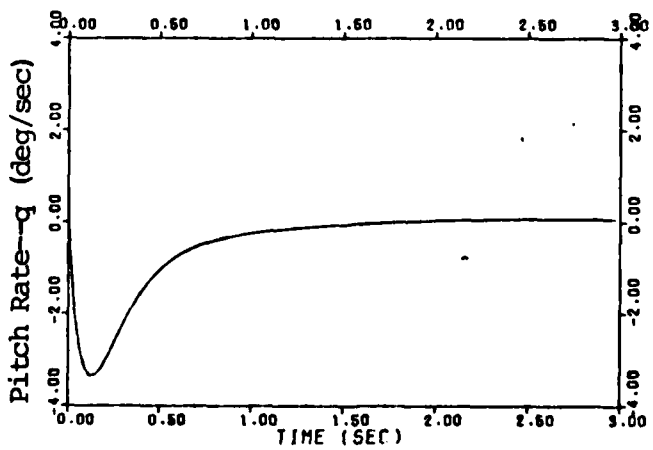

Fig. 5-18(a). Pitch Rate Response from Elevator Hardover, Flight Condition Two

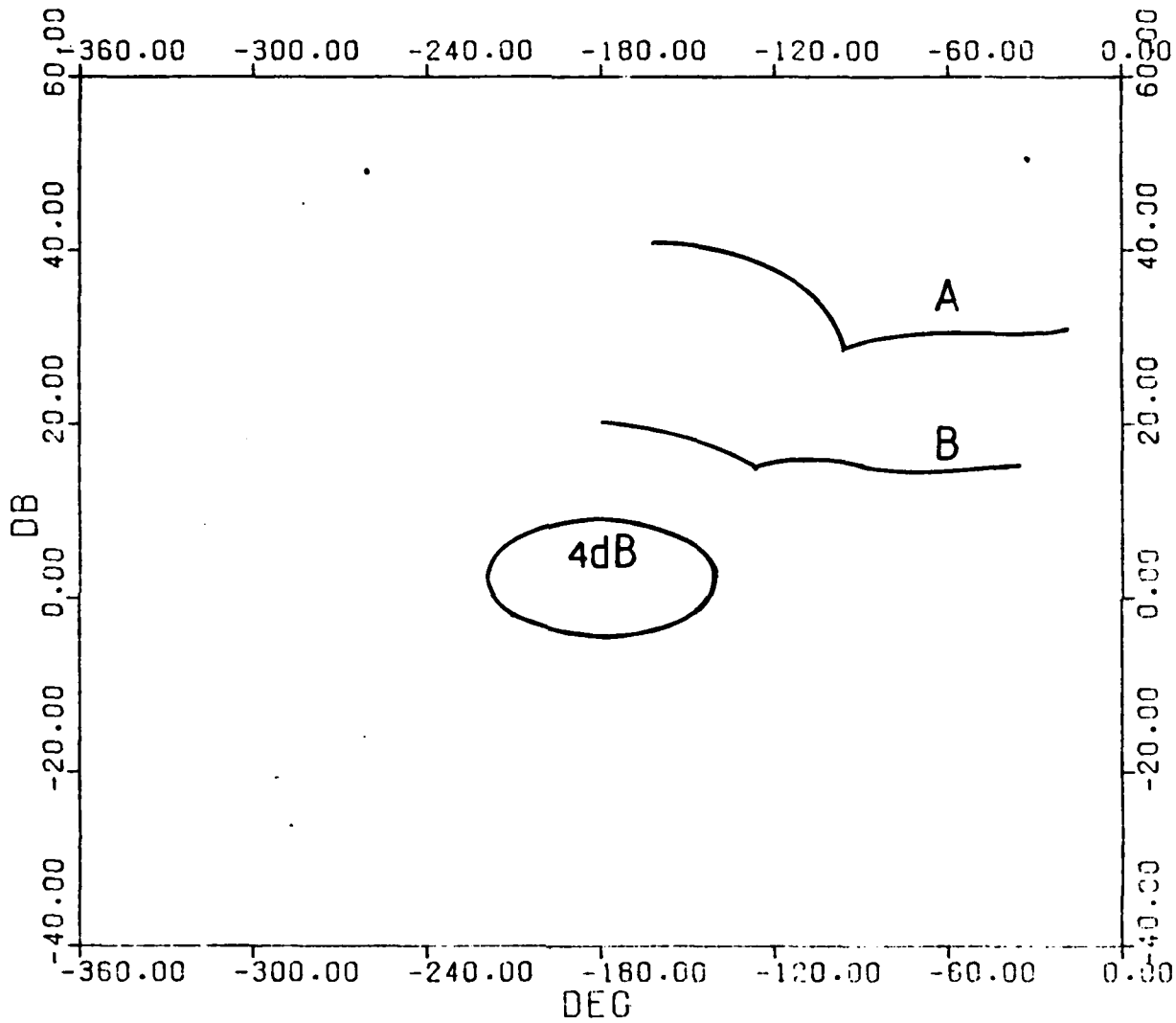

Fig. 5-17. Bounds on L Resulting from τ_{11} Demands
(Bound A = $\delta_1{}^a = \delta_1{}^b = 0$, Bound B = $\delta_1{}^a = \delta_1{}^b \neq 0$)

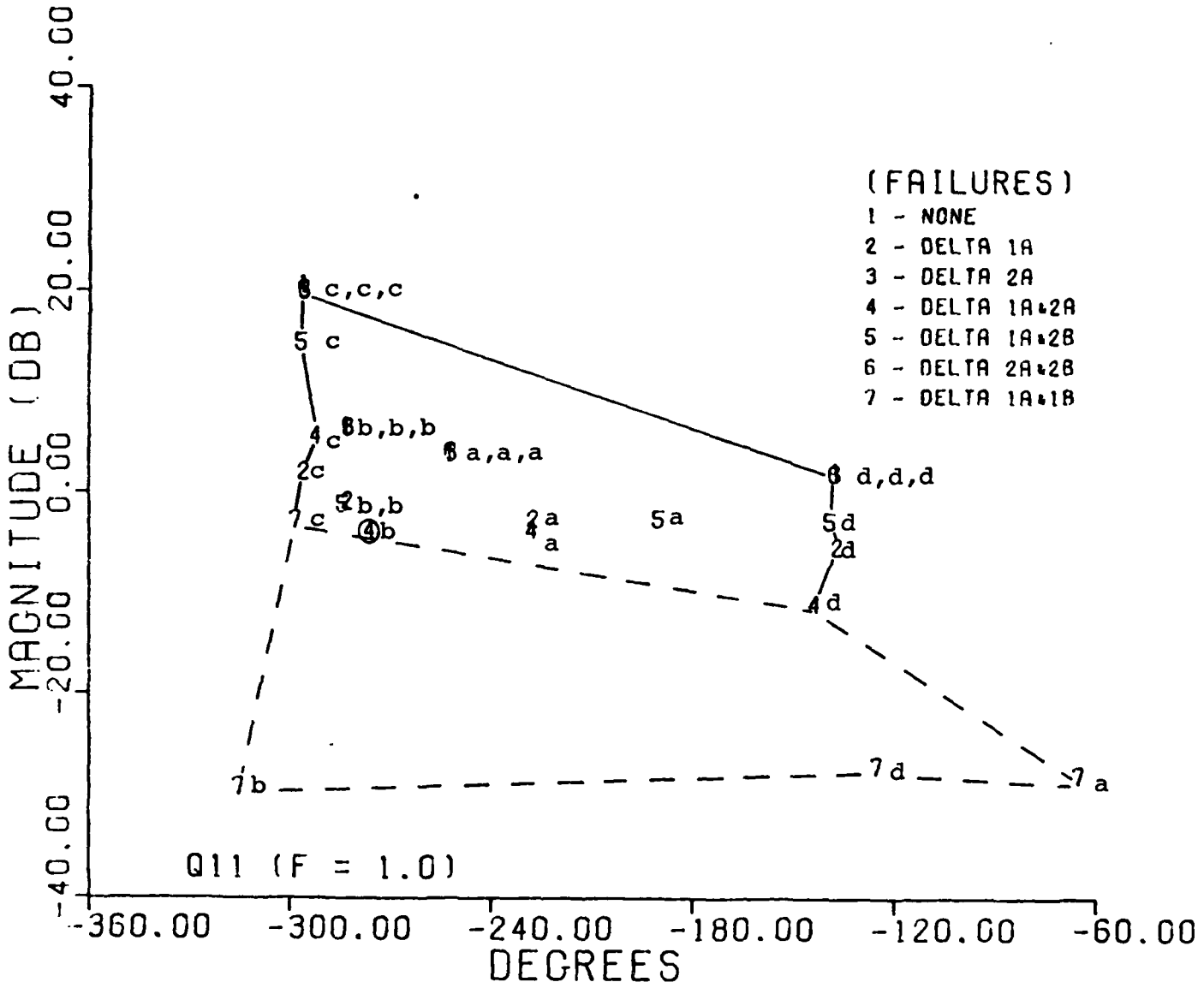

Fig. 5-16. Template of Q_{11} at $\omega = 1.0$ r/s, Includes $\delta_1^a = \delta_1^b = 0$

Figure 5-16. The additional area of plant uncertainty is enclosed by the dashed line. Flight conditions one through four are identified, respectively, by the letters a, b, c, and d. The difference between the bound on L at ω = 1.0 r/s with and without the plant uncertainty due to both elevators failed is seen in Figure 5-17. The bounds in Figure 5-17 represent the demands on L due to the command response τ_{11}. Bound A is developed from the Q_{11} template with the additional uncertainty of both elevators failed, while bound B is developed from the same template without the extra uncertainty. Clearly, it is seen from Figure 5-17 that the larger the amount of plant uncertainty the higher is the bound on L, and higher bounds mean a larger loop transmission bandwidth. The L bandwidth is increased by more than one and one-half octaves from bound B to bound A.

This example further illustrates the utility of QFT as a design technique for FCS reconfiguration. This method provides the designer with valuable insights very early in the design process as to the "cost" of feedback.

V.5 Control Surface "Hardover"

A condition known as "hardover" occurs when a surface without command suddenly deflects to its maximum position and remains there. The output from this control surface may be treated as an external disturbance vector which is to be attenuated by the feedback system. As an

true when the p input is ramped with a slope of 50 deg/sec^2 (1 sec to peak value); initial rates are also well below saturation levels as seen in Figure 5-15. Figures 5-14 and 5-15 may be compared with Figures 5-4a and 5-8a where the inputs are pulsed to see the marked reduction in the surface rates.

V.4 QFT Insights

Quantitative feedback theory provides the designer with insight at the initial design stages into the nature of the loop transmission. By examining the extent of plant uncertainty, and the narrowness of the performance specifications, the designer gains valuable insight about the bounds on L and, hence, on L itself. For instance, the larger the area of plant uncertainty and/or the tighter the performance specifications, the higher are the bounds on L. Thus, the designer has a feel early in the design for the compensation required. If he feels that the demands on L are too high he may choose to reduce the amount of plant uncertainty in the design or relax the performance tolerances. For this thesis, it was initially planned that the compensator designs would be robust when both elevators are failed. This was decided against after examining the template of Q_{11} and seeing the extra "cost" in terms of loop transmission bandwidth for including this configuration. The additional plant uncertainty in the pitch channel when both elevators are failed is seen in

TABLE A-3

AIRCRAFT DATA FOR FLIGHT CONDITION THREE
(Mach = 0.9 and 20,000 feet)

$\bar{q}$ (dynamic pressure--lbs/ft^2) = 552.113

V_T (trim velocity--ft/sec) = 933.23

α_T (trim angle-of-attack--deg) = 1.96

Longidutinal Body Axis Primed Dimensional Derivatives		
$Z_\alpha{}'$ = -1.48446	$M_\alpha{}'$ = 4.27171	$X_\alpha{}'$ = 38.2906
$Z_{\delta_e}{}'$ = -0.149227	$M_{\delta_e}{}'$ = -24.0581	$X_{\delta_e}{}'$ = 2.00593
$Z_{\delta_f}{}'$ = -0.244924	$M_{\delta_f}{}'$ = -6.47269	$X_{\delta_f}{}'$ = 2.31681
$Z_q{}'$ = 0.994789	$M_q{}'$ = -0.777221	$X_q{}'$ = -30.1376
$Z_u{}'$ = -0.000022	$M_u{}'$ = -0.000130	$X_u{}'$ = -0.012075
$Z_\theta{}'$ = -0.001120	$M_\theta{}'$ = 0.000309	$X_\theta{}'$ = -32.1830

Lateral-Directional Body Axis Primed Dimensional Derivatives		
$N_\beta{}'$ = 7.2370	$L_\beta{}'$ = -55.2526	$Y_\beta{}'$ = -0.343554
$N_p{}'$ = -0.023184	$L_p{}'$ = -2.80004	$Y_p{}'$ = 0.032636
$N_r{}'$ = -0.362530	$L_r{}'$ = 0.145674	$Y_r{}'$ = -0.997556
$N_{\delta_r}{}'$ = -5.80890	$L_{\delta_r}{}'$ = 10.3955	$Y_{\delta_r}{}'$ = 0.037032
$N_{\delta_a}{}'$ = -1.25006	$L_{\delta_a}{}'$ = -51.0502	$Y_{\delta_a}{}'$ = -0.001371
$N_{\delta_{DT}}{}'$ = -5.13710	$L_{\delta_{DT}}{}'$ = -50.7290	$Y_{\delta_{DT}}{}'$ = 0.026609
$N_{\delta_c}{}'$ = 5.89254	$L_{\delta_c}{}'$ = 5.53185	$Y_{\delta_c}{}'$ = 0.026734

TABLE A-4

AIRCRAFT DATA FOR FLIGHT CONDITION FOUR
(Mach = 1.6 and 30,000 feet)

$\bar{q}$ (dynamic pressure--lbs/ft^2) = 1129.31

V_T (trim velocity--ft/sec) = 1591.75

α_T (trim angle-of-attack--deg) = 1.68

Longitudinal Body Axis Primed Dimensional Derivatives		
$Z_\alpha' = -1.25100$	$M_\alpha' = -43.8012$	$X_\alpha' = 45.1941$
$Z_{\delta_e}' = -0.115337$	$M_{\delta_e}' = -32.8919$	$X_{\delta_e}' = 9.40431$
$Z_{\delta_f}' = -0.075084$	$M_{\delta_f}' = -5.85004$	$X_{\delta_f}' = -13.3021$
$Z_q' = 0.995991$	$M_q' = -0.351737$	$X_q' = -46.5132$
$Z_u' = -0.000002$	$M_u' = 0.000802$	$X_u' = -0.030046$
$Z_\theta' = -0.000593$	$M_\theta' = -0.000075$	$X_\theta' = -32.1861$

Lateral-Directional Body Axis Primed Dimensional Derivatives		
$N_\beta' = 7.42422$	$L_\beta' = -100.032$	$Y_\beta = -0.358564$
$N_p' = -0.005040$	$L_p' = -2.46287$	$Y_p' = 0.029374$
$N_r' = -0.383316$	$L_r' = 0.160287$	$Y_r' = -0.998410$
$N_{\delta_r}' = -3.27086$	$L_{\delta_r}' = 4.96942$	$Y_{\delta_r}' = 0.010313$
$N_{\delta_a}' = -2.37673$	$L_{\delta_a}' = -14.1689$	$Y_{\delta_a}' = 0.006763$
$N_{\delta_{DT}}' = -3.45190$	$L_{\delta_{DT}}' = -46.6078$	$Y_{\delta_{DT}}' = 0.005250$
$N_{\delta_c}' = 9.36290$	$L_{\delta_c}' = 12.0662$	$Y_{\delta_c}' = 0.028790$

Appendix B: Reconfiguration Theory

This appendix contains quantitative inherent reconfiguration theory developed by Dr. Isaac Horowitz. Reconfiguration synthesis theory is developed for 2 input-2 output, 5 input-3 output, and 10 input-6 output systems utilizing control of individual flight control surfaces. Theory to optimize the division of control surface effort under no failure and failure conditions is also presented.

A QUANTITATIVE INHERENT RECONFIGURATION THEORY FOR A CLASS OF SYSTEMS

Isaac Horowitz*

Summary

In aircraft flight control, most control surfaces are in pairs (elevators, ailerons, canards etc), with each pair normally controlled as a single unit. If a surface fails, the usual approach is to attempt explicit identification and switch-in of compensation prepared for that contingency. In this paper each surface is separately controlled, permitting "inherent reconfiguration", wherein the design is apriori made such that despite one or several simultaneous surface failures, the system still satisfies the original performance tolerance (of course over a smaller dynamic range), with the same original fixed compensation.

Inherent reconfiguration is a natural extension of "Quantitative Feedback Theory". (QFT), wherein the system design is tuned to the plant uncertainty set $\mathcal{P} = \{P\}$, and to the acceptable system output set A. In QFT one apriori designs so that the system output is in A for all P in $\mathcal{P}$. Surface failures simply enlarge the set $\mathcal{P}$. The transparency of QFT enables the designer to readily see the extra "cost of feedback" for this enlargement of $\mathcal{P}$ by inclusion of surface failures.

*Cohen Professor of Applied Mathemtics, Weizmann Institute of Science, Israel and Department of Electrical and Computer Engineering, University of Colorado, Boulder.

This research was supported under Contract F33615-82-C-3000 by Universal Energy Systems Inc., Dayton, Ohio and National Science Foundation Grant ECS-8303333 at the University of Colorado.

A QUANTITATIVE INHERENT RECONFIGURATION THEORY FOR A CLASS OF SYSTEMS

Isaac Horowitz

1. INTRODUCTION

Consider a system with uncertain constrained multiple input - multiple output (MIMO) part denoted as the plant P with m control inputs and n outputs to be controlled. If m>n then m-n degrees of freedom are available for optimization purposes. In an "output-controllable" plant (Horowitz and Shaked 1975), the n desired outputs uniquely determine the remaining n free inputs. If n>m, only m outputs are independently achievable. Hence, an effective n×n plant is normally assumed in uncertain MIMO systems, if the problem is to achieve desired input-output relations despite uncertainty (Horowitz 1979, 1982).

There is an important plant class wherein one or more of the n plant inputs is actually a <u>pair</u> e.g. elevator, canard and aileron pairs in an aircraft. The elevator pair is usually counted as one control input, because its two parts are tied or driven together to achieve longitudinal mode control, and therefore do not affect the lateral variables such as roll and yaw. Similarly the two ailerons are usually tied or driven differentially for lateral control, and therefore this pair does not affect longitudinal variables such as pitch and normal acceleration. However, the individual elements of each of these pairs do affect both the longitudinal and lateral variables and this fact is indeed used for "reconfiguration" purposes in case of significant control surface damage. Such reconfiguration

requires explicit identification of the failure and the switch-in of standby compensation elements designed for this specific purpose. The challenge (Rubertus 1983, Chandler 1984, Chandler and Potts 1983) treated in this paper is to devise a design theory in which no explicit identification is required. Rather, even under severe control surface failures, the tolerances are to be satisfied automatically, with no need for switching in of new compensations. The same compensation functions are to be adequate under normal (no failure) and under the maximum possible control surface failures. This is denoted here as "inherent reconfiguration". The question of how optimum such a single design is for the variety of failure conditions, is discussed in Section 5. Three configurations of increasing complexity are treated in Sections 2-4.

1.1 Synthesis objectives

A linear time-invariant plant model is assumed. (See Section 5 for discussion of nonlinear plants). There are specified tolerances on the closed-loop system responses to commands r_i in Figure 1, as follows. Let $y = Tr$, $T = [t_{ij}]$, and each t_{ij} has its set of acceptable functions $\mathcal{T}_{ij}$ either in the time or frequency domain. It is particularly convenient to assume "basically noninteracting" (BNIA) tolerances of the form $|t_{ij}(j\omega)| \leq b_{ij}(\omega)$ for $i \neq j$ (see Section 5 for discussion). There is also a set of possible external disturbance vectors $\mathcal{D} = \{d\}$ acting on the plant whose effect on the system output is given by $y_d = T_d d$, $T_d = [t_{d_{ij}}]$, with tolerances of the form $|t_{d_{ij}}| \leq b_{d_{ij}}(\omega)$, giving sets of acceptable disturbance response functions $\mathcal{T}_d$. These tolerances on the elements of T and T_d

are to be achieved over the entire set of plant variation (different flight conditions in flight control) and over the maximum possible simultaneous control input failures, by means of a fixed set of compensation functions.

2. A TWO-PAIR STRUCTURE

2.1 Introduction

The simplest plant for illustrating the theory is shown (in darker lines), together with its compensations, in Figure 1. For example, the (δ_1^a, δ_1^b) pair could be the right and left elevators (δ_2^a, δ_2^b) the right and left ailerons, y_1 the pitch angle, y_2 the roll angle. The effect of each individual j surface on each i output is given explicitly by p_{ij}^a, p_{ij}^b with $p_{ij}^a = p_{ij}^b$ under normal (no failure) conditions. If δ_2^a, δ_2^a (or δ_1^a, δ_1^b) have equal values, i.e. the right and left ailerons (or elevators) are deflected equally in the same direction, then $y_2(\text{roll}) = \Sigma(\delta_i^a p_{2i}^a - \delta_i^b p_{2i}^b) = 0$. That is why minus signs are associated with p_{12}^b, p_{22}^b in Figure 1, and plus signs for all p_{1i}^a, p_{1i}^b.

If the command inputs (r_1, r_2) and the plant outputs (y_1, y_2), but no internal plant variables can be measured (Horowitz 1982a), then the most general feedback structure has 16 free functions: $8f_{ij}$ from the two r_j to the four δ_i and $8m_{ij}$ to the four δ_i from the two y_j in Figure 1. But it is assumed here that in the normal (no failure) case, zero interaction between the lateral and longitudinal outputs is desired i.e. $t_{ij} = 0$ for $i \neq j$, also that $p_{ij}^a = p_{ij}^b$. This

accounts for the various symmetries in the f_{ij}, m_{ij} of Figure 1. Thus, if $r_1 = 0$, $r_2 \neq 0$ the desired $y_1 = 0$, $y_2 \neq 0$ are achievable by $\delta_1^a = -\delta_1^b$, $\delta_2^a = -\delta_2^b$, so opposite signals via $(m_{12},-m_{12})$, $(m_{22},-m_{22})$ $(f_{12},-f_{12})$, $(f_{22},-f_{22})$ are needed. However, the same (m_{11},m_{11}) (m_{21},m_{21}) and f_{j1} give $\delta_i^a = \delta_i^b$ if $y_1 \neq 0$, $y_2 = 0$ are wanted in response to $r_1 \neq 0$, $r_2 = 0$. Hence, only 8 free compensating functions are left. Note that Figure 1 is only one of an infinitude of possible canonic structures (Horowitz 1963) exploiting the available freedom. Simple equivalence relations permit any one to be replaced by another structure with no need for redesign.

2.2 Development of Synthesis Theory

In Figure 1, $y = Tr = P \quad = P(Fr-My)$, so

$$T = [t_{ij}] = (I+PM)^{-1}PF \qquad \text{with} \tag{1}$$

$$P = \begin{bmatrix} p_{11}^a & p_{11}^b & p_{12}^a & p_{12}^b \\ p_{21}^a & -p_{21}^b & p_{22}^a & -p_{22}^b \end{bmatrix}, \quad \delta = [\delta_1^a, \delta_1^b, \delta_2^a, \delta_2^b]'$$

$$r=[r_1,r_2]', \; M = \begin{bmatrix} m_{11} & m_{12} \\ m_{11} & -m_{12} \\ m_{21} & m_{22} \\ m_{21} & -m_{22} \end{bmatrix}, \quad F = \begin{bmatrix} f_{11} & f_{12} \\ f_{11} & -f_{12} \\ f_{21} & f_{22} \\ f_{21} & -f_{22} \end{bmatrix} \tag{2a-e}$$

This gives, with all elements $f_{ij}, m_{ij}, p_{ij}(s)$ transfer functions,

$$PM = \begin{bmatrix} (p_{11}+p_{12}\frac{m_{21}}{m_{11}})m_{11} & (\Delta p_{12}+\frac{m_{12}}{m_{22}}\Delta p_{11})m_{22} \\ (\Delta p_{21}+\frac{m_{21}}{m_{11}}\Delta p_{22})m_{11} & (p_{22}+p_{21}\frac{m_{12}}{m_{22}})m_{22} \end{bmatrix} \tag{3a}$$

$$PF = \begin{bmatrix} (p_{11}+p_{12}\frac{f_{21}}{f_{11}})f_{11} & (\Delta p_{12}+\frac{f_{12}}{f_{22}}\Delta p_{11})f_{22} \\ (\Delta p_{21}+\frac{f_{21}}{f_{11}}\Delta p_{22})f_{11} & (p_{22}+\frac{f_{12}}{f_{22}}p_{21})f_{22} \end{bmatrix} \tag{3b}$$

$$p_{ij} = p^a_{ij}+p^b_{ij}\ , \quad \Delta p_{ij} = p^a_{ij}-p^b_{ij} \tag{3c}$$

Quantitative synthesis theories for satisfying each of the n^2 t_{ij} tolerances of (1) despite the uncertainty, have been developed (Horowitz 1979, 1982b) and applied (Horowitz and Loecher 1981, Horowitz et al 1981, 1982, Betzold et al 1984) to significant examples. These techniques have the merit of reducing the n×n MIMO problem into a number of single input - single output (SISO) single-loop problems, whose solutions are guaranteed to solve the original MIMO problem. It would be very desirable to apply this theory to the present problem class (see also Section 2.2.2). For this purpose it is necessary to identify a n×n equivalent plant P_e and compensator M_e, F_e matrices (n=2 in this section), such that

$$T = (I+PM)^{-1}PF \text{ of Eq(1)} = (I+P_eM_e)^{-1}P_eF_e \tag{4}$$

Also for the BNIA tolerances of Section 1.1, M_e and F_e should be diagonal. Examination of (3a-c) reveals this is achieved by setting

$$\frac{m_{21}}{m_{11}} = \frac{f_{21}}{f_{11}} \triangleq \mu_{21}(s), \quad \frac{m_{12}}{m_{22}} = \frac{f_{12}}{f_{22}} \triangleq \mu_{12}(s), \text{ giving} \tag{5a,b}$$

$$P_e = [p_{ije}] = \begin{bmatrix} p_{11}+\mu_{21}p_{12} & \Delta p_{12}+\mu_{12}\Delta p_{11} \\ \Delta p_{21}+\mu_{21}\Delta p_{22} & p_{22}+\mu_{12}p_{21} \end{bmatrix} \tag{6a}$$

$$M_e = \mathrm{diag}[m_{ii}], \quad F_e = \mathrm{diag}[f_{ii}] \tag{6b,c}$$

The available quantitative design theory is directly applicable to the new equivalent P_e, M_e, F_e system, including surface failures, as is next seen. Note in (6a) that $p_{ije}(i \neq j) = 0$ in the no failure case. See Section 2.2.2 for additional strong justification of relations (5a,b).

2.2.1 Failure cases

Various kinds of failure are possible. Total failure of δ_1^a is defined as $p_{i1}^a = 0$ for all i, which may involve new values of the other p_{ij}, if the aerodynamic coefficients involved in these p_{ij} are affected by the failure. The design theory easily accommodates this with the new value $p_{ije}(i \neq j)$ no longer zero, but $p_{12e} = -\mu_{12}p_{11}^b$, $p_{21e} = -p_{21}^b$ and $p_{11e} = p_{11}^b+\mu_{21}p_{12}$, $p_{22e} = p_{22}+\mu_{12}p^b{}_{21}$. Partial failures likewise result in new values of the p_{ije}, without changing the form of the MIMO problem. The quantitative feedback theory (QFT) of (Horowitz 1979, 1982b) was devised precisely for such situations of the p_{ije} assuming different values due to uncertainty. The various failure cases simply give additional elements in the set $P_e = \{[p_{ije}]\}$ of possible plant matrices. Suppose a fixed compensation design is being made for m_1 representative flight conditions involving different Mach and altitude values and m_2 different failure cases. Then at most

$m_1 m_2$ (instead of m_1) sets pf P_e matrix element values constitute the plant uncertainty set P_e, to which the design theory is applied in precisely the same manner as if there were only m_1 sets. It is even conceivable that the extent of the new uncertainty (measured by the ranges of the individual frequency responses $\{p_{ije}(j\omega)\}$ at any ω) is not much enlarged by the various failure cases.

"Hardover" is a type of failure in which one or more control surfaces are frozen at some fixed values and can no longer be changed. If δ_1^a is so frozen at (say) its maximum value δ_{1x}, then let its resulting vector of output components $(p_{11}^a \delta_{1x}, p_{21}^a \delta_{1x})' = d_e$ be treated as an external disturbance vector, which is to be suitably attenuated by the feedback system, in order to satisfy the system performance tolerances. The effective plant upon which d_e acts is P_e of (6a) in which $p_{11}^a = p_{21}^a = 0$, because δ_1^a is no longer controllable. The synthesis theory can handle simultaneous disturbance attenuation and command input response under plant uncertainty.

2.2.2. Additional justification of constraints (5a,b)

One might argue that (5,ab) may not be optimum relations inasmuch as they are apparently required only so that the specific synthesis techniques of Horowitz (1979, 1982b) may be directly used. It is next shown that they are in fact necessary in order that failures may lead to small and controllable channel interaction despite plant uncertainty. Thus, consider the system transfer matrix T under δ_1^a failure, for which $p_{11}^a = p_{21}^a = 0$, giving

$$T = \frac{\begin{bmatrix} (f_{11}p^b_{11}+f_{21}p_{12})(1+m_{22}p_{22}) + f_{21}p_{12}m_{12}p^b_{21} & p^b_{11}p_{22}(m_{12}f_{22}-m_{22}f_{12})-f_{12}p^b_{11} \\ p_{12}p^b_{21}(m_{11}f_{21}-f_{11}m_{21})-f_{21}p^b_{21} & (f_{12}p^b_{21}+f_{22}p_{22})(1+m_{21}p_{12}) + f_{22}p_{22}m_{11}p^b_{11} \end{bmatrix}}{(1+m_{21}p_{12})(1+m_{12}p^b_{21}+m_{22}p_{22}) + m_{11}p^b_{11}(1+m_{22}p_{22})} \quad (7)$$

The dominant terms in the numerator of any t_{uv} involve $m_{..}p_{..}p_{..}$ products, so small t_{uv} $(u \neq v)$ relative to t_{uu} require such products disappear in the numerators of t_{uv} independently of the actual p values. This is achieved in (7) only by (5a,b), because the other alternative of setting for example $p^b_{11}p_{22}(m_{12}f_{22}-m_{22}f_{12}) = f_{12}p^b_{11}$ is impractical when there is non-negligible plant uncertainty. It is readily found that (5a,b) suffice for this purpose for δ^a_1, δ^b_1, δ^a_2, δ^b_2 failures one at a time, or any two at a time.

It is arguable that the same result is achieved in (7) by setting $m_{ij} = f_{ij} = 0$ for all $i \neq j$, which is a special case of (5a,b). However it would then be impossible to achieve t_{22} under simultaneous failure of δ^a_2 and δ^b_2, or to achieve t_{11} if both δ^a_1 and δ^a_2 failed. Also δ^a_2, δ^b_2 would not contribute to y_1 when $r_1 \neq 0$ and δ^a_1, δ^b_1 would not contribute to y_2 when $r_2 \neq 0$. Thus (5a,b) are inherently necessary in any synthesis technique which achieves the objectives in this paper.

2.2.3 Division of control effort

(a) No failure case. In order to find the δ's needed to achieve the desired outputs note that $\delta = Fr - My = (F-MT)r$. Take any $r_i \neq 0$ the other $r_j = 0$ so $Fr = f^i$ the ith column of F, and $Tr = t^i$ the ith

column of T. In the no failure case if i=1, and if $p^a_{ij} = p^b_{ij}$ giving $t_{21} = 0$, the result is $\delta^a_1 = \delta^b_1 = f_{11}-m_{11}t_{11}$ and $\delta^a_2 = \delta^b_2 = f_{21}-m_{21}t_{11}$, so that due to (5a), $\delta^a_1/\delta^a_2 = f_{11}/f_{21} = 1/\mu_{21}(s)$. Similarly for $r_2 \neq 0$, $r_1=0$ and $p^a_{ij} = p^b_{ij}$, in the no failure case $\delta^a_1 = -\delta^b_1 = f_{12}-m_{12}t_{22}$, $\delta^a_2 = -\delta^b_2 = f_{22}-m_{22}t_{22}$, so (5b) gives $\delta^a_1/\delta^a_2 = f_{12}/f_{22} = \mu_{12}(s)$. The designer may choose μ_{21}, μ_{12} to achieve the optimum division of control effort between δ_1 and δ_2. Note that in the traditional older design procedure where the lateral and longitudinal modes are decoupled, there is no such division of control effort -- only the δ_i are used to achieve y_i.

The following appears a reasonable way to select the μ_{ij}. Under r_1 command $t_{11} = p_{11}\delta^a_1 + p_{12}\delta^a_2$. Let $\delta^a_2 = \delta^a_1\phi_{21}p_{11}/p_{12}$, ϕ_{21} a constant, so that $t_{11} = p_{11}\delta^a_1(1+\phi_{21})$, in order that δ^a_1, δ^b_1 work together to achieve t_{11}; ϕ_{21} can possibly be chosen on the basis of the relative saturation levels of δ^a_1, δ^a_2. This gives (see 2.2.3) $\mu_{21} = \phi_{21}p_{11}/p_{12}$. Similarly, consideration of r_2 command leads to $\delta^a_1 = \delta^a_2\phi_{12}p_{22}/p_{21}$ $(r_2 \neq 0, r_1=0) = \mu_{12}\delta^a_2$. Of course, the p_{ij} values change for various flight conditions, but the ratios p_{11}/p_{12}, p_{22}/p_{21} change much less. A compromise fixed p_{ii}/p_{ij} ratio can be chosen. Also, if scheduling is used, then the μ_{ij} values may also be scheduled.

(b) <u>Control effort division under failure</u> The above equation $\delta = (f^i-Mt^i)r_i$ must be properly used under failure, because it refers to the commanded δ values. Hence, if for example δ^a_1 fails, the above gives the commanded but not actual δ^a_1 value. Simple equations are obtained for the δ's, but the difficulty is in the

t_{ij} values. If δ_1^a fails, then t_{12}, t_{21} are no longer zero so for $r_2=1$, $r_1=0$

$$\delta_2^a = f_{22}-(m_{21}t_{12}+m_{22}t_{22}) = (f_{22}-m_{22}t_{22})-\mu_{21}m_{11}t_{12}$$

$$\delta_2^b = -(f_{22}-m_{22}t_{22}) - \mu_{21}m_{11}t_{12} \tag{8}$$

$$\delta_1^b = -\mu_2(f_{22}-m_{22}t_{22}) - m_{11}t_{12}$$

It is readily found (Horowitz 1982b), that

$$t_{ij}(i\neq j) = \frac{t_{jj}p_{ije}}{p_{jje}(1+\ell_i)},$$

$$f_{ii}-m_{ii}t_{ii} = \frac{m_{ii}t_{ii}(1+\ell_j-\gamma)}{\ell_i(1+\ell_j)}, \tag{9}$$

where $\gamma = p_{12e}p_{21e}/p_{11e}p_{22e}$, $\ell_u = m_{uu}q_{uu}$,

$$p_e^{-1} = [1/q_{uv}] .$$

The above are actually general results, giving

$$\frac{2\delta_1^b}{\delta_2^a-\delta_2^b} = \frac{-\left[\ell_1\frac{p_{12e}}{p_{11e}} + \mu_{12}(1+\ell_1-\gamma)\right]}{1+\ell_1-\gamma} \tag{10}$$

which is $-\mu_{12}$ in the no fail case, because then $p_{12e} = 0$. If δ_1^a fails, $p_{11}^a = p_{21}^a = 0$ so (10) gives, recalling (6a), $-\mu_{12}\mu_{21}p_{12}/(p_{11}^b+\mu_{21}p_{12})$ in the control-frequency range where $|\ell_i(j\omega)|>>1-\gamma$. For $r_1=1$, the result is in general

$$\frac{2\delta_1^b}{\delta_2^a+\delta_2^b} = \frac{1}{\mu_{21}}\left[1 + \frac{\mu_{12}\ell_2p_{21e}}{p_{22e}(1+\ell_2-\gamma)}\right] \tag{11}$$

which is $1/\mu_{21}$ in the no fail case where $p_{21e} = 0$, and

REFERENCES

Betzold, R.W., Horowitz, I., Houpis, C.W., 1984, Proc. Naecon, Dayton, Ohio 1984.

Chandler, P.R., 1984, IEEE Proc. Naecon, 1, 586-590; "Self-Repairing Flight Control, AFWAL, WPAFB, Feb. 9, 1984.

Chandler, P.R., and Potts, D.W., 1983, Proc. IEEE 22nd Conf. Dec. and Control, 1068-73.

Horowitz, I., 1963, Synthesis of Feedback Systems, Academic Press, N.Y.

Horowitz, I., 1976, Proc. IEEE, 64 123-130; 1979, Int. J. Control, 30, 81-106; 1980a, ibid, 32 199-219; 1980b, ibid, 32, 749-757; 1981a, ibid, 34, 547-560; 1981b, ibid, 34, 749-64; 1981c, Int. J. Sys. Sci., 12 539-563; 1982a, Proc. IEE. D, 129, 215-226; 1982b, Int. J. Control, 36, 977-988.

Horowitz, I., and Breiner, M., 1981, Int. J. Sys. Sci., 12, 539-63.

Horowitz, I., and Loecher, C., 1981, Int. J. Control, 33, 677-99.

Horowitz, I. et al, 1982, Multivariable Flight Control Design with Uncertain Parameters, Report AFWAL-TR-83-3036, Sept. 1982. AFFDL, AFWAL, WFAFB, Ohio 45433.

Horowitz, I., and Shaked, U., 1975, IEEE Trans. AC-28, 84-97.

Robertus, D.P., 1983, IEEE National Aerospace and Electronics Conf., 5, 1280-6.

the inputs r_i to the systems of Figures 1-3. Suppose that the desired response function set for mode x is T_{ix}. H is designed so that its outputs are $T_{ix}c_{ix}$ in response to command input number x of value c_x. Then the r_i of the systems in this paper have the values $r_i = T_{ix}c_{ix}$. H has as amny input points as the modes F being considered, and new ones can be added without disturbing the designs of F, M of this paper. The latter point is the principal advantage of this approach, but the optimum under BNIA design may not be optimum for each or any of the various modes. Clearly compromises between these two approaches are feasible with the design theory presented here.

It is also worth noting that the well-known "scheduling" technique is obviously easily accommodated into the synthesis procedure. An advantage of quantitative synthesis is that the designer clearly sees the relations between "cost of feedback" (Horowitz et al 1982) and the range of uncertainty and the tolerances, so the trade-off between scheduling complexity and cost of feedback reduction is highly transparent.

condition for obtaining the equivalent linear set is to solve the nonlinear plant equations backwards - given the plant outputs to find the plant inputs. This means the parameters equivalent to the μ_{ij} of this paper must first be chosen i.e. one must first decide how to use the freedom due to the plant having more inputs than outputs.

BNIA design

Optimization with respect to the μ_{ij} has been previously discussed. The assumption of desired "basically noninteracting closed-loop tolerances" is related to the optimization problem, as follows. In advanced fighter aircraft there are many different operating modes. In mode i, a specific combination of outputs may be wanted in response to command r_i (a specific set of t_{ji} for j = 1 to n). In mode m an entirely different set of t_{jm} in response to r_m, may be specified with its set of tolerances. It is conceivable that the optimum use of the available freedom (more plant inputs than outputs), may be significantly different for the different modes. If this is sufficiently important, different designs with conceivably different compensations inside the feedback loops, may be made, and the new systems switched in accordance with the mode desired. The design theory presented here is clearly readily applied to this alternative, as the design technique is not exclusively for BNIA systems (Horowitz and Loecher 1981).

This paper offers an alternative approach to the many-mode design problem. A prefilter H is added whose output provides

based upon control effort division, have been discussed in the paper. Another way of using the available design freedom, is to minimize the P_e uncertainty. Thus in (6a), $p_{11e} = p_{11}+\mu_{21}p_{12}$ with correlations often between the parameters of p_{11} and p_{12}. One could consider choosing μ_{21} so as to minimize the uncertainty range of p_{11e} due to the various flight conditions and failures. Other optimality criterion could also be considered, e.g. drag minimization.

Sections 2-4 presented the synthesis theory by application to structures whose complexity ranged from (4 plant inputs - 2 outputs) to (10 plant inputs - 6 outputs). In all of these, two "groups" (longitudinal and lateral for aircraft) were assumed. But it is obvious that there can be as many groups as outputs. Recall also (Section 2.1) that different compensation structures may be used, in particular G = M in the forward path, and a new F' prefilter in place of F with GF' = F and the outputs of -P and F' being the inputs into G.

Nonlinear uncertain plants

Linear time-invariant plant models were used in this paper, permitting use of transform equations. The synthesis theory is readily extended to uncertain nonlinear MIMO systems by means of the "linear plant set equivalence technique" (Horowitz 1976, 1981a,b,c, 1982c, Horowitz et al 1980a,b). In this technique the uncertain nonlinear plant set is replaced by linear time invariant equivalent sets. The solutions (compensations) for the latter problem are guaranteed to work for the original nonlinear problem for the set of command and disturbance inputs for which the equivalence has been developed. A necessary

5. DISCUSSION

This paper has presented a unified synthesis procedure for flight control design which apriori takes into account in a precise, quantitative manner many possible combinations of control surface failures, the various flight conditions and external disturbances (gusts etc.). This can all be done by means of a fixed compensation design, providing the equivalent plant matrix P_e satisfies the usual necessary conditions (Horowitz 1982b). The minimum-phase condition (det P_e has no right half-plane zeros) guarantees that any arbitrarily narrow tolerances can be satisfied. If P_e is nonminimum-phase it is necessary that the performance tolerances are compatible with the constrained loop bandwidths achievable.

It is conceivable that a single fixed compensation design to handle such a large variety of conditions, may require impractically large loop bandwidths. If so, one could consider scheduling for different classes of mach number and altitude, in order to reduce the range of uncertainty. Scheduling is quite reliable, whereas failure identification may sometimes be fairly unreliable.

Optimization

Since each control surface is assumed separately controllable, the number of plant control inputs exceeds the outputs to be controlled in the no failure condition. The exploitation of this freedom constitutes an optimization problem, which must be solved before the design for uncertainty and failure can proceed. The difficulties involved when optimization is

$m_{33}t_{31} \doteq p_{31e}\phi/p_{33e}$, $\phi = f_{11}-m_{11}t_{11}$. From the matrix equation $\delta = (F-MT)r$, for $r_1 = 1$ and other $r_i = 0$, there result five scalar equations $\delta_i = \phi\mu_{i1}-(\mu_{i2}m_{22}t_{21}+\mu_{i3}m_{33}t_{31})$, $\mu_{ii} = 1$ for $i = 1$ to 5. The $m_{22}t_{21}$, $m_{33}t_{31}$ are replaced by $p_{21e}\phi/p_{22e}$, $p_{31e}\phi/p_{33e}$ of above, giving four equations for $j = 2$ to 5:

$$\lambda_{j1} = (\delta/\delta_1)_{r_1} \doteq \frac{\mu_{j1}p_{22e}p_{33e}-(\mu_{j2}p_{21e}p_{33e}+\mu_{j3}p_{22e}p_{31e})}{p_{22e}p_{33e}-(\mu_{12}p_{21e}p_{33e}+\mu_{13}p_{22e}p_{31e})} \quad (20)$$

The p_{uve} are of course functions of the μ_{ij} as per (18,19), so the above equation relates the μ_{ij} to the p_{ij} and λ_{j1}. Similarly four equations relationg λ_{j2} (j=1,3,4,5) to the μ_{ij} and p_{ij} are obtained by setting only $r_2 = 1$, the others zero, etc. By this means ($r_i = 1$, all others zero for $i = 1$ to 6), a total of 24 equations relating the λ_{ij} to the 24 μ_{ij} are obtained.

4.2 Number of tolerable failures

At least six independent control inputs are needed to achieve linear control of the six outputs in Figure 3, so any four of the ten control surfaces may fail simultaneously. The design can be apriori made so that the desired performance tolerances on all 36 t_{ij} of T are satisfied for any such four simultaneous failures. Five failures will permit only twenty-five t_{ij} tolerances satisfied, and again this can be incorporated into the design, etc. - all this to be achieved by a single fixed set of compensators.

As in Sections 2, 3 interaction between the two sets (1-3 and 4-6) is zero in the no fail case. But as in Sections 2, 3, the paired δ_i of set 1 (δ_1, δ_2 here) participate in achieving set 2 outputs in response to set 2(r_3-r_6) commands, and vice versa. The design procedure is the same as in Sections 2, 3. Once the μ_{ij} are chosen, the P_e set is available by listing all flight conditons and surface failures for which the design is to apply, and proceeding precisely as in any quantitative MIMO synthesis problem.

4.1 Choice of μ_{ij}

Essentially the choice of μ_{ij} is an optimization problem — how to use the available freedom (more plant inputs than outputs) for each r_i input. There are 30 each m_{ij}, f_{ij} to be chosen: Setting $m_{ij}/m_{jj} = f_{ij}/f_{jj}$ of (20b) gives 24 relations, the actual μ_{ij} values gives 24 more and finally quantitative design leads to six each of diagonal m_{ii} , f_{ii}. However, quantitative design can proceed only after the μ_{ij} of (20b) have been chosen, permitting P_e of (18,19) to be evaluated for the various flight conditions and surface failure cases. Suppose the $\lambda_{ij} = (\delta_i/\delta_j)_{r_j \neq 0}$ (all $r_i = 0$ for $i \neq j$) have been chosen, if optimum division of control effort under no fail is the optimality criterion. Then, as in Section 3.1, the λ_{ij} must be related to the μ_{ij} and a procedure similar to that in Section 3.1 can be followed: e.g. for $r_1 = 1$ (all other $r_i = 0$), only t_{11} , t_{21} , t_{31} exist. From $(I+P_eM_e)T = P_eF_e$ and neglecting t_{31} or t_{21} cf t_{11} (justifiable in BNIA systems) and $|\ell_i| >> 1$ (highly justifiable in control frequency range), one gets $m_{22}t_{21} \doteq P_{21e}\phi/P_{22e}$,

The $\alpha_{3i} = 0$ for $i = 4\text{-}6$ in order that $\delta_3 = 0$ for r_4, r_5 or r_6 commands as it is assumed that $t_{3i} = 0$ is desired. Similarly $\alpha_{6j} = 0$ for $j = 1\text{-}3$ so $\delta_6 = 0$ for r_1, r_2 or r_3 commands, as $t_{6j} = 0$ is assumed desired.

P_e is derived and the μ_{ij} defined in the same manner as in Sections 2.2, 3 for the reasons given in 2.2, 2.2.2 giving $T = (I+P_eM_e)^{-1}P_eF_e$, and

First three columns of

$$P_e = \begin{bmatrix} p_{11} & p_{12} & p_{13} & p_{14} & p_{15} \\ p_{21} & p_{22} & p_{23} & p_{24} & p_{25} \\ p_{31} & p_{32} & p_{33} & p_{34} & p_{35} \\ \Delta p_{41} & \Delta p_{42} & 0 & \Delta p_{44} & \Delta p_{45} \\ \Delta p_{51} & \Delta p_{52} & 0 & \Delta p_{54} & \Delta p_{55} \\ \Delta p_{61} & \Delta p_{62} & 0 & \Delta p_{64} & \Delta p_{65} \end{bmatrix} \begin{bmatrix} 1 & \mu_{12} & \mu_{13} \\ \mu_{21} & 1 & \mu_{23} \\ \mu_{31} & \mu_{32} & 1 \\ \mu_{41} & \mu_{42} & \mu_{43} \\ \mu_{51} & \mu_{52} & \mu_{53} \end{bmatrix} \tag{18}$$

Last three columns of

$$P_e = \begin{bmatrix} \Delta p_{11} & \Delta p_{12} & \Delta p_{14} & \Delta p_{15} & 0 \\ \Delta p_{21} & \Delta p_{22} & \Delta p_{24} & \Delta p_{25} & 0 \\ \Delta p_{31} & \Delta p_{32} & \Delta p_{34} & \Delta p_{35} & 0 \\ p_{41} & p_{42} & p_{44} & p_{45} & p_{46} \\ p_{51} & p_{52} & p_{54} & p_{55} & p_{56} \\ p_{61} & p_{62} & p_{64} & p_{65} & p_{66} \end{bmatrix} \begin{bmatrix} \mu_{14} & \mu_{15} & \mu_{16} \\ \mu_{24} & \mu_{25} & \mu_{26} \\ 1 & \mu_{45} & \mu_{46} \\ \mu_{54} & 1 & \mu_{56} \\ \mu_{64} & \mu_{65} & 1 \end{bmatrix} \tag{19}$$

$$\Delta p_{ij} = p^a_{ij} - p^b_{ij} \quad (j \neq 3,6), \quad \mu_{ij} = \frac{m_{ij}}{m_{jj}} = \frac{f_{ij}}{f_{jj}},$$

$$p_{ij} = p^a_{ij} + p^b_{ij} \quad (j \neq 3,6). \tag{20a-e}$$

$$M_e = \text{diag.}m_{ii}, \qquad F_e = \text{diag.}f_{ii}$$

situations can be included in the design.

4. TEN INPUT - SIX OUTPUT PLANT

The final structure treated here (Figure 3) has one single and two pairs of control surfaces for one set of variables (e.g. longitudinal) and a similar number for a second set (e.g. lateral). The resulting P,F,M matrices are

$$P = \begin{bmatrix} p_{11}^a & p_{11}^b & p_{12}^a & p_{12}^b & p_{13} & p_{14}^a & p_{14}^b & p_{15}^a & p_{15}^b & 0 \\ p_{21}^a & p_{21}^b & p_{22}^a & p_{22}^b & p_{23} & p_{24}^a & p_{24}^b & p_{25}^a & p_{25}^b & 0 \\ p_{31}^a & p_{31}^b & p_{32}^a & p_{32}^b & p_{33} & p_{34}^a & p_{34}^b & p_{35}^a & p_{35}^b & 0 \\ p_{41}^a & -p_{41}^b & p_{42}^a & -p_{42}^b & 0 & p_{44}^a & -p_{44}^b & p_{45}^a & -p_{45}^b & p_{46} \\ p_{51}^a & -p_{51}^b & p_{52}^a & -p_{52}^b & 0 & p_{54}^a & -p_{54}^b & p_{55}^a & -p_{55}^b & p_{56} \\ p_{61}^a & -p_{61}^b & p_{62}^a & -p_{62}^b & 0 & p_{64}^a & -p_{64}^b & p_{65}^a & -p_{65}^b & p_{66} \end{bmatrix} \tag{16}$$

It is assumed δ_6 affects only the second set of outputs and δ_3 only the first set, hence $p_{i6} = 0$ for $i = 1\text{-}3$, $p_{j3} = 0$ for $j = 4\text{-}6$.

$$M,F = \begin{bmatrix} \alpha_{11} & \alpha_{12} & \alpha_{13} & \alpha_{14} & \alpha_{15} & \alpha_{16} \\ \alpha_{11} & \alpha_{12} & \alpha_{13} & -\alpha_{14} & -\alpha_{15} & -\alpha_{16} \\ \alpha_{21} & \alpha_{22} & \alpha_{23} & \alpha_{24} & \alpha_{25} & \alpha_{26} \\ \alpha_{21} & \alpha_{22} & \alpha_{23} & -\alpha_{24} & -\alpha_{25} & -\alpha_{26} \\ \alpha_{31} & \alpha_{32} & \alpha_{33} & 0 & 0 & 0 \\ \alpha_{41} & \alpha_{42} & \alpha_{43} & \alpha_{44} & \alpha_{45} & \alpha_{46} \\ \alpha_{41} & \alpha_{42} & \alpha_{43} & -\alpha_{44} & -\alpha_{45} & -\alpha_{46} \\ \alpha_{51} & \alpha_{52} & \alpha_{53} & \alpha_{54} & \alpha_{55} & \alpha_{56} \\ \alpha_{51} & \alpha_{52} & \alpha_{53} & -\alpha_{54} & -\alpha_{55} & -\alpha_{56} \\ 0 & 0 & 0 & \alpha_{64} & \alpha_{65} & \alpha_{66} \end{bmatrix} \tag{17}$$

done as follows. As noted in 2.2.3, in general in Figures 1,2 $\delta = (F-MT)r$, giving for r_1 command in Figure 2:

$$\delta_1^a = f_{11}-(m_{11}t_{11}+m_{12}t_{21}),$$

$$\delta_2 = f_{21}-(m_{21}t_{11}+m_{22}t_{21}) = \mu_{21}(f_{11}-m_{11}t_{11}) - m_{22}t_{21}$$

$$\delta_3^a = f_{31}-(m_{31}t_{11}+m_{32}t_{21}) = \mu_{31}(f_{11}-m_{11}t_{11})-\mu_{32}m_{22}t_{12} .$$

Equations (9) are used to eliminate t_{21} , $f_{11}-m_{11}t_{11}$.
The result, after writing the P_{ije} in terms of p_{uv} and μ_{uv} of (13), is

$$x_1(\lambda_{21}p_{22}+p_{21}) + x_2p_{23}+x_3\lambda_{21}p_{23} - \frac{\mu_{21}}{m_{22}} = \frac{-\lambda_{21}}{m_{22}}$$

$$x_1p_{22}\lambda_{31} \quad -x_2p_{22}+x_3(\lambda_{31}p_{23}+p_{21}) - \frac{\mu_{31}}{m_{22}} = \frac{-\lambda_{31}}{m_{22}} \qquad (15)$$

$$x_1 = 1-\mu_{12}\mu_{21} , \quad x_2 = \mu_{31}-\mu_{21}\mu_{32} , \quad x_3 = \mu_{32}-\mu_{12}\mu_{31}$$

Two more equations are obtained for $r_2 \neq 0$, $r_1=0$, setting $\delta_1^a/\delta_2 = \lambda_{12}$, $\delta_3^a/\delta_2 = \lambda_{32}$ giving a total of four equations in the four μ_{ij} unknowns. Unfortunately the as yet unknown m_{22} appears in the first two and m_{11} in the last two, but the terms containing these m_{ii} appear small compared to the others, so the result should be relatively insensitive to the m_{ii} values.

3.2 Number of tolerable failures

It is readily seen that there exists a linear range of control of all three outputs in Figure 2, even if any two (of the five) surfaces totally fail simultaneously. But failure of any three leaves only two outputs or any two independent combinations, independently controllable, while failure of four leaves only one output controllable. All these

inherently necessary for it to be possible to achieve under failure longitudinal output with small lateral effect, and vice versa.

3.1 Division of control effort and choice of μ_{ij}

One is tempted to follow the procedure in Section 2.2.3, if optimum control effort division is desired i.e. for $r_1 \neq 1$, $r_2 = r_3 = 0$ in $t_{11} = p_{11}\delta_1^a + p_{12}\delta_2 + p_{13}\delta_3^a$, let $\delta_2/\delta_1^a = \phi_{21}p_{11}/p_{12}$, $\delta_3^a/\delta_1^a = \phi_{31}p_{11}/p_{13}$ with ϕ_{21}, ϕ_{31} constants, in order that the three δ's work together to achieve t_{11}. However, the resulting $t_{21} = p_{11}\delta_1^a(1+\phi_{21}+\phi_{31})$ is then not independently realizable, so the above cannot be followed for r_1, r_2 commands. It can be applied to the r_3 command because $t_{13} = t_{23} = 0$, $t_{33} = p_{31}\delta_1^a + p_{33}\delta_3^a$. Let $\delta_1^a/\delta_3^a = \phi_{13}p_{33}/p_{31}$. Also $\delta_1^a = f_{13} - m_{13}t_{33} = \mu_{13}(f_{33} - m_{33}t_{33})$, $\delta_3^a = f_{33} - m_{33}t_{33}$ so $\delta_1^a/\delta_3^a = \mu_{13}$ which gives $\mu_{13} = \phi_{13}p_{33}/p_{31}$ once the optimum choice of δ_1^a/δ_3^a has been made. But for r_1, r_2 commands the optimal division of the control effort is more complicated as it is subject to the constaints of t_{21}, t_{12} satisfying their BNIA tolerances of the form $|t_{21}(j(\omega))/t_{11}(j\omega)| \leq \varepsilon_{21}(\omega)$, $|t_{12}, t_{22}| \leq \varepsilon_{12}(\omega)$ with $\varepsilon_{21}, \varepsilon_{12}$ known. Thus if $t_{11}/t_{21} = \Sigma p_{1i}\delta_i^a/\Sigma p_{2i}\delta_i^a = 1/\varepsilon_{21}$, with ε_{21} very small, this gives the constraint $p_{21} + p_{22}\lambda_{21} + p_{23}\lambda_{31} \doteq 0$ where $\lambda_{i1} = (\delta_i/\delta_1)_{r_1 \neq 0}$; for r_2 command the resulting constraint due to t_{12} is $p_{11}\lambda_{12} + p_{12} + p_{13}\lambda_{32} \doteq 0$, $\lambda_{i2} = (\delta_i/\delta_2)_{r_2 \neq 0}$.

Suppose the λ_{ij} values have been "optimally" chosen, it is then necessary to realte them to the μ_{ij} of (14-c) in order for P_e of (13) to be known and the design to proceed. This can be

$$P = \begin{bmatrix} p_{11}^a & p_{11}^b & p_{12} & p_{13}^a & p_{13}^b \\ p_{21}^a & p_{21}^b & p_{22} & p_{23}^a & p_{23}^b \\ p_{31}^a & -p_{31}^a & 0 & p_{33}^a & -p_{33}^b \end{bmatrix} \quad ; \; M,F = \begin{bmatrix} \alpha_{11} & \alpha_{12} & \alpha_{13} \\ \alpha_{11} & \alpha_{12} & -\alpha_{13} \\ \alpha_{21} & \alpha_{22} & 0 \\ \alpha_{31} & \alpha_{32} & \alpha_{33} \\ \alpha_{31} & \alpha_{32} & -\alpha_{33} \end{bmatrix} \tag{12a,b}$$

$\alpha = m$ for M, $\alpha = f$ for F.

Note that $p_{32} = 0$ as the rudder has no effect on the longitudinal output; $\alpha_{23} = 0$ as $\delta_2 = 0$ is desired for r_3 command giving y_3 output with desired $y_1 = y_2 = 0$; as before $p_{ij}^a = p_{ij}^b$ is assumed.

As in Section 2.2, one demands $T = (I+P_eM_e)^{-1}P_eF_e = (I+PM)^{-1}PF$ with 3×3 P_e and diagonal M_e, F_e giving for the analogs of (5,6)

$$P_e = \begin{bmatrix} p_{11} & p_{12} & p_{13} \\ p_{21} & p_{22} & p_{23} \\ \Delta p_{31} & 0 & \Delta p_{33} \end{bmatrix} \begin{bmatrix} 1 & \mu_{12} \\ \mu_{21} & 1 \\ \mu_{31} & \mu_{32} \end{bmatrix} \text{ for its first 2 columns,}$$

$$\begin{bmatrix} \Delta p_{11} & \Delta p_{13} \\ \Delta p_{21} & \Delta p_{23} \\ p_{31} & p_{33} \end{bmatrix} \begin{bmatrix} \mu_{13} \\ 1 \end{bmatrix} \text{ for its third column} \tag{13}$$

$$\Delta p_{ij} = p_{ij}^a - p_{ij}^b, \; p_{ij} = p_{ij}^a + p_{ij}^b \; , \; \mu_{ij} = \frac{m_{ij}}{m_{jj}} = \frac{f_{ij}}{f_{jj}} \tag{14a-e}$$

$$M_e = \text{diag. } m_{ii} \; , \quad F_e = \text{diag. } f_{ii}$$

Note that $p_{31e}, p_{32e}, p_{13e}, p_{23e} = 0$ in the no fail case. The results in Sections 2.2.1, 2.2.2 apply as again (14c) is

be incorporated in the design, to guarantee the desired performance under these circumstances.

2.2.5 Design procedure

The plant of Figure 1 has four control inputs (the four δs) and only two outputs, so there exist two degrees of freedom (μ_{12}, μ_{21}) available for optimization. It was shown in Section 2.2.3 how these may be chosen for optimum division of the control effort. However other optimal criteria may be perferable (see Section 5). In any case, it is assumed that μ_{12}, μ_{21} have been chosen, which determines P_e. The various modes and conditions for which the system is to operate are listed by the designer, the flight conditions, the failure cases, the disturbances (gusts etc) etc. These give the sets $\mathcal{P}_e$, $\mathcal{D}$ of Sections 1.1, 2.2.1 and the performance tolerances T, T_d of Section 1.1. The design technique of (Horowitz 1979, 1982b) is then applied, resulting in required $m_{ii}(s)$, $f_{ii}(s)$, i=1,2. The values of the m_{ij}, f_{ij} for $i \neq j$ are available from (5a,b) and the design is complete.

3. A FIVE INPUT - THREE OUTPUT PLANT

The slight increase in plant complexity in Figure 2 results in a more difficult problem of μ_{ij} selection, if control effort division is the optimality criterion. The added single control input δ_2 and the pair (δ_1^a, δ_2^a) are assumed all of one type say lateral e.g. δ_2 is a rudder, (δ_1^a, δ_1^b) is an aileron pair while (δ_3^a, δ_3^b) is a longitudinal type, e.g. elevator pair. If so the P,M,F matrices are

$\approx p_{22}/\mu_{21}(p_{22}+\mu_{12}p_{21}^{b})$ in the control frequency range where $|\ell_2(j\omega)|>>1-\gamma$. Equations (10,11) can be used to obtain the control effort ratios for other failure cases.

Thus, if μ_{12},μ_{21} provide the optimum division of control efforts between δ_1 and δ_2 in the no fail case, then in view of the above, the division under failure may no longer be optimum. But in failure cases, the dominating concern is acceptable performance, giving more time for reliable identification and switching in of compensations optimum for the failure situation, should this be considered justifiable.

2.2.4 Performance under failures

The quantitative MIMO synthesis techniques (Horowitz 1979, 1982b) guarantee the achievement, theoretically, of arbitrarily narrow performance tolerances for a large class of uncertain MIMO plants. The design may not be practical if the sensors are not sufficiently accurate or have unduly large noise levels. The principal condition for this theoretical ability is that the MIMO plant is minimum-phase over its range of uncertainty i.e. det. P_e has no right half-plane zeros and that P_e is output controllable (Horowitz and Shaked 1975, Horowitz 1982b) meaning that despite the failures, the remaining control surfaces still have the physical ability to achieve two independent outputs (of course for a smaller output range). This is so in the present problem for any single, or any two simultaneous control surface failures. If there are three simultaneous failures, then only one output is achievable and the second output is not independently achievable. Such cases too can

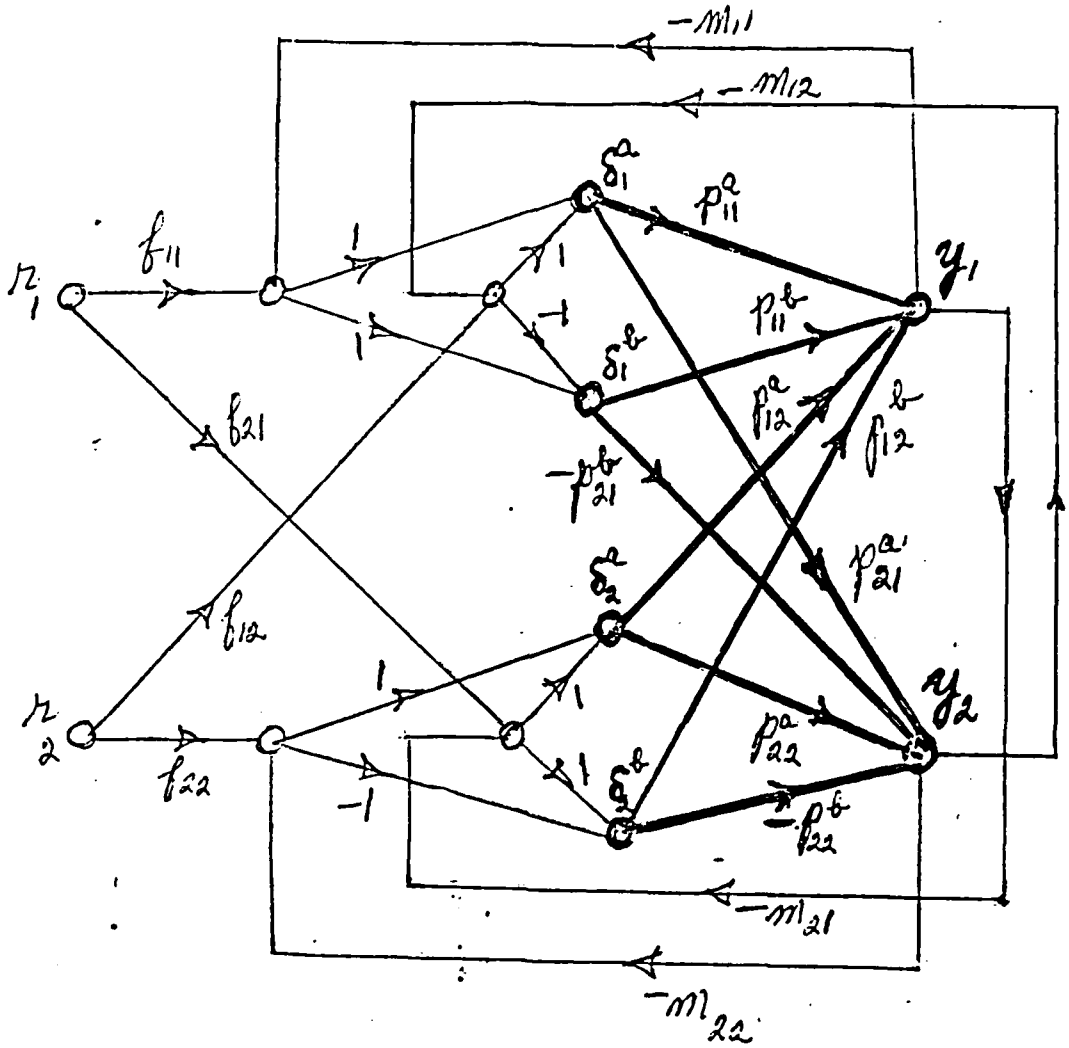

Fig. B-1. A 4-input, 2-output, 2 mode structure.

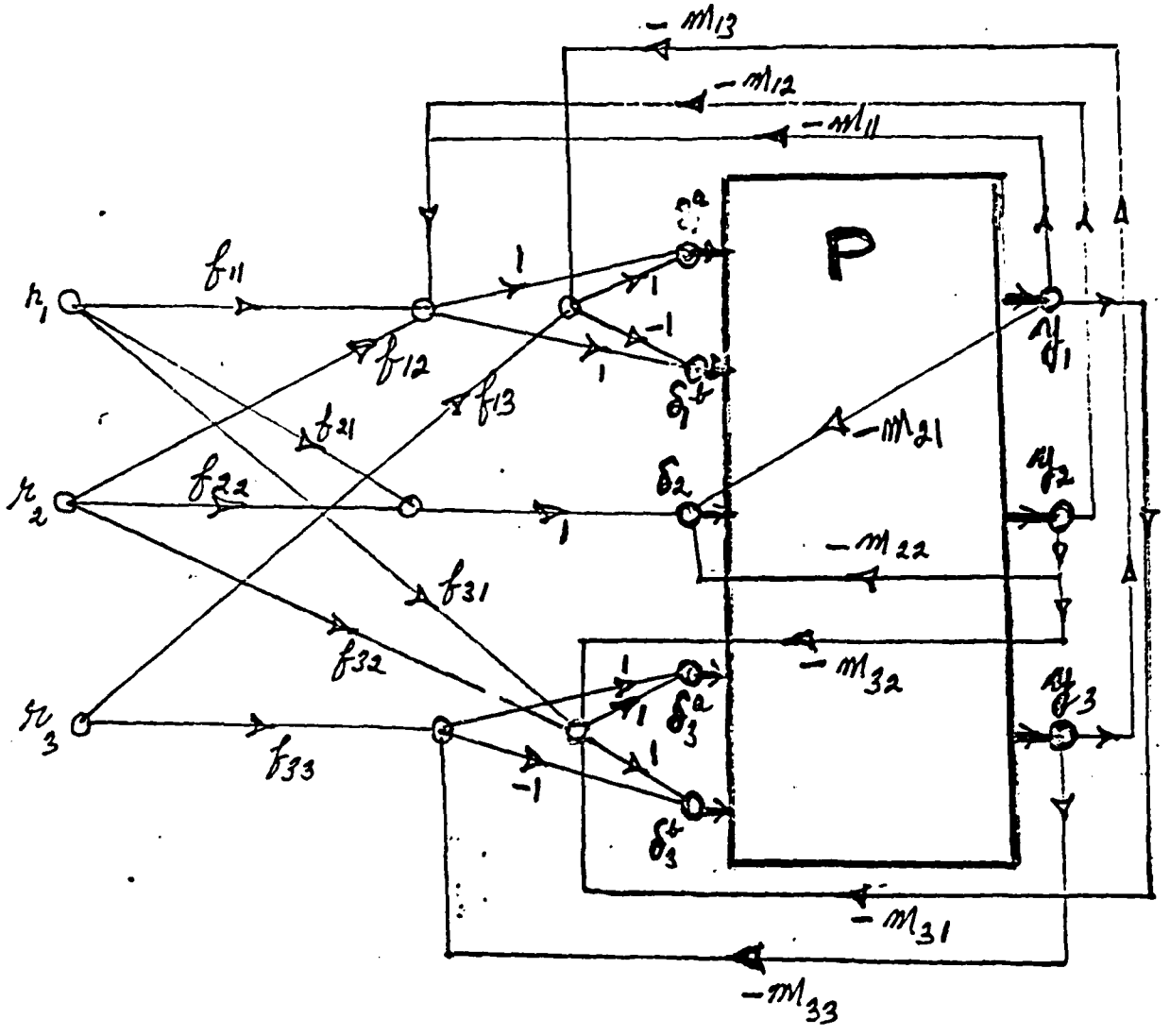

Fig. B-2. A 5-input, 3-output, 2-mode structure.

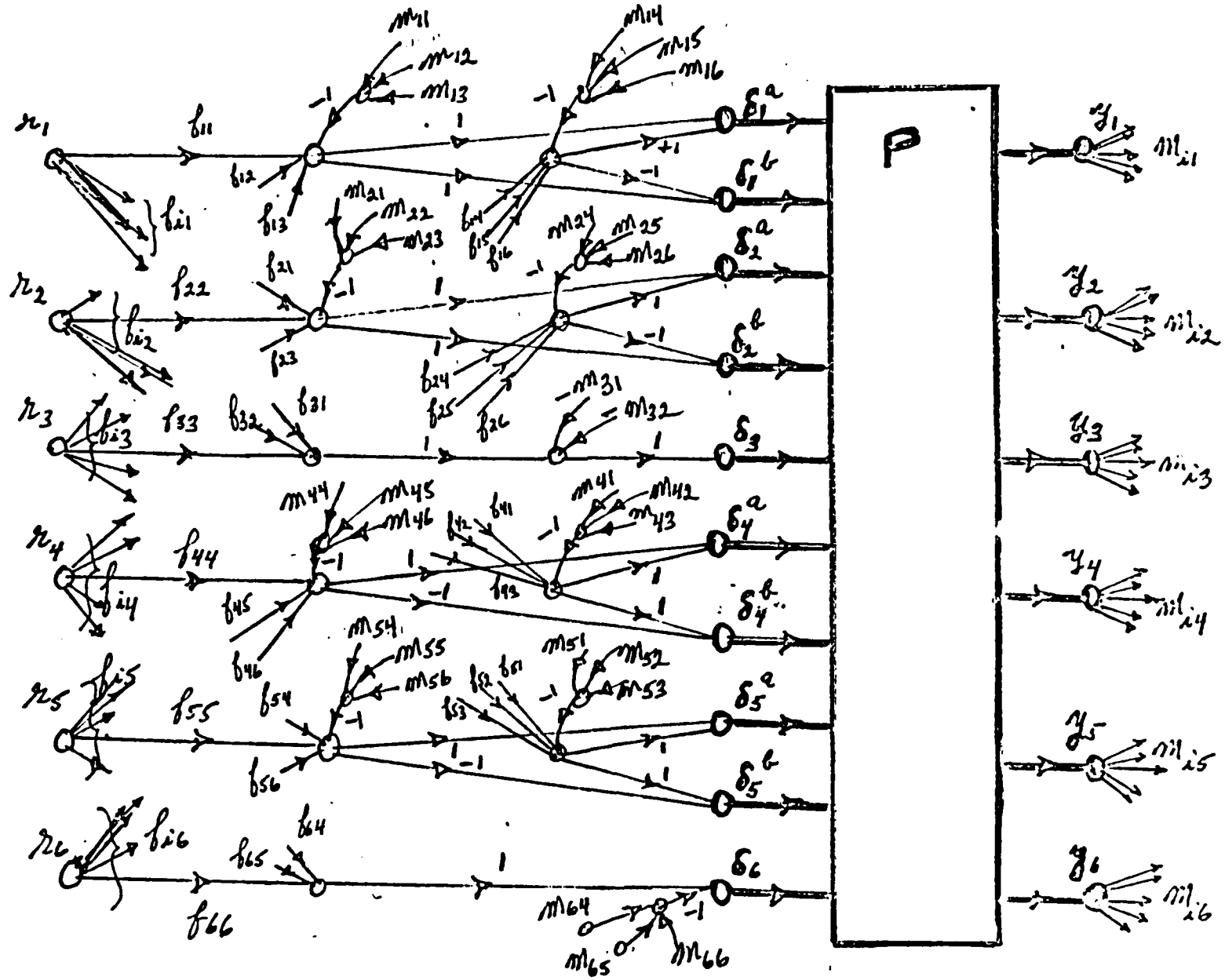

Fig. B-3. A 10-input, 6-output, 2-mode structure.

Appendix C: Equivalent Plant Transfer Function Matrices

The equivalent plant transfer function matrices are listed in this appendix for each flight condition and control surface configuration mode. These matrices are derived from the $\underline{P}_e$ matrix below using the basic plant transfer function equations developed in Chapter II.

$$\underline{P}_e = \begin{bmatrix} P_{11} + \mu P_{12} & \Delta P_{12} + \mu \Delta P_{11} \\ \Delta P_{21} + \mu \Delta P_{22} & P_{22} + \mu P_{21} \end{bmatrix}$$

where

$$P_{ij} = P_{ij}^{a} + P_{ij}^{b} \text{ and } \Delta P_{ij} = P_{ij}^{a} - P_{ij}^{b}$$

The reciprocal plant expressions $(1/Q_{ij})$ for the SISO systems of Figure 4-5 are obtained by inverting the $\underline{P}_e$ matrices. These transfer functions are expressed in terms of the Q_{ij} equations in this appendix. $\underline{P}_e^{-1} = (1/Q_{ij})$.

TABLE C-1

EQUIVALENT PLANT MATRICES FOR FLIGHT CONDITION ONE

Mode 1:	P_{11e}*	P_{12e}*
	$\frac{-2.176(0)(-.0175)(-.4617)}{(.363)(-1.3)(-.0768\pm j.207)}$	--
	P_{21e}*	P_{22e}*
	--	$\frac{-5.549(0)(-.2237\pm j1.029)}{(-.104)(-.684)(-.274\pm j1.91)}$
Mode 2:	P_{11e}	P_{12e}
	$\frac{-1.058(0)(-.01677)(-.4669)}{(.363)(-1.3)(-.0768\pm j.207)}$	$\frac{.2795(0)(-.01822)(-.4568)}{(.363)(-1.3)(-.0768\pm j.207)}$
	P_{21e}	P_{22e}
	$\frac{2.142(0)(-.3017\pm j1.562)}{(-.104)(-.684)(-.274\pm j1.91)}$	$\frac{-5.041(0)(-.2153\pm j.9547)}{(-.104)(-.684)(-.274\pm j1.91)}$
Mode 3:	P_{11e}	P_{12e}
	$\frac{-2.206(0)(-.01787)(-.4592)}{(.363)(-1.3)(-.0768\pm j.207)}$	$\frac{-.121(0)(-.0654)(-.259)}{(.363)(-1.3)(-.0768\pm j.207)}$
	P_{21e}	P_{22e}
	$\frac{.56(0)(-.21\pm j.853)}{(-.104)(-.684)(-.274\pm j1.91)}$	$\frac{-3.3(0)(-.2363\pm j1.13)}{(-.104)(-.684)(-.274\pm j1.91)}$

*Equivalent Plant.

TABLE C-1--Continued

Mode 4:	P_{11e}	P_{12e}
	$\frac{-1.09(0)(-.0175)(-.462)}{(.363)(-1.3)(-.0768\pm j.207)}$	$\frac{.159(0)(-.003)(-.587)}{(.363)(-1.3)(-.0768\pm j.207)}$
	P_{21e}	P_{22e}
	$\frac{2.7(0)(-.282\pm j1.45)}{(-.104)(-.684)(-.274\pm j1.91)}$	$\frac{-2.78(0)(-.224\pm j1.03)}{(-.104)(-.684)(-.274\pm j1.91)}$
Mode 5:	P_{11e}	P_{12e}
	$\frac{-1.09(0)(-.0175)(-.462)}{(.363)(-1.3)(-.0768\pm j.207)}$	$\frac{.4(0)(-.027)(-.402)}{(.363)(-1.3)(-.0768\pm j.207)}$
	P_{21e}	P_{22e}
	$\frac{1.582(0)(-.336\pm j1.74)}{(-.104)(-.684)(-.274\pm j1.91)}$	$\frac{-2.78(0)(-.224\pm j1.03}{(-.104)(-.684)(-.274\pm j1.91)}$
Mode 6:	P_{11e}	P_{12e}
	$\frac{-2.236(0)(-.0182)(-.457)}{(.363)(-1.3)(-.0768\pm j.207)}$	--
	P_{21e}	P_{22e}
	--	$\frac{-1.07(0)(-.302\pm j1.56)}{(-.104)(-.684)(-.274\pm j1.91)}$

TABLE C-2

EQUIVALENT PLANT MATRICES FOR FLIGHT CONDITION TWO

Mode 1:	P_{11e}*	P_{12e}*
	$\frac{-5.92(0)(-.0099)(-.562)}{(1.167)(-2.02)(-.0065\pm j.078)}$	--
	P_{21e}*	P_{22e}*
	—	$\frac{-20.8(0)(-.223\pm j1.697)}{(.078)(-.827)(-.211\pm j1.95)}$
Mode 2:	P_{11e}	P_{12e}
	$\frac{-2.98(0)(-.0098)(-.574)}{(1.167)(-2.02)(-.0065\pm j.078)}$	$\frac{.73(0)(-.01)(-.55)}{(1.167)(-2.02)(-.0065\pm j.078)}$
	P_{21e}	P_{22e}
	$\frac{6.79(0)(-.244\pm j2.101)}{(-.078)(-.827)(-.211\pm j1.95)}$	$\frac{-19.14(0)(-.221\pm j1.66)}{(.078)(-.827)(-.211\pm j1.95)}$
Mode 3:	P_{11e}	P_{12e}
	$\frac{-5.89(0)(-.01)(-.56)}{(1.167)(-2.02)(-.0065\pm j.078)}$	$\frac{.106(0)(-.0067)(-1.86)}{(1.167)(-2.02)(-.0065\pm j.078)}$
	P_{21e}	P_{22e}
	$\frac{2.18(0)(-.219\pm j1.61)}{(-.078)(-.827)(-.211\pm j1.95)}$	$\frac{-12.12(0)(-.22\pm j1.7)}{(.078)(-.827)(-.211\pm j1.95)}$

*Equivalent Plant.

TABLE C-2--Continued

	P_{11e}	P_{12e}
Mode 4:	$\frac{-2.96(0)(-.01)(-.56)}{(1.167)(-2.02)(-.0065\pm j.078)}$	$\frac{.84(0)(-.01)(-.72)}{(1.167)(-2.02)(-.0065\pm j.078)}$
	P_{21e}	P_{22e}
	$\frac{8.97(0)(-.24\pm j1.99)}{(-.078)(-.827)(-.211\pm j1.95)}$	$\frac{-10.4(0)(-.22\pm j1.7)}{(.078)(-.827)(-.211\pm j1.95)}$
	P_{11e}	P_{12e}
Mode 5:	$\frac{-2.96(0)(-.01)(-.56)}{(1.167)(-2.02)(-.0065\pm j.078)}$	$\frac{.63(0)(-.013)(-.326)}{(1.167)(-2.02)(-.0065\pm j.078)}$
	P_{21e}	P_{22e}
	$\frac{4.6(0)(-.256\pm j2.3)}{(-.078)(-.827)(-.211\pm j1.95)}$	$\frac{-10.4(0)(-.22\pm j1.7)}{(.078)(-.827)(-.211\pm j1.95)}$
	P_{11e}	P_{12e}
Mode 6:	$\frac{-2.93(0)(-.01)(-.55)}{(1.167)(-2.02)(-.0065\pm j.078)}$	—
	P_{21e}	P_{22e}
	—	$\frac{-1.7(0)(-.244\pm j2.1)}{(.078)(-.827)(-.211\pm j1.95)}$

TABLE C-3

EQUIVALENT PLANT MATRICES FOR FLIGHT CONDITION THREE

Mode 1:	P_{11e}*	P_{12e}*
	$\frac{-25.7(0)(-.013)(-1.52)}{(.965)(-3.22)(-.0076\pm j.538)}$	--
	P_{21e}*	P_{22e}*
	--	$\frac{-63.7(0)(-.358\pm j3.07)}{(-.0272(-2.7)(-.39\pm j2.96)}$
Mode 2:	P_{11e}	P_{12e}
	$\frac{-13.7(0)(-.0126)(-1.526)}{(.965)(-3.22)(-.0076\pm j.538)}$	$\frac{3.75(0)(-.013)(-1.52)}{(.965)(-3.22)(-.0076\pm j.538)}$
	P_{21e}	P_{22e}
	$\frac{25.4(0)(-.375\pm j3.58)}{(-.0272)(-2.7)(-.39\pm j2.96)}$	$\frac{-57.4(0)(-.354\pm j3.01}{(-.0272(-2.7)(-.39\pm j2.96)}$
Mode 3:	P_{11e}	P_{12e}
	$\frac{-24.9(0)(-.0126)(-1.514)}{(.965)(-3.22)(-.0076\pm j.538)}$	$\frac{3.24(0)(-.013)(-1.65)}{(.965)(-3.22)(-.0076\pm j.538)}$
	P_{21e}	P_{22e}
	$\frac{6.38(0)(-.354\pm j2.93)}{(-.0272)(-2.7)(-.39\pm j2.96)}$	$\frac{-22.9(0)(-.352\pm j2.84)}{(-.0272(-2.7)(-.39\pm j2.96)}$

*Equivalent Plant.

TABLE C-3--Continued

	P_{11e}	P_{12e}
Mode 4:	$\frac{-12.8(0)(-.0126)(-1.52)}{(.965)(-3.22)(-.0076\pm j.538)}$	$\frac{6.24(0)(-.0125)(-1.58)}{(.965)(-3.22)(-.0076\pm j.538)}$
	P_{21e}	P_{22e}
	$\frac{31.7(0)(-.37\pm j3.46)}{(-.0272)(-2.7)(-.39\pm j2.96)}$	$\frac{-31.8(0)(-.358\pm j3.07)}{(-.0272)(-2.7)(-.39\pm j2.96)}$
	P_{11e}	P_{12e}
Mode 5:	$\frac{-12.8(0)(-.0126)(-1.52)}{(.965)(-3.22)(-.0076\pm j.538)}$	$\frac{-.229(0)(-.012)(-3.44)}{(.965)(-3.22)(-.0076\pm j.538)}$
	P_{21e}	P_{22e}
	$\frac{19(0)(-.382\pm j3.77)}{(-.0272)(-2.7)(-.39\pm j2.96)}$	$\frac{31.8(0)(-.358\pm j3.07)}{(-.0272)(-2.7)(-.39\pm j2.96)}$
	P_{11e}	P_{12e}
Mode 6:	$\frac{-12.03(0)(-.0126)(-1.51)}{(.965)(-3.22)(-.0076\pm j.538)}$	—
	P_{21e}	P_{22e}
	—	$\frac{-6.34(0)(-.375\pm j3.58)}{(-.0272)(-2.7)(-.39\pm j2.96)}$

TABLE C-4

EQUIVALENT PLANT MATRICES FOR FLIGHT CONDITION FOUR

Mode 1:	P_{11e}*	P_{12e}*
	$\frac{-34.4(0)(-.03)(-1.08)}{(-.0152\pm j.0234)(-8.01\pm j6.6)}$	—
	P_{21e}*	P_{22e}*
	--	$\frac{-25.8(0)(-.394\pm j4.47)}{(-.035)(-2.17)(-.5\pm j3.13)}$
Mode 2:	P_{11e}	P_{12e}
	$\frac{-17.9(0)(-.0302)(-1.06)}{(-.0152\pm j.0234)(-8.01\pm j6.6)}$	$\frac{4.11(0)(-.03)(-1.1)}{(-.0152\pm j.0234)(-.801\pm j6.6)}$
	P_{21e}	P_{22e}
	$\frac{23.3(0)(-.38\pm j3.85)}{(-.035)(-2.17)(-5\pm j3.13)}$	$\frac{-20(0)(-.4\pm j4.63)}{(-.035)(-2.17)(-.5\pm j3.13)}$
Mode 3:	P_{11e}	P_{12e}
	$\frac{-33.6(0)(-.03)(1.09)}{(-.0152\pm j.0234)(-8.01\pm j6.6)}$	$\frac{2.93(0)(-.035)(-.686)}{(-.0152\pm j.0234)(-.801\pm j6.6)}$
	P_{21e}	P_{22e}
	$\frac{1.77(0)(-.408\pm j4.92)}{(-.035)(-2.17)(-5\pm j3.13)}$	$\frac{-18.7(0)(-.39\pm j4.28)}{(-.035)(-2.17)(-.5\pm j3.13)}$

*Equivalent Plant.

TABLE C-4--Continued

Mode 4:	P_{11e}	P_{12e}
	$\frac{-17.2(0)(-.03)(-1.08)}{(-.0152\pm j.0234)(-8.01\pm j6.6)}$	$\frac{7.04(0)(-.03)(-.927)}{(-.0152\pm j.0234)(-.801\pm j6.6)}$
	P_{21e}	P_{22e}
	$\frac{25.1(0)(-.38\pm j3.93)}{(-.035)(-2.17)(-5\pm j3.13)}$	$\frac{-12.9(0)(-.394\pm j4.47)}{(-.035)(-2.17)(-.5\pm j3.13)}$
Mode 5:	P_{11e}	P_{12e}
	$\frac{-17.2(0)(-.03)(-1.08)}{(-.0152\pm j.0234)(-8.01\pm j6.6)}$	$\frac{1.19(0)(-.026)(-2.1)}{(-.0152\pm j.0234)(-.801\pm j6.6)}$
	P_{21e}	P_{22e}
	$\frac{21.5(0)(-.37\pm j3.75)}{(-.035)(-2.17)(-5\pm j3.13)}$	$\frac{-12.9(0)(-.39\pm j4.45)}{(-.035)(-2.17)(-.5\pm j3.13)}$
Mode 6:	P_{11e}	P_{12e}
	$\frac{-32.9(0)(-.03)(-1.1)}{(-.0152\pm j.0234)(-8.01\pm j6.6)}$	—
	P_{21e}	P_{22e}
	—	$\frac{-11.7(0)(-.38\pm j3.85)}{(-.035)(-2.17)(-.5\pm j3.13)}$

TABLE C-5

EQUIVALENT PLANT EQUATIONS FOR THE SINGLE INPUT-SINGLE OUTPUT SYSTEMS FOR FLIGHT CONDITION ONE ($\underline{P}_e^{-1} = [1/Q_{ij}]$)

Mode 1:	Q_{11}*	Q_{12}*
	$\frac{-2.18(0)(-.0175)(-.462)}{(.363)(-1.3)(-.0768\pm j.206)}$	--
	Q_{21}*	Q_{22}*
	--	$\frac{-5.55(0)(-.224\pm j1.03)}{(-.104)(-.684)(-.274\pm j1.91)}$
Mode 2:	Q_{11}	Q_{12}
	$\frac{-.939(0)(-.0162)(-.471)}{(.363)(-1.3)(-.0768\pm j.206)}$	$\frac{-16.8(0)(-.203\pm j.847)}{(-.104)(.684)(-.274\pm j1.91)}$
	Q_{21}	Q_{22}
	$\frac{-2.2(0)(-.0162)(-.471)(-.203\pm j.847)}{(.363)(-1.3)(-.0768\pm j.207)(-.302\pm j1.56)}$	$\frac{-4.45(0)(-.203\pm j.847)}{(-.104)(-.684)(-.274\pm j1.91)}$

*Equivalent Plant.

TABLE C-5--Continued

Mode 3:	Q_{11}	Q_{12}
	$\frac{-2.23(0)(-.018)(-.458)}{(.363)(-1.3)(-.0768\pm j.206)}$	$\frac{-60.9(0)(-.458)(-.236\pm j1.3)}{(-.104)(-.259)(-.684)(-.274\pm j1.91)}$
	Q_{21}	Q_{22}
	$\frac{-13.2(0)(-.018)(-.458)(-.236\pm j1.13)}{(.363)(-1.3)(-.078\pm j.207)(-.205\pm j.853)}$	$\frac{-3.34(0)(-.236\pm j1.13)}{(-.104)(-.684)(-.274\pm j1.91)}$
Mode 4:	Q_{11}	Q_{12}
	$\frac{-.934(0)(-.0256)(-.412)}{(.363)(-1.3)(-.0768\pm j.206)}$	$\frac{-16.3(0)(-.226\pm j.937)}{(-.104)(-.684)(-.274\pm j1.91)}$
	Q_{21}	Q_{22}
	$\frac{-.959(0)(-.412)(-.0256)(-.226\pm j.937)}{(.363)(-1.3)(-.0768\pm j.207)(-.282\pm j1.45)}$	$\frac{-2.38(0)(-.226\pm j.937)}{(-.104)(-.684)(-.274\pm j1.91)}$

Lower Bound--a_{22}

$$\frac{p}{R} = \frac{6.937}{(s + 0.75)(s + 2.5)(s + 3.7)}$$

Figures of Merit:

Peak Time, T_p = Very Large

Settling Time, T_s = 5.99 sec

Peak Value, M_p = 50.0

Loop Interaction Bound--b_{12}

$$\frac{q}{R} = \frac{0.04s\ (s + 1)(s + 10)}{(s + 0.75)(s + 5)(s^2 + 2s + 2)}$$

Figures of Merit:

Peak Time, M_p = 0.992 sec

Settling Time, T_s = 4.30 sec

Peak Value, M_p = 1.4 deg/sec

Loop Interaction Bound--b_{21}

$$\frac{p}{R} = \frac{0.335s\ (s + 1)(s + 10)}{(s + 0.75)(s + 5)(s^2 + 2s + 2)}$$

Figures of Merit:

Peak Time, T_p = 0.992 sec

Settling Time, T_s = 4.30 sec

Peak Value, M_p = 2.344 deg/sec

Roll Rate Models

Upper Bound--b_{22}

$$\frac{p}{R} = \frac{2.136\ (s+1.3)}{(s^2 + 2.667s + 2.776)}$$

Figures of Merit:

Peak Time, T_p = 1.538 sec

Settling Time, T_s = 3.01 sec

Peak Value, M_p = 55.0 deg/sec

Pitch Rate Models

Upper Bound--b_{11}

$$\frac{q}{R} = \frac{4.167\ (s + 2.667)}{(s^2 + 5.334s + 11.113)}$$

Figures of Merit:

Peak Time, T_p = 0.785 sec

Settling Time, T_s = 1.5 sec

Peak Value, M_p = 11.0 deg/sec

Lower Bound--a_{11}

$$\frac{q}{R} = \frac{63.75}{(s + 1.5)(s + 4.25)(s + 10)}$$

Figures of Merit:

Peak Time, T_p = Very Large

Settling Time, T_s = 3.01 sec

Peak Value, M_p = 10 deg/sec

Appendix D: Pitch Rate and Roll Rate Response Models

This appendix contains the transfer function models for pitch rate and roll rate. These models are synthesized with desired specifications in mind, and the models are used to develop bounds on the loop transmission. Also listed in this appendix are the figures of merit for the response models. See Chapter IV for the time and frequency domain plots of these models.

TABLE C-8--Continued

	Q_{11}	Q_{12}
Mode 5:	$\frac{-19.2(0)(-.03)(-1.06)}{(.152\pm j.0234)(-.801\pm j6.59)}$	$\frac{-208.2(0)(-1.16)(-.406\pm j4.39)}{(-.0345)(-2.17)(-2.1)(-.5\pm j3.13)}$
	Q_{21}	Q_{22}
	$\frac{-11.5(0)(-.03)(-1.16)}{(-.0152\pm j.0234)(-.801\pm j6.59)}$	$\frac{-14.4(0)(-.406\pm j4.39)}{(-.0345)(-2.17)(.5\pm j3.13)}$
	Q_{11}	Q_{12}
Mode 6:	$\frac{-32.9(0)(-.03)(-1.1)}{(.152\pm j.0234)(-.801\pm j6.59)}$	--
	Q_{21}	Q_{22}
	—	$\frac{-11.7(0)(-.377\pm j3.85)}{(-.0345)(-2.17)(.5\pm j3.13)}$

TABLE C-8--Continued

	Q_{11}	Q_{12}
Mode 3:	$\frac{-33.4(0)(-.03)(-1.09)}{(.152\pm j.0234)(-.801\pm j6.59)}$	$\frac{-213.6(0)(-1.09)(-.388\pm j4.28)}{(-.686)(-2.17)(-.036)(-.5\pm j3.13)}$
	Q_{21}	Q_{22}
	$\frac{-352.7(0)(-.03)(-1.09)(-.388\pm j4.28)}{(-.0151\pm j.0234)(-.408\pm j4.92)(-.801\pm j6.59)}$	$\frac{-18.6(0)(-.39\pm j4.28)}{(-.0345)(-2.17)(.5\pm j3.13)}$
	Q_{11}	Q_{12}
Mode 4:	$\frac{-3.5(0)(-.03)(-1.34)}{(.152\pm j.0234)(-.801\pm j6.59)}$	$\frac{-6.44(0)(-1.34)(-.62\pm j6.08)}{(-.0345)(-.927)(-2.17)(-.5\pm j3.13)}$
	Q_{21}	Q_{22}
	$\frac{-1.81(0)(-.0286)(-1.34)(-.621\pm j6.08)}{(-.0152\pm j.0234)(-.38\pm j3.93)(-.801\pm j6.59)}$	$\frac{-2.64(0)(-.621\pm j6.08)}{(-.0345)(-2.17)(.5\pm j3.13)}$

TABLE C-8

EQUIVALENT PLANT EQUATIONS FOR THE SINGLE INPUT-SINGLE OUTPUT SYSTEMS FOR FLIGHT CONDITION FOUR ($\underline{P}_e^{-1} = [11Q_{ij}]$)

Mode 1:	Q_{11}*	Q_{12}*
	$\frac{-34.4(0)(-.03)(-1.08)}{(.152\pm j.0234)(-.801\pm j6.59)}$	--
	Q_{21}*	Q_{22}*
	--	$\frac{-25.8(0)(-.394\pm j4.47)}{(-.0345)(-2.17)(.5\pm j3.13)}$
Mode 2:	Q_{11}	Q_{12}
	$\frac{-13.1(0)(-.0303)(-1.06)}{(.152\pm j.0234)(-.801\pm j6.59)}$	$\frac{-63.8(0)-.405\pm j4.89)}{(-.0345)(-2.17)(-.5\pm j3.13)}$
	Q_{21}	Q_{22}
	$\frac{(-11.3(0)(-.0303)(-1.06)(-.405\pm j4.89)}{(-.0152\pm j.0234)(-.38\pm j3.85)(-.801\pm j6.59)}$	$\frac{-14.6(0)(-.405\pm j4.89)}{(-.0345)(-2.17)(.5\pm j3.13)}$

*Equivalent Plant.

TABLE C-7--Continued

	Q_{11}	Q_{12}
Mode 5:	$\frac{-12.98(0)(-.0126)(-1.55)}{(.965)(-3.22)(-.0076\pm j.0538)}$	$\frac{1810.(0)(-1.55)(.354\pm j3.08)}{(-2.7)(-3.44)(-.0272)(-.391\pm j2.96)}$
	Q_{21}	Q_{22}
	$\frac{-21.8(0)(-.0126)(-1.55)(-.354\pm j3.08)}{(.965)(-3.22)(-.0076\pm j.0538)(-.382\pm j3.77)}$	$\frac{-32.2(0)(-.354\pm j3.08)}{(-.0272)(-2.7)(-.39\pm j2.96)}$
Mode 6:	Q_{11}	Q_{12}
	$\frac{-24.1(0)(-.0126)(-1.51)}{(.965)(-3.22)(-.0076\pm j.0538)}$	—
	Q_{21}	Q_{22}
	—	$\frac{-12.68(0)(-.375\pm j3.58)}{(-.0272)(-2.7)(-.39\pm j2.96)}$

TABLE C-7--Continued

Mode 3:	Q_{11}	Q_{12}
	$\frac{-23.97(0)(-.0126)(-1.51)}{(.965)(-3.22)(-.0076\pm j.0538)}$	$\frac{-169.2(0)(-.352\pm j2.84}{(-.0272(-2.7)(-.39\pm j2.96)}$
	Q_{21}	Q_{22}
	$\frac{-85.8(0)(-.0126)(-1.61)}{(.0076)(.965)(-3.22)}$	$\frac{-22.02(0)(-.352\pm j2.84)}{(-.0272)(-2.7)(-.39\pm j2.96)}$
Mode 4:	Q_{11}	Q_{12}
	$\frac{-6.62(0)(-.0127)(-1.43)}{(.965)(-3.22)(-.0076\pm j.0538)}$	$\frac{-33.8(0)(-.364\pm j\pm 2.64)}{(-.0272)(-2.7)(-.391\pm j2.96)}$
	Q_{21}	Q_{22}
	$\frac{-6.62(0)(-.013)(-1.43)(-.364\pm j2.64)}{(.965)(-.0076\pm j.0538)(-3.22)(-.371\pm j3.46)}$	$\frac{-16.4(0)(-.364\pm j2.64)}{(-.0272)(-2.7)(-.39\pm j2.96)}$

TABLE C-7

EQUIVALENT PLANT EQUATIONS FOR THE SINGLE INPUT-SINGLE OUTPUT SYSTEMS FOR FLIGHT CONDITION THREE ($\underline{P}_e^{-1} = [11Q_{ij}]$)

Mode 1:	Q_{11}*	Q_{12}*
	$\frac{-25.7(0)(-.0126)(-1.52)}{(.965)(-3.22)(-.0076\pm j.0538)}$	--
	Q_{21}	Q_{22}*
	--	$\frac{-63.7(0)(-.358\pm j3.07)}{(-.0272)(-2.7)(-.39\pm j2.96)}$
Mode 2:	Q_{11}	Q_{12}
	$\frac{-14.98(0)(-.0126)(-1.52)}{(.965)(-3.22)(-.0076\pm j.0538)}$	$\frac{285.9(0)(-.358\pm j3.06)}{(-.0272)(2.7)(-.39\pm j2.96)}$
	Q_{21}	Q_{22}
	$\frac{-33.9(0)(-.013)(-1.5)(-.358\pm j3.06)}{(-.0076\pm j.0538)(-.375\pm j3.58)(.965)(-3.22)}$	$\frac{-62.99(0)(-.358\pm j3.06)}{(-.0272)(-2.7)(-.39\pm j2.96)}$

*Equivalent Plant.

TABLE C-6--Continued

	Q_{11}	Q_{12}
Mode 5:	$\frac{-2.68(0)(-.0096)(-.609)}{(1.167)(-2.02)(-.0065\pm j.078)}$	$\frac{-44.6(0)(-.208\pm j1.63)}{(-.078)(-.326)(-.211\pm j1.95)}$
	Q_{21}	Q_{22}
	$\frac{-6.06(0)(-.0096)(-.609)(-.208\pm j1.63)}{(1.167)(-.0065\pm j.078)(-.256\pm j2.3}$	$\frac{-9.44(0)(-.208\pm j1.63)}{(-.078)(-.827)(-.211\pm j1.95)}$
	Q_{11}	Q_{12}
Mode 6:	$\frac{-5.86(0)(-.01)(-.55)}{(1.167)(-2.02)(-.0065\pm j.078)}$	--
	Q_{21}	Q_{22}
	--	$\frac{-3.396(0)(-.244\pm j2.1)}{(-.078)(-.827)(-.211\pm j1.95)}$

TABLE C-6--Continued

Mode 3:	Q_{11}	Q_{12}
	$\frac{-2.72(0)(-.0098)(-.577)}{(1.167)(-2.02)(-.0065\pm j.078)}$	$\frac{-71.2(0)(-.218\pm j1.61)}{(-.078)(-.827)(-.211\pm j1.95)}$
	Q_{21}	Q_{22}
	$\frac{-7.68(0)(-.0098)(-.577)(-.218\pm j1.61)}{(1.167)(-2.03)(-.0065\pm j.078)(-.244\pm j2.1)}$	$\frac{-17.5(0)(-.218\pm j1.61)}{(-.078)(-.827)(-.211\pm j1.95)}$
Mode 4:	Q_{11}	Q_{12}
	$\frac{-2.24(0)(-.011)(-.485)}{(1.167)(-2.02)(-.0065\pm j.078)}$	$\frac{-27.8(0)(-.485)(-.232\pm j1.59)}{(-.078)(-.716)(-.827)(-.211\pm j1.95}$
	Q_{21}	Q_{22}
	$\frac{-2.6(0)(-.011)(-.485)(-.232\pm j1.59}{(1.167)(-2.03)(-.0065\pm j.078)(-.238\pm j1.99)}$	$\frac{-7.88(0)(-.232\pm j1.59)}{(-.078)(-.827)(-.211\pm j1.95)}$

TABLE C-6

EQUIVALENT PLANT EQUATIONS FOR THE SINGLE INPUT-SINGLE OUTPUT SYSTEMS FOR FLIGHT CONDITION TWO ($\underline{P}_e^{-1} = [1/Q_{ij}]$)

Mode 1:	Q_{11}*	Q_{12}*
	$\frac{-5.92(0)(-.01)(-.562)}{(1.167)(-2.02)(-.0065\pm j.078)}$	—
	Q_{21}*	Q_{22}*
	--	$\frac{-20.8(0)(-.223\pm j1.7)}{(-.078)(-.827)(-.211\pm j1.95)}$
Mode 2:	Q_{11}	Q_{12}
	$\frac{-5.87(0)(-.01)(-.552)}{(1.167)(-2.02)(-.0065\pm j.078)}$	$\frac{-577.2(0)(-.223\pm j1.7)}{(.078)(-.827)(-.211\pm j1.95)}$
	Q_{21}	Q_{22}
	$\frac{-28.03(0)(-.01)(-.552)}{(1.167)(-2.03)(-.0065\pm j.078)}$	$\frac{-10.4(0)(-.223\pm j1.7)}{(-.078)(-.827)(-.211\pm j1.95)}$

*Equivalent Plant.

TABLE C-5--Continued

Mode 5:	Q_{11}	Q_{12}
	$\frac{-.86(0)(-.0071)(-.534)}{(.363)(-1.3)(-.0768\pm j.206)}$	$\frac{-5.96(0)(-.17\pm.743)}{(-.104)(-.684)(-.274\pm j1.91)}$
	Q_{21}	Q_{22}
	$\frac{-1.51(0)(-.0071)(-.534)(-.17\pm j.743)}{(.363)(-1.3)(-.077\pm j.207)(-.336\pm j1.74)}$	$\frac{-2.19(0)(.17\pm j.743)}{(-.104)(-.684)(-.274\pm j1.91)}$
Mode 6:	Q_{11}	Q_{12}
	$\frac{-2.24(0)(-.018)(-.457)}{(.363)(-1.3)(-.0768\pm j.206)}$	--
	Q_{21}	Q_{22}
	--	$\frac{-1.07(0)(-.302\pm j1.56)}{(-.104)(-.684)(-.274\pm j1.91)}$

Appendix E: Templates of Q_{11} and Q_{22}

This appendix contains templates of Q_{11} and Q_{22} at various frequencies.

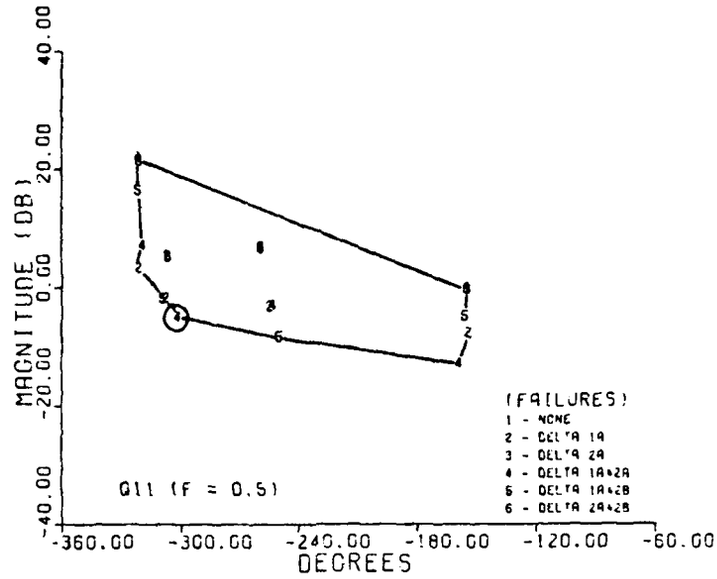

Fig. E-1(a). Template of Q_{11} at ω = 0.5 Rad/Sec

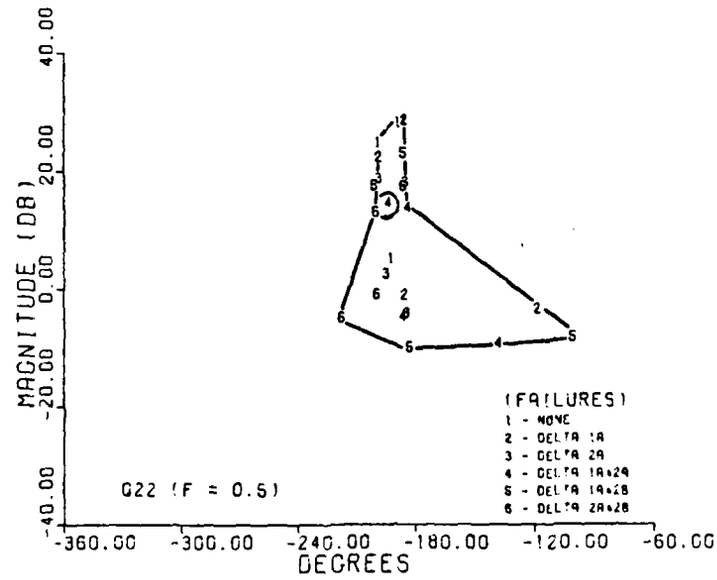

Fig. E-1(b). Template of Q_{22} at ω = 0.5 Rad/Sec

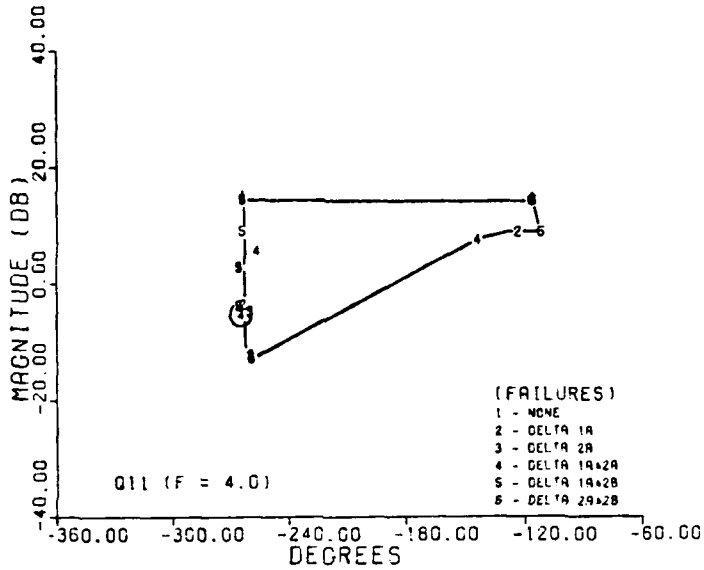

Fig. E-2(a). Template of Q_{11} at ω = 4.0 Rad/Sec

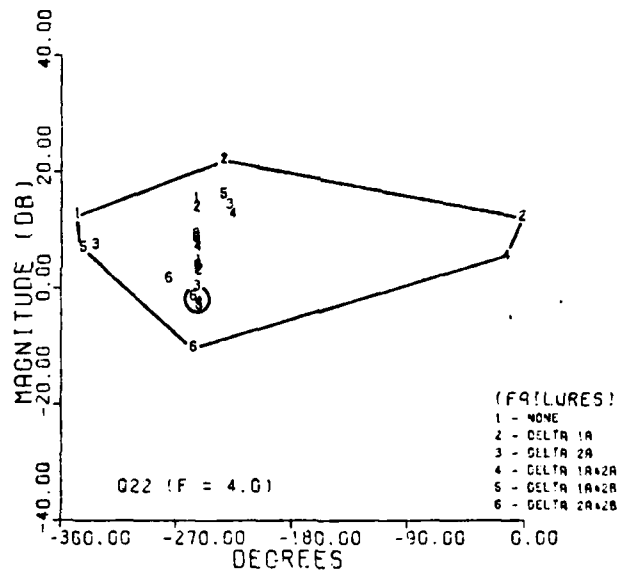

Fig. E-2(b). Template of Q_{22} at ω = 4.0 Rad/Sec

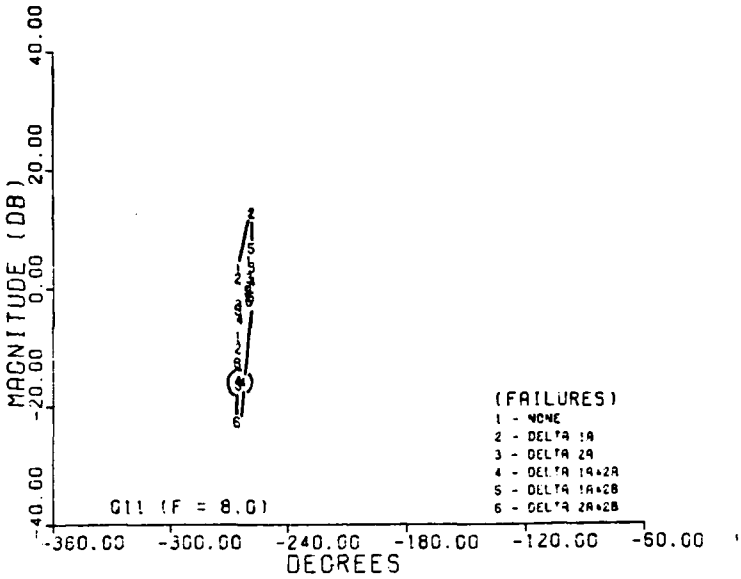

Fig. E-3(a). Template of Q_{11} at ω = 8 Rad/Sec

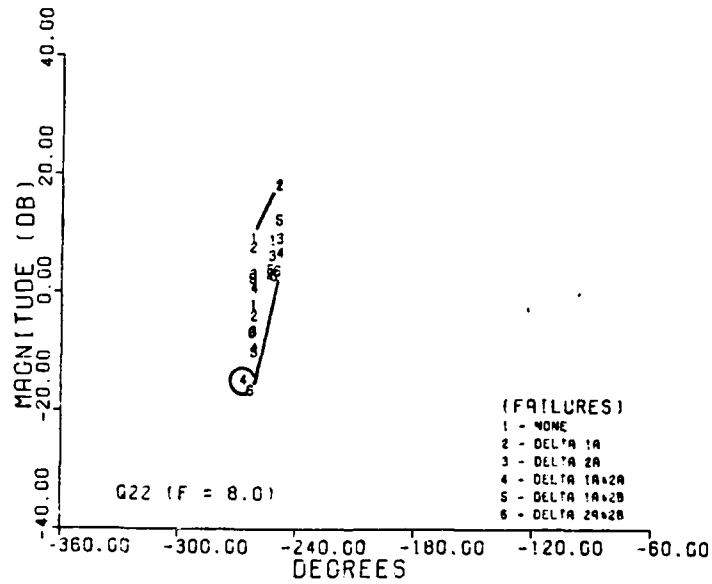

Fig. E-3(b). Template of Q_{22} at ω = 8 Rad/Sec

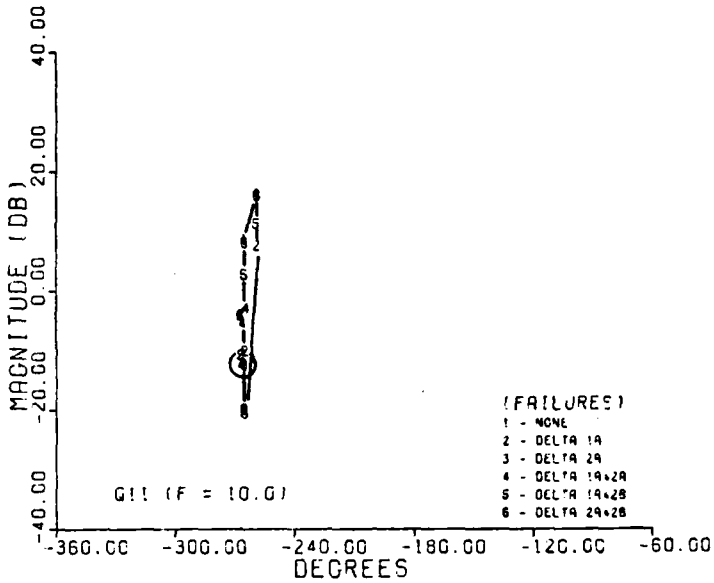

Fig. E-4(a). Template of Q_{11} at ω = 10 Rad/Sec

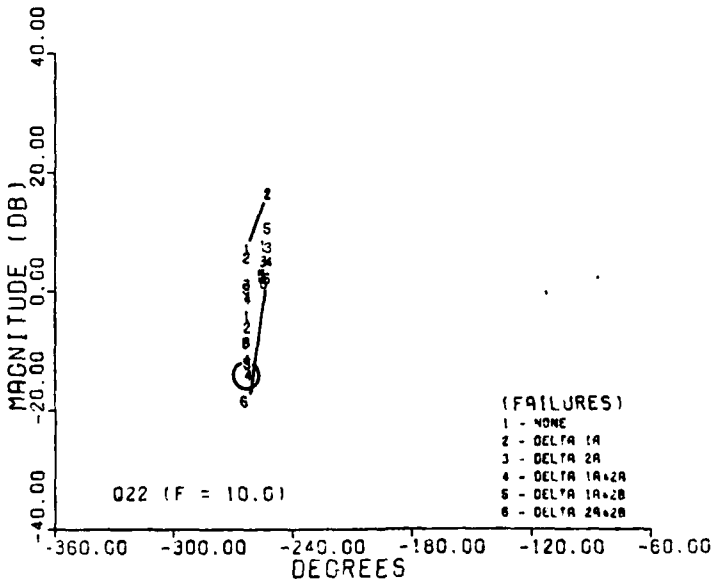

Fig. E-4(b). Template of Q_{22} at ω = 10 Rad/Sec

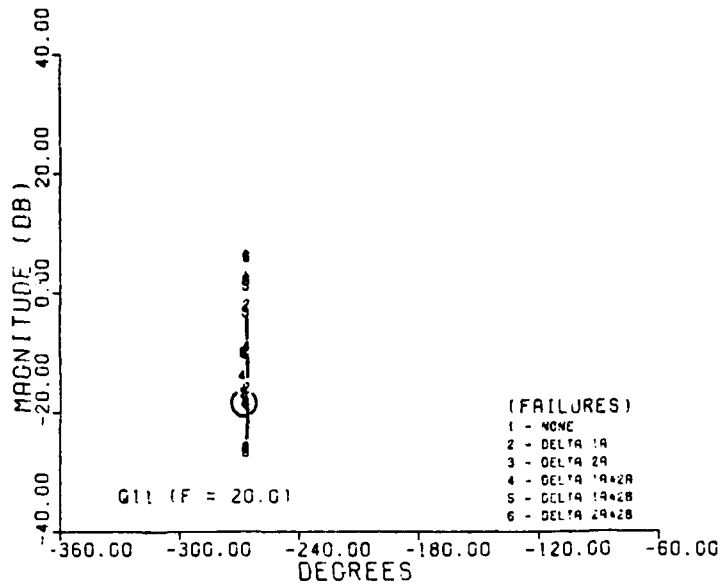

Fig. E-5(a). Template of Q_{11} at ω = 20 Rad/Sec

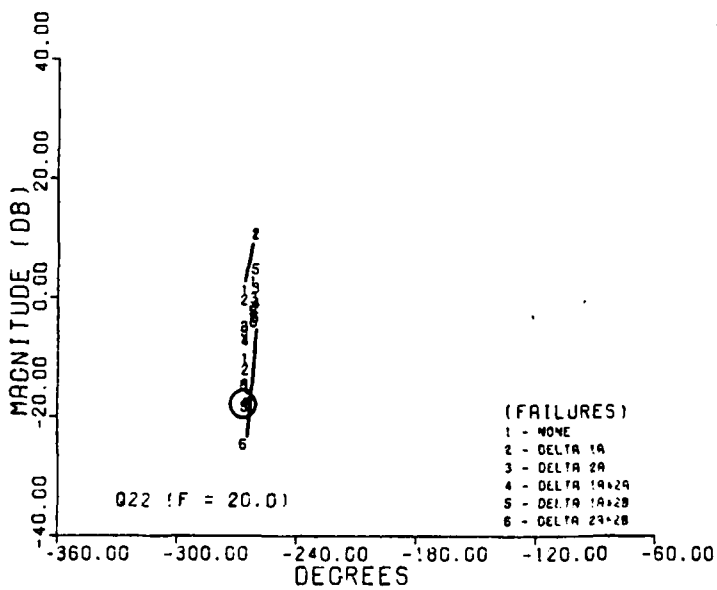

Fig. E-5(b). Template of Q_{22} at ω = 20 Rad/Sec

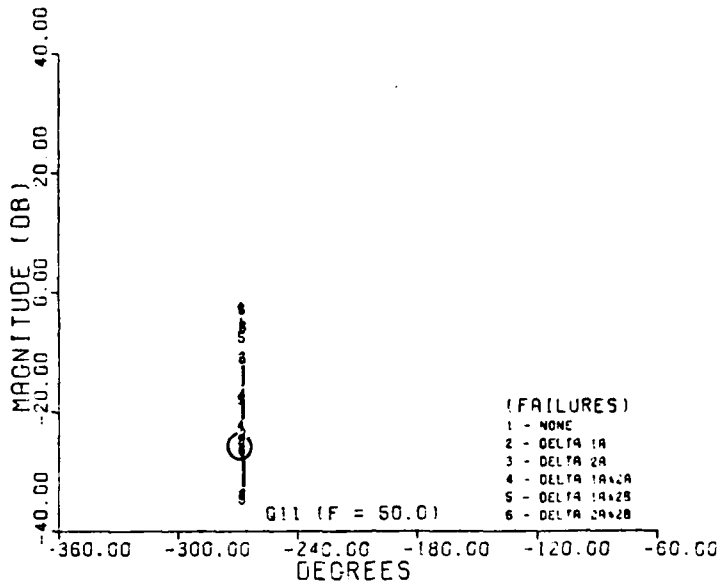

Fig. E-6(a). Template of Q_{11} at ω = 50 Rad/Sec

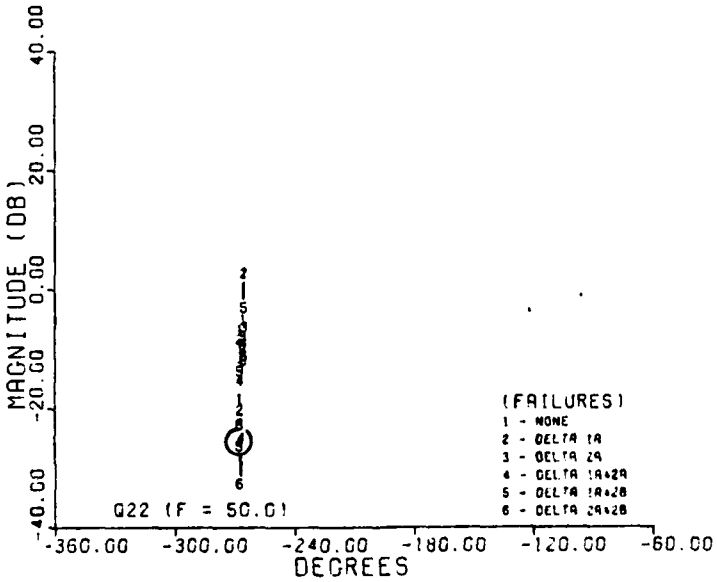

Fig. E-6(b). Template of Q_{22} at ω = 50 Rad/Sec

Appendix F: Simulation Programs

The computer programs listed in this appendix are the programs used to conduct the simulation of the system represented by Figure 2-1. The simulation is structured around a main program and three subroutines. The main program is called Zsimu; Zsimu calls subroutines Derv, Zdata, and Degol. Poles and zeros of the basic plant equations are listed in Zdata.

Data for the four basic plant equations (P_{ij}) at each flight condition are listed in Zdata. These data are passed as poles and zeros to Zsimu. Derivatives of the output variables are passed from Derv to Zsimu.

Subroutine Derv uses the state-variable format to write basic plant, prefilter, and compensator equations. Desired outputs are derived from the state equations based upon the structure of the system being simulated. For this simulation, a maximum of 30 state-variables can be defined in Derv. This limitation is due to the subroutine Degol. Position saturation for the elevators and flaperons is also included in this subroutine. Derivatives of the output variables are passed to the main program for integration.

The main program Zsimu takes the outputs of Derv and integrates these using the subroutine Degol. Degol is an integration routine for linear, ordinary differential equations similar to the program ODE. The "case" block of Zsimu allows inputs (IR), flight conditions (IC), or CSC modes (IM) to be selected as desired. The "integration" block allows the integration time and the number of points in the integration to be specified. For this simulation the outputs of Zsimu are pitch rate, roll rate, and the four surface deflections. These outputs are identified by the variables YY1 to YY6, respectively. Integration time is denoted by the variable XX. If other outputs are desired, they are defined in Derv. A step or ramp command input may be specified in the "Degol" block.

Zsimu

```
      PROGRAM ZSIMU(INPUT,OUTPUT,DATALP,DATAOUT,PLOT,TAPE9,
     +TAPE6=OUTPUT,TAPE7=DATALP,TAPE8=DATAOUT)

C
C
C  UPDATE% AUG. 15,  1984
C  ORIGINAL% AUG.12,  1984
C
C***************   DIMENSION   ***************
C
C
C-----  DEGOL  -----
      REAL Y(30)
      EXTERNAL DERV
      DIMENSION XX(500),YY(500),YY1(500),YY2(500),YY3(500),
      DIMENSION YY4(500),YY5(500),YY6(500)
C
C-----  PLANT  -----
C
      DIMENSION VP11K(4),VP11Z1(4),VP11Z2(4),VP11Z3(4)
C
      DIMENSION VP12K(4),VP12Z1(4),VP12Z2(4),VP12Z3(4)
C
      COMPLEX VP11P1(4),VP11P2(4),VP11P3(4),VP11P4(4)
C
      DIMENSION VP21K(4),VP21Z1(4)
      COMPLEX VP21Z2(4),VP21Z3(4)
C
      DIMENSION VP22K(4),VP21()
      COMPLEX VP22Z2(4),VP22Z3(4)
C
      DIMENSION VP22P1(4),VP22P2(4)
      COMPLEX VP22P3(4),VP22P4(4)

C
C***************   COMMON   ***************
C
C-----  DERV  -----
C
      COMMON/P11Z/ P11K,P11Z1,P11Z2,P11Z3
      COMMON/P11P/ P11P1,P11P2,P11P3,P11P4
C
      COMMON/P12Z/ P12K,P12Z1,P12Z2,P12Z3
C
      COMMON/P21Z/ P21K,P21Z1,P21Z2,P21Z3
```

```
C
      COMMON /P22Z/ P22K,P22Z1,P22Z2,P22Z3
      COMMON /P22P/ P22P1,P22P2,P22P3,P22P4
C
C
      COMMON /F/ F1K,F1P,F2K,F2P
C
      COMMON /G1Z/G1K,G1Z1,G1Z2,G1Z3,G1Z4
      COMMON /G1P/G1P1,G1P2,G1P3,G1P4
C
      COMMON /G2Z/G2K,G2Z1,G2Z2,G2Z3,Z2Z4
      COMMON /G2P/G2P1,22G2P3,G2P4
C
      COMMON /R/ R1,R2
      COMMON /U/ U12,U21
      COMMON /C/ C1,C2
      COMMON /D/ D1A,D1B,D2A,D2B
      COMMON /IS/ IS1A,IS1B,IS2A,IS2B
C
C-----  MONITOR  -----
      COMMON /M/ F1,F2,G1,G2,E1,E2,D11,D12,D21,D22,
      COMMON /M/ C11,C12,C21,C22
C-----  ZDATA  -----
C
      COMMON /VP11Z/VP11K,VP11Z1,VP11Z2,VP11Z3
      COMMON /VP11P/VP11P1,VP11P2,VP11P3,VP11P4
C
      COMMON /VP12Z/VP12K,VP12Z1,VP12Z2,VP12Z3
C
      COMMON /VP21Z/VP21K,VP21Z1,VP21Z2,VP21Z3
C
      COMMON /VP22Z/VP22K,VP22Z1,VP22Z2,VP22Z3
      COMMON /BP22P/VP22P1,VP22P2,VP22P3,VP22P4
C
C-----  CASE  -----
C
      DIMENSION IRV(30),ICV(30),IMV(30)
C
      DATA NC/1/
      DATA IRV/1,1,1,1,1,1,2,23*0/
      DATA ICV/2,2,4,2,4,2,2,23*0/
      DATA IMV/4,2,3,4,5,6,7,23*0/
C
C***************  MAIN PROGRAM  ***************
C
C-----  P(S)  -----
C
      CALL ZDATA
C
C-----  F1(S)  -----
```

```
      F1K = 2.
      F1P = 2.
C
C-----  F2(S) -----
      F2K = 2.
C
      F2P = 2.
C
C-----  G1(S)  -----
      G1K = -660000.
C
      G1Z1 = 4.
      G1Z2 = 100.
      G1Z3 = .013
      G1Z4 = .006
C     G1Z3 = .013 + .006
C     G1Z4 = .013*.006
C
      G1P1 = .0223
      G1P2 = 25.
C     G1P3 = 630.
C     G1P4 = 630.
      G1P3 =60 + 630.
      G1P4 = 630.*630.
C
C-----  G2(S)  -----
      G2K = -36800.
      G2Z1 = 3.
      G2Z2 = 900.
      G2Z3 = 2.
      G2Z4 = 4.
C     G2Z3 = 1. + 10.
C     G2Z4 = 10.
C
      G2P1 = .25
      G2P2 = 50.
C     G2P3 = 158.
C     G2P4 = 3750.
      G2P3 = 158. + 3750.
      G2P4 = 158.*3750.
C
C
C-----  INPUT R(I)  -----
      R1 = 10.
      R2 = 50.
C
C-----  SCALE U(I,J)  -----
      U12 = .25
      U21 = .25
C
C
```

```
C***************  DO CASES  ***************
C
      DO 10 III = 1,NC
C
         IR = IRV(III)
         IC = ICV(III)
         IM = IMV(III)
C        R1 = 0.
         R2 = 0.
C        FIR.EQ. 1) R1 = 10.
C        IF(IR .EQ. 2) R2 = 50.
C
         IS1A = 1
         IS1B = 1
         IS2A = 1
         IS2B = 1
         IF(IM .EQ. 2) IS1A = 0
         IF(IM .EQ. 3) IS2A = 0
         IF(IM .EQ. 4) IS1A = 0
         IF(IM .EQ. 4) IS2A = 0
         IF(IM .EQ. 5) IS1A = 0
         IF(IM .EQ. 5) IS2B = 0
         IF(IM .EQ. 6) IS2A = 0
         IF(IM .EQ. 6) IS2B = 0
         IF(IM .EQ. 7) IS1A = 0
         IF(IM .EQ. 7) IS1B = 0
C
C-----  P11(S)  -----
         P11K = VP11K(IC)*.5
         P11Z1 =-VP11Z1(IC)
C        P11Z2 = VP11Z2(IC)
C        P11Z3 = VP11Z3(IC)
         P11Z2 = -VP11Z2(IC) - VP11Z3(IC)
         P11Z3 = VP11Z2(IC) 1Z3(IC)
C
C        P11P1 = -2.*REAL(VP11P1(IC))
C        P11P2 = CABS(VP11P1(IC))*2
         P11P1 = -REAL(VP11P1(IC)+VP11P2(IC))
         P11P2 = REAL(VP11P1(IC)*VP11P2(IC))
         P11P3 = -2.*REAL(VP11P3(IC))
         P11P4 = CABS(VP11P3(IC))*2
C-----  P12(S)  -----
         P12K = VP12K(IC)*.5
         P12Z1 = -VP12Z1(IC)
C        P12Z2 = VP12Z2(IC)
C        P12Z3 = VP12Z3(IC)
         P12Z2 = -VP12Z2(IC) - VP12Z3(IC)
         P12Z3 = VP12Z2(IC)*VP12Z3(IC)
C
C-----  P21(S)  -----
         P21K =VP21K(IC)*.5
```

```
          P21Z1 = -VP21Z1(IC)
          P21Z2 = -2.*REAL(VP21Z2(IC))
          P21Z3 = CABS(VP21Z2(IC))*2
C
C-----  P22(S)  -----
      P22K =VP22K(IC)*.5
          P22Z1 = -VP22Z1(IC)
          P22Z2 = -2.*REAL(VP22Z2(IC))
          P22Z3 = CABS(VP22Z2(IC))*2
C
C         P22P1 = VP22P1(IC)
C         P22P2 = VP22P2(IC)
          P22P1 = -VP22P1(IC) - VP22P2(IC)
          P22P2 = VP22P1(IC)*VP22P2(IC)
          P22P3 = -2.*REAL(VP22P3(IC))
          P22P4 = CABS(VP22P3(IC))*2
C
C
C***************  INTEGRATION  ***************
C
      NE = 28
      AE = 1.E-5
      RE = 1.E-6
      MAX = 1000
      H = 1.E-4
      N = 60000
      NP = 300
      T0 = 0.
      T1 = H
C
C-----  INITIAL CONDITION  -----
      C1 = 0.
      C2 = 0.
      D1A = 0.
      D1B = 0.
      D2A = 0.
      2 = 0.
C
      DO 30 I = 1,NE
 30      Y(I) = 0.
C
C-----  ITERATION  -----
      II = 0
      IIXY = 1
      KKXY = N/NP
      IF(KKXY .LT. 1) KKXY = 1
C
      DO 40 I = 1,N
C
```

AD-A151 771 FLIGHT CONTROL SYSTEM RECONFIGURATION DESIGN USING QUANTITATIVE FEEDBACK THEORY(U) AIR FORCE INST OF TECH WRIGHT-PATTERSON AFB OH SCHOOL OF ENGI.. P B ARNOLD 3/3

UNCLASSIFIED DEC 84 AFIT/GE/ENG/84D-15 F/G 1/4 NL

END

FILMED

DTIC

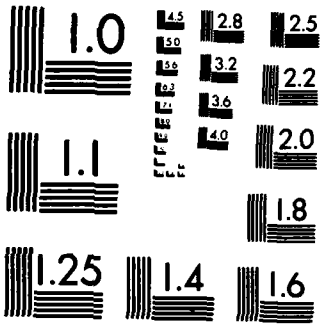

MICROCOPY RESOLUTION TEST CHART
NATIONAL BUREAU OF STANDARDS-1963-A

```
C-----  YY(II)  -----
         IF(I .EQ. IIXY) THEN
            II = II + 1
C           WRITE(8,122)II,G1,G2,D11,D12,D21,D22
C           WRITE(8,122)II,C1,C2,C11,C12,C21,C22
            PRINT 122,II,T0,C1,C2,D1A,D1B,D2A,D2B
            XX(II)= T0
            YY1(II) = C1
            YY2(II) = C2
            YY3(II) = D1A
            YY4(II) = D1B
            YY5(II) = D2A
            YY6(II) = D2B
            IIXY = IIXY + KKXY
         END IF
C
C-----  CALL DEGOL  -----
C        PRINT 122,I,T0,C1,C2,D1A,D1B,D2A,D2B
         IK = 1
         CALL DEGOL(DERV,NE,Y,T0,T1,RE,AE,IK,MAX)
         IF(IK .NE. 2) THEN
            PRINT *,IK,T0,T1
            STOP
         END IF
         T1 =T1 + H
C
C         IF(T1 .GT. 5.) R1 = 0.
C         IF(T1 .GT. 5.) R2 = 0.
C     IF(IR .EQ. 1 .AND. T1 .LE. .5) R1 = 20.*T1
      IF(IR .EQ. 1 .AND. T1 .GT. .5) R1 = 10.
      IF(IR .EQ. 1 .AND. T1 .GE. 5.) R1 = 0.
C
     .IF(IR .EQ. 2 .AND. T1 .LE. 1.) R2 = 50.*T1
      IF(IR .EQ. 2 .AND. T1 .GT. 1.) R2 = 50.
      IF(IR .EQ. 2 .AND. T1 .GE. 5.) R2 = 0.
C
 40   CONTINUE
C
C***************  PLOT  ***************
    NY = II
      PRINT *,NXY
C
      WRITE(8,121)NXY
C     WRITE(7,121)NXY
      DO 50 I = 1,NXY
         WRITE(8,122)I,XX(I),YY1(I),YY2(I),YY3(I),
           YY4(I),YY5(I),YY6(I)
         WRITE(7,122)I,XX(I),YY1(I),YY2(I),YY3(I),
           YY4(I),YY5(I),YY6(I)
 50   CONTINUE
C
      CALL LPL(NXY, XX, YY1,IM)
```

```
C
C-----  END CASES LOOP  -----
 10   CONTINUE
C
C***************  PRINT OUT  ***************
C
      CALL LPRINT(1)
      CALL LPL1(NXY,XX,YY2,1)
      CALL LPRINT(2)
C
C
C***************  FORMAT  ***************
 121  FORMAT(1X,I5)
 122  FORMAT(1X,I5,7(1X,E9.3))
C
      RETURN
      END
C
```

Degol

```
C     SUBROUTINE DEGOL
C
      SUBROUTINE DEGOL(F,NEQN,Y,T,TOUT,RELERR,ABSERR,IFLAG,
         ITMAX)
      INTEGER K
      REAL HOLD
      LOGICAL START,CRASH,STIFF
      DIMENSION Y(NEQN),PSI(12)
      DIMENSION YY(30),WT(30),PHI(30,16),P(30),YP(30),
         YPOUT(30)
      EXTERNAL F
      DATA FOURU/.44E-15/
      MAXNUM=MAX0(500,ITMAX)
      IF(NEQN .LT. 1 .OR. NEQN .GT. 30) GO TO 10
      IF(T .EQ. TOUT) GO TO 10
      IF(RELERR .LT. 0.0 .OR. ABSERR .LT. 0.0) GO TO 10
      EPS = AMAX1(RELERR,ABSERR)
      IF(EPS .LE. 0.0) GO TO 10
      IF(IFLAG .EQ. 0) GO TO 10
      ISN = ISIGN(1,IFLAG)
      IFLAG = IABS(IFLAG)
      IF(IFLAG .EQ. 1) GO TO 20
      IF(IFLAG .GE. 2 .AND. IFLAG .LE. 5) GO TO 20
 10   IFLAG = 6
      RETURN
 20   DEL = TOUT - T
      ABSDEL = ABS(DEL)
      TEND = T + 10.0*DEL
      IF(ISN .LT. 0) TEND = TOUT
      NOSTEP = 0
      KLE4 = 0
      STIFF = .FALSE.
      RELEPS = RELERR/EPS
      ABSEPS = ABSERR/EPS
      IF(IFLAG .EQ. 1) GO TO 30
      IF(ISNOLD .LT. 0) GO TO 30
      IF(DELSGN*DEL .GT. 0.0) GO TO 50
C
C   ON START AND RESTART ALSO SET WORK VARIABLES X AND YY(*),
C   STORE THE DIRECTION OF INTEGRATION AND INITIALIZE THE
C   STEP SIZE
C
 30   START = .TRUE.
      X = T
      DO 40 L = 1,NEQN
```

```
 40       YY(L) = Y(L)
      DELSGN = SIGN(1.0,DEL)
      H = SIGN(AMAX1(ABS(TOUT-X),FOURU*ABS(X)),TOUT-X)
C
C   IF ALREADY PAST OUTPUT POINT,  INTERPOLATE AND RETURN
C
 50   IF(ABS(X-T) .LT. ABSDEL) GO TO 60
      CALL INTRP(X,YY,TOUT,Y,YPOUT,NEQN,KOLD,PHI,PSI)
      IFLAG = 2
      T = TOUT
      TOLD = T
      ISNOLD = ISN
      RETURN
C
C   IF CANNOT GO PAST OUTPUT POINT AND SUFFICIENTLY CLOSE,
C   EXTRAPOLATE AND RETURN
C
 60   IF(ISN .GT. 0 .OR. ABS(TOUT-X) .GE. FOURU*ABS(X))
         GO TO 80
      H = TOUT - X
      CALL F(X,YY,YP)
      DO 70 L = 1,NEQN
 70      Y(L) = YY(L) + H*YP(L)
      IFLAG = 2
      T = TOUT
      TOLD = T
      ISNOLD = ISN
      RETURN
C
C   TEST FOR TOO MUCH WORK
C
 80   IF(NOSTEP .LT. MAXNUM) GO TO 100
      IFLAG = ISN*4
      IF(STIFF) IFLAG = ISN*5
      DO 90 L = 1,NEQN
 90      Y(L) = YY(L)
      T = X
      TOLD = T
      ISNOLD = 1
      RETURN
C
C   LIMIT STEP SIZE, SETWEIGHT VECTOR AND A STEP
C
 100  H = SIGN(AMIN1(ABS(H),ABS(TEND-X)),H)
      DO 110 L = 1,NEQN
 110     WT(L) = RELEPS*ABS(YY(L)) + ABSEPS
      CALL STEP(X,YY,F,NEQN,H,EPS,WT,START,
     +   HOLD,K,KOLD,CRASH,PHI,P,YP,PSI)
C
C   TEST FOR TOLERANCE S TOO SMALL
      IF( .NOT. CRASH) GO TO 130
```

```
      IFLAG = ISN*3
      RELERR = EPS*RELEPS
      ABSERR = EPS*ABSEPS
      DO 120 L = 1,NEQN
 120     Y(L) = YY(L)
      T = X
      TOLD = T
      ISNOLD = 1
      RETURN
C
C   AUGMENT COUNTER ON WORK AND TEST FOR STIFFNESS
C
 130  NOSTEP = NOSTEP + 1
      KLE4 = KLE4 + 1
      IF(KOLD .GT. 4) KLE4 = 0
      IF(KLE4. GE. 50) STIFF = .TRUE.
      GO TO 50
      END
C*************************************************
C     SUBROUTINE STEP
C*************************************************
      SUBROUTINE STEP(X,Y,F,NEQN,H,EPS,WT,START,
     +   HOLD,K,KOLD,CRASH,PHI,P,YP,PSI)
      LOGICAL START,CRASH,PHASE1,NORND
      DIMENSION Y(NEQN),WT(NEQN),PHI(NEQN,16),P(NEQN),
     +   YP(NEQN),PSI(12)
      DIMENSION ALPHA(12),BETA(12),SIG(13),W(12),V(12),G(13),
     +   GSTR(13),TWO(13)
      EXTERNAL F
      DATA TWOU/.22E-15/
      DATA FOURU/.44E-15/
      DATA TWO/2.0,4.0,8.0,16.0,32.0,64.0,128.0,256.0,512.0,
     +   1024.0,2048.0,4096.0,8192.0/
      DATA GSTR/0.500,0.0833,0.0417,0.0264,0.0188,0.0143,
     +   0.0114,0.00936,0.00789,0.00679,0.00592,0.00524,
     +   0.00468/
      DATA G(1),G(2)/1.0,0.5/,SIG(1)/1.0/
      CRASH = .TRUE.
      IF(ABS(H) .GE. FOURU*ABS(X)) GO TO 5
      H = SIGN(FOURU*ABS(X),H)
      RETURN
 5    P5EPS = 0.5*EPS
C
C   IF ERROR TOLERANCE IS TOO SMALL, INCREASE IT TO AN
C   ACCEPTABLE VALUE
C
      ROUND = 0.0
      DO 10 L = 1,NEQN
 10      ROUND = ROUND + (Y(L)/WT(L))**2
      ROUND = TWOU*SQRT(ROUND)
```

```
      IF(P5EPS .GE. ROUND) GO TO 15
      EPS = 2.0*ROUND*(1.0 + FOURU)
      RETURN
 15   CRASH = .FALSE.
      IF(.NOT.START) GO TO 99
C
C   INITIALIZE.   COMPUTE APPROPRIATE STEP SIZE FOR FIRST
 C  STEP
C     CALL F(X,Y,YP)
      SUM = 0.0
      DO 20 L = 1,NEQN
      PHI(L,1) = YP(L)
      PHI(L,2) = 0.0
 20   SUM = SUM + (YP(L)/WT(L))**2
      SUM = SQRT(SUM)
      ABSH = ABS(H)
      IF(EPS.LT. 16.0*SUM*H*H) ABSH = 0.25*SQRT(EPS/SUM)
      H = SIGN(AMAX1(ABSH,FOURU*ABS(X)),H)
      HOLD = 0.0
      K = 1
      KOLD = 0
      START = .FALSE.
      PHASE1 = .TRUE.
      NORND = .TRUE.
      IF(P5SEPS
 .GT. 100.0*ROUND) GO TO 99
      NORND = .FALSE.
      DO 25L = 1,NEQN
 25      PHI(L,15) = 0.0
 99   IFAIL = 0
C        ***     END BLOCK 0     ***
C        ***     BEGIN BLOCK 1     ***
C   COMPUTE COEFFICIENTS OF FORMULAS FOR THIS STEP.  AVOID
C   COMPUTING THOSE QUANTITIES NOT CHANGED WHEN STEP SIZE IS
C   NOT CHANGED.
C        ***
C
 100  KP1 = K+1
      KP2 = K+2
      KM1 = K-1
      KM2 = K-2
C
C   NS IS THE NUMBER OF STEPS TAKEN WITH SIZE H, INCLUDING
C   THE CURRENT ONE.  WHEN K.LT.NS,  NO COEFFICIENTS CHANGE
C
      IF(N .NE. HOLD) NS = 0
      NS = MIN0(NS+1,KOLD+1)
      NSP1 = NS+1
      IF(K .LT. NS) GO TO 199
C
```

```
C   COMPUTE THOSE COMPONENTS OF ALPHA(*),BETA(*)PSI(*),
C   SIG(*) WHICH ARE CHANGED
      BETA(NS) = 1.0
      REALNS = NS
      ALPHA(NS) = 1.0/REALNS
      TEMP1 = H*REALNS
      SIG(NSP1) = 1.0
      IF(K .LT. NSP1) GO TO 110
      DO 105 I = NSP1,K
         IM1 = I-1
            TEMP2 = PSI(IM1)
            PSI(IM1) = TEMP1
         BETA(I) = BETA(IM1)*PSI(IM1)/TEMP2
         TEMP1 = TEMP2 + H
         ALPHA(I) = H/TEMP1
         REALI = I
 105     SIG(I+1) = REALI*ALPHA(I)*SIG(I)
 110  PSI(K) = TEMP1
C
C   COMPUTE COEFFICIENTS G(*)
C
C   INITIALIZE V(*) AND W(*),  G(2) IS SET DATA STATEMENT
C     IF(NS .GT. 1) GO TO 120
      DO 115 IQ = 1,K
         TEMP3 = IQ*(IQ+1)
         V(IQ) = 1.0/TEMP3
 115     W(IQ) = V(IQ)
      GO TO 140
C
C   IF ORDER WAS RAISED, UPDATE DIAGONAL PART OF V(*)
C
 120  IF(K .LE. KOLD) GO TO 130
      TEMP4 = K*KP1
      V(K) = 1.0/TEMP4
      NSM2 = NS-2
      IF(NSM2 .LT. 1) GO TO 130
      DO 125 J = 1,NSM2
         I = K-J
 125     V(I) = V(I) - ALPHA(J+1)*V(I+1)
C
C
C   UPDATE V(*) AND SET W(*)
C
 130  LIMIT1 = KP1 - NS
      TEMP5 = ALPHA(NS)
      DO 135 IQ = 1,LIMIT1
         V(IQ) = V(IQ) - TEMP5*V(IQ+1)
 135     W(IQ) = V(IQ)
      G(NSP1) = W(1)
C
```

```
C   COMPUTE THE G(*) IN THE WORK VECTOR W(*)
C
 140  NSP2 = NS +2
      IF(KP1 .LT. NSP2) GO TO 199
      DO 150 I = NSP2,KP1
         LIMIT2 = KP2 -I
         TEMP 6 = ALPHA(I-1)
      DO 145 IQ = 1,LIMIT2
 145     W(IQ) = W(IQ) - TEMP6*W(IQ+1)
 150  G(I) = W(1)
 199  CONTINUE
C        ***     END BLOCK 1     ***
C
C        ***     BEGIN BLOCK 2     ***
C   PREDICT A SOLUTION P(*), EVALUATE DERIVATIVES USING
C   PREDICTED SOLUTION, ESTIMATE LOCAL ERROR AT ORDER K
C   AND ERRORS AT ORDERS K, K-1, K-I AS IF CONSTANT STEP
C   SIZE WERE USED.
C
C
C   CHANGE PHI TO PHI STAR
C
      IF(K .LT. NSP1) GO TO 215
      DO 210 I = NSP1,K
         TEMP1 = BETA(I)
         DO 205 L = 1,NEQN
 205        PHI( L,I ) = TEMP1*PHI(L,I)
 210     CONTINUE
C
C   PREDICT SOLUTION AND DIFFERENCES
C
 215  DO 220 L = 1,NEQN
         PHI(L,KP2) = PHI(L,KP1)
         PHI(L,KP1) = 0.0
 220     P(L) = 0.0
      DO 230 J = 1,K
         I = KP1 - J
         IP1 = I+1
         TEMP2 = G(I)
         DO 225 L = 1,NEQN
            P(L) = P(L) + TEMP2*PHI(L,I)
 225     PHI(L,I) = PHI(L,I) + PHI(L,IP1)
 230  CONTINUE
      IF(NORND) GO TO 240
      DO 235 L = 1,NEQN
         TAU = H*P(L) - PHI(L,15)
         P(L) = Y(L) + TAU
 235     PHI(L,16) = (P(L) - Y(L)) - TAU
      GO TO 250
 240  DO 245 L = 1,NEQN
```

```
 245      P(L) = Y(L) + H*P(L)
 250   XOLD = X
       X = X + H
       ABSH = ABS(H)
       CALL F(X,P,YP)
C
C   ESTIMATE ERRORS AT ORDERS K, K-1, K-2
C
       ERKM2 = 0.0
       ERKM1 = 0.0
       ERK = 0.0
       DO 265 L = 1,NEQN
          TEMP3 = 1.0/WT(L)
          TEMP4 = YP(L) - PHI(L,1)
          IF(KM2)265,260,255
 255   ERKM2 = ERKM2 + ((PHI(L,KM1)+TEMP4)*TEMP3)**2
 260   ERKM1 = ERKM1 + ((PHI(L,K)+TEMP4)*TEMP3)**2
 265   ERK = ERK + (TEMP4*TEMP3)**2
       IF(KM2)280,275,270
 270   ERKM2 = ABSH*SIG(KM1)*GSTR(KM2)*SQRT(ERKM2)
 275   ERKM1 = ABSH*SIG(K)*GSTR(KM1)*SQRT(ERKM1)
 280   TEMP5 = ABSH*SQRT(ERK)
       ERR = TEMP5*(G(K) - G(KP1))
       ERK = TEMP5*SIG(KP1)*GSTR(K)
       KNEW = K
C
C   TEST IF ORDER SHOULD BE LOWERED
C
       IF(KM2)299,290,285
 285   IF(AMAX1(ERKM1,ERKM2) .LE. ERK) KNEW = KM1
       GO TO 299
 290   IF(ERKM1 .LE. 0.5*ERK) KNEW = KM1
C
C   TEST IF STEP SUCCESSFUL
C
 299   IF(ERR .LE. EPS) GO TO 400
C
C
  ***      END BLOCK 2     ***
C
C          ***      BEGIN BLOCK 3      ***
C   THE STEP IS UNSUCCESSFUL.  RESTORE X, PHI(*,*), PSI(*).
C   IF THIRD CONSECUTIVE FAILURE,  SET ORDER TO ONE.  IF
C   STEP FAILS MORE THAN THREE TIMES,  CONSIDER AN OPTIMAL
C   STEP SIZE.  DOUBLE ERROR TOLERANCE AND RETURN IF
C   ESTIMATED STEP SIZE IS TOO SMALL FOR MACHINE PRECISION.
C     ***
C
C   RESTORE X, PHI(*,*) AND PSI(*)
C
```

```
      PHASE1 = .FALSE.
      X = XOLD
      DO 310 I = 1,K
         TEMP1 = 1.0/BETA(I)
         IP1 = I+1
         DO 305 L = 1,NEQN
 305        PHI(L,I) = TEMP1*(PHI(L,I) - PHI(L,IP1))
 310     CONTINUE
      IF(K .LT. 2) GO TO 320
      DO 315 I = 2,K
 315     PSI(I-1) = PSI(I) - H

C   ON THIRD FAILURE, SET ORDER TO ONE.   THEREAFTER, USE
C   OPTIMAL STEP SIZE
C     IFAIL = IFAIL + 1
      TEMP2 = 0.5
      IF(IFAIL - 3) 335,330,325
 325  IF(P5EPS .LT. 0.25*ERK) TEMP2 = SQRT(P5EPS/ERK)
 330  KNEW = 1
 335  H = TEMP2*H
      K = KNEW
      IF(ABS(H) .GE. FOURU*ABS(X)) GO TO 340
      CRASH = .TRUE.
      H = SIGN(FOURU*ABS(X),H)
      EPS = EPS + EPS
      RETURN
 340  GO TO 100
C        ***     END BLOCK 3     ***
C
C        ***     BEGIN BLOCK 4     ***
C   THE STEP IS SUCCESSFUL.  CORRECT THE PREDICTED SOLUTION,
C   EVALUATE THE DERIVATIVES USING THE CORRECTED SOLUTION
C   AND UPDATE THE DIFFERENCES.  DETERMINE BEST AND SIZE FOR
C   NEXT STEP.
C
 400  KOLD = K
      HOLD = H
C
C   CORRECT AND EVALUATE
C
      TEMP1 = H*G(KP1)
      IF(NORND) GO TO 410
      DO 405 L = 1,NEQN
         RHO = TEMP1*(YP(L) - PHI(L,1)) - PHI(L,16)
         Y(L) = P(L) + RHO
 405  PHI(L,15) = (Y(L) - P(L)) - RHO
      GO TO 420
 410  DO 415 L = 1,NEQN
 415     Y(L) = P(L) + TEMP1*(YP(L) - PHI(L,1))
 420  CALL F(X,Y,YP)
C
```

```
C   UPDATE DIFFERENCES FOR NEXT STEP
C
      DO 425 L = 1,NEQN
         PHI(L,KP1) = YP(L) - PHI(L,1)
 425     PHI(L,KP2) = PHI(L,KP1) - PHI(L,KP2)
      DO 435 I = 1,K
         DO 430 L = 1,NEQN
 430        PHI(L,I) = PHI(L,I) + PHI(L,KP1)
 435  CONTINUE
C
C   ESTIMATE ERROR AT ORDER K+1 UNLESS
C   IN FIRST PHASE WHEN ALWAYS RAISE ORDER,
C   ALWAYS RECIDED TO LOWER ORDER,
C   STEP SIZE NOT CONSTANT SO ESTIMATE UNRELIABLE
C
      ERKP1 = 0.0
      IF(KNEW .EQ. KM1  .OR.  K.EQ. 12) PHASE1 = .FALSE.
      IF(PHASE1) GO TO 450
      IF(KNEW .EQ. KM1) GO TO 455
      IF(KP1 .GT. NS) GO TO 460
      DO 440 L = 1,NEQN
 440     ERKP1 = ERKP1 = (PHI(L,KP2)/WT(L))**2
      ERKP1 = ABSH*GSTR(KP1)*SQRT(ERKP1)
C
C   USING ESTIMATED ERROR AT ORDER K+1, DETERMINE
C   APPROPRIATE ORDER FOR NEXT STEP
C
      IF(K .GT. 1) GO TO 445
      IF(ERKP1 .GE. 0.5*ERK) GO TO 460
      GO TO 450
 445  IF(ERKM1 .LE. AMIN1(ERK,ERKP1)) GO TO 455
      IF(ERKP1 .GE. ERK .OR.  K .EQ. 12) GO TO 460
C
C   HERE ERKP1 .LT. ERK .LT. AMAX1(ERKM1,ERKM2) ELSE ORDER
C   WOULD HAVE BEEN LOWERED IN BLOCK 2.  THUS ORDER IS TO
C   BE RAISED
C
C   RAISE ORDER
C
 450  K = KP1
      ERK = ERKP1
      GO TO 460
C
C   LOWER ORDER
 455     K = KM1
      ERK = ERKM1
C
C   WITH NEW ORDER DETERMINE APPROPRIATE STEP SIZE FOR
C   NEXT STEP
C
```

```
 460  HNEW = H + H
      IF(PHASE1) GO TO 465
      IF(P5EPS .GE. ERK*TWO(K+1)) GO TO 465
      HNEW = H
      IF(P5EPS .GE. ERK) GO TO 465
      TEMP2 = K+1
      R = (P5EPS/ERK)**(1.0/TEMP2)
      HNEW = ABSH*AMAX1(0.5,AMAX1(0.9,R))
      HNEW = SIGN(AMAX1(HNEW,FOURU*ABS(X)),H)
 465. H = HNEW
      RETURN
         ***     END BLOCK 4     ***
      END
C*********************************************
C     SUBROUTINE INTRP
C*********************************************
      SUBROUTINE INTRP(X,Y,XOUT,YOUT,YPOUT,NEQN,KOLD,PHI,PSI)
      DIMENSION Y(NEQN),YOUT(NEQN),YPOUT(NEQN),PHI(NEQN,16),
          PSI(12)
      DIMENSION G(13),W(13),RHO(13)
      DATA G(1)/1.0/,RHO(1)/1.0/
      HI = XOUT - X
      KI = KOLD + 1
      KIP1 = KI + 1
C
C   INITIALIZE W(*) FOR COMPUTING G(*)
C
      DO 5 I = 1,KI
         TEMP1 = I
 5       W(I) = 1.0/TEMP1
      TERM = 0.0
C
C   COMPUTE G(*)
C
      DO 15 J = 2,KI
         JM1 = J - 1
         PSIJM1 - PSI(JM1)
         GAMMA = (HI + TERM)/PSIJM1
         ETA = HI/PSIJM1
         LIMIT1 = KIP1 - J
         DO 10 I = 1,LIMIT1
 10         W(I) = GAMMA*W(I) - ETA*W(I+1)
         G(J) = W(1)
         RHO(J) = GAMMA*RHO(JM1)
 15      TERM = PSIJM1
C
C
C   INTERPOLATE
C
```

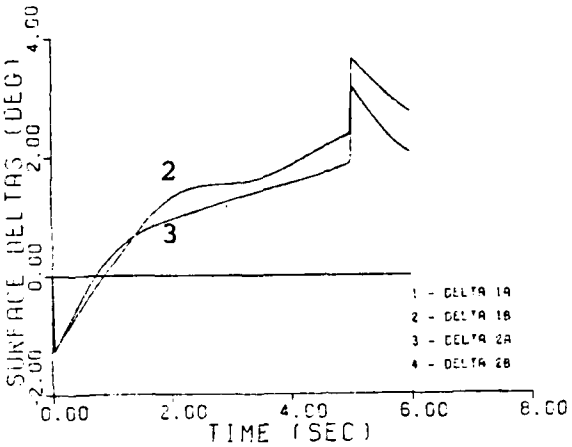

Fig. G-2(e). Control Surface Deflections for Pitch Rate Command, Flight Condition 3--CSC Mode 5

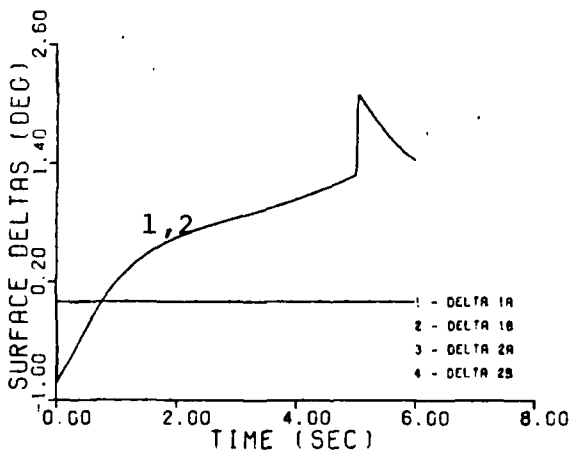

Fig. G-2(f). Control Surface Deflections for Pitch Rate Command, Flight Condition 3--CSC Mode 6

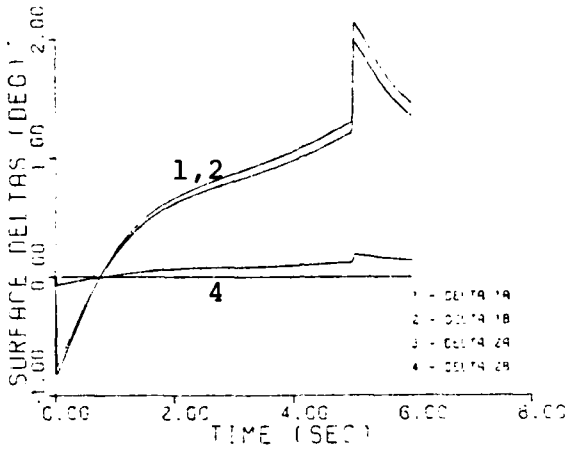

Fig. G-2(c). Control Surface Deflections for Pitch Rate Command, Flight Condition 3--CSC Mode 3

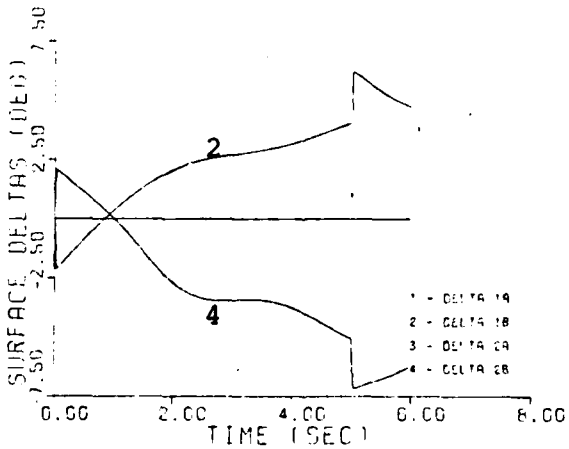

Fig. G-2(d). Control Surface Deflections for Pitch Rate Command, Flight Condition 3--CSC Mode 4

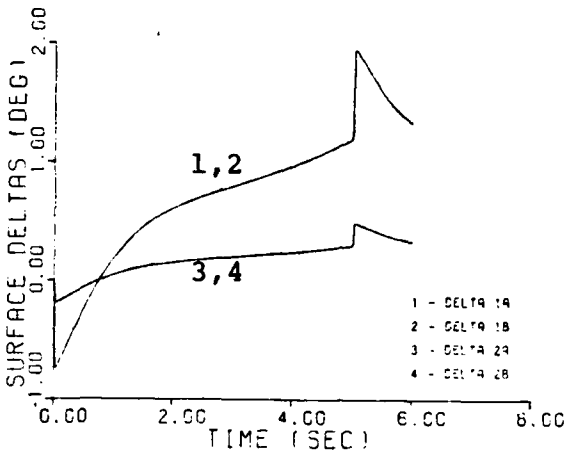

Fig. G-2(a). Control Surface Deflections for Pitch Rate Command, Flight Condition 3--CSC Mode 1

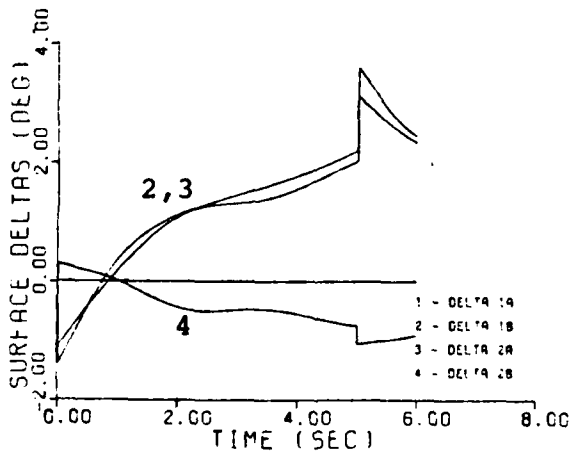

Fig. G-2(b). Control Surface Deflections for Pitch Rate Command, Flight Condition 3--CSC Mode 2

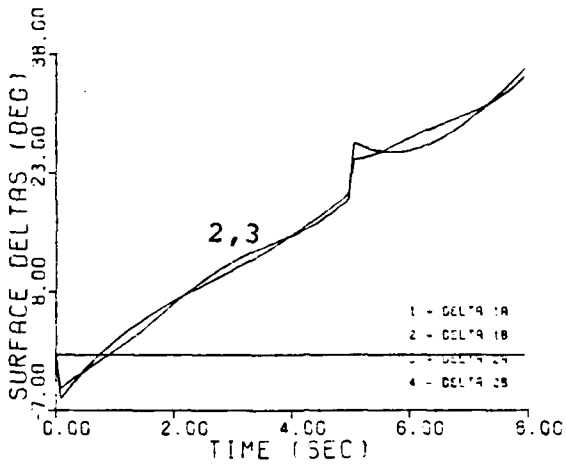

Fig. G-1(e). Control Surface Deflections for Pitch Rate Command, Flight Condition 2--CSC Mode 5

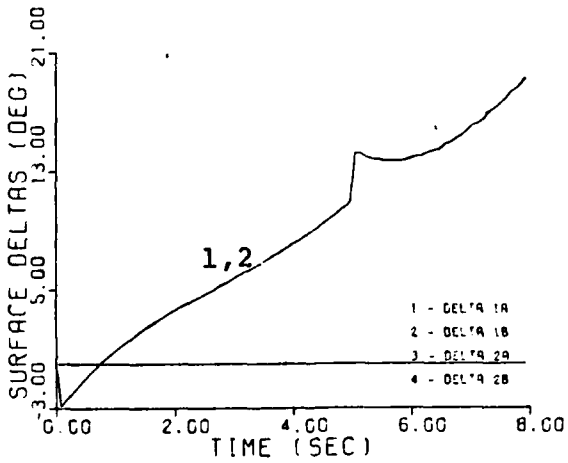

Fig. G-1(f). Control Surface Deflections for Pitch Rate Command, Flight Condition 2--CSC Mode 6

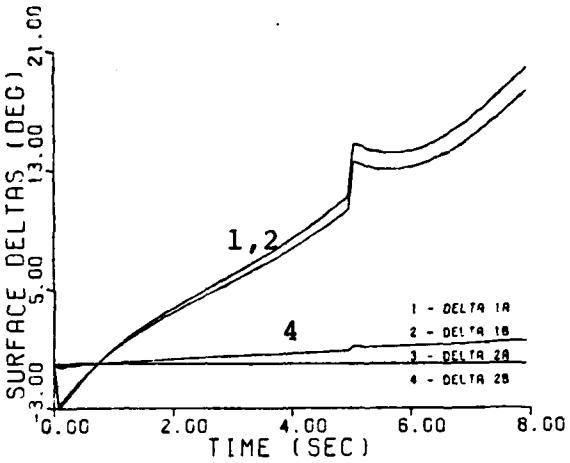

Fig. G-1(c). Control Surface Deflections for Pitch Rate Command, Flight Condition 2--CSC Mode 3

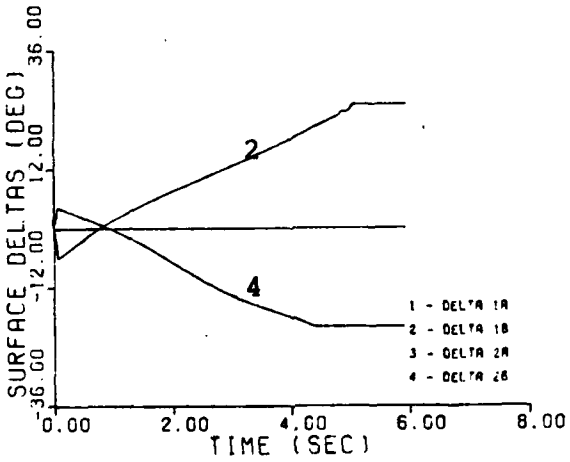

Fig. G-1(d). Control Surface Deflections for Pitch Rate Command, Flight Condition 2--CSC Mode 4

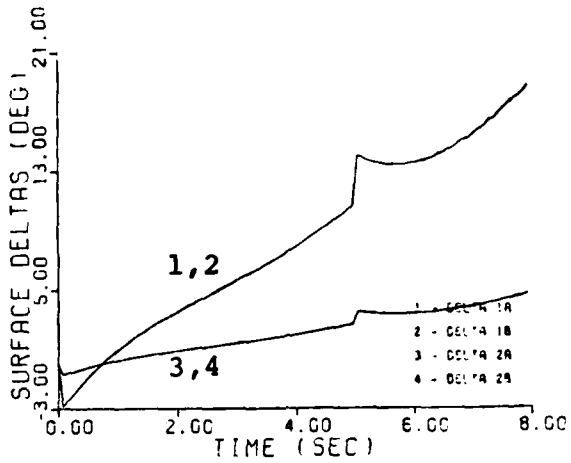

Fig. G-1(a). Control Surface Deflections for Pitch Rate Command, Flight Condition 2--CSC Mode 1

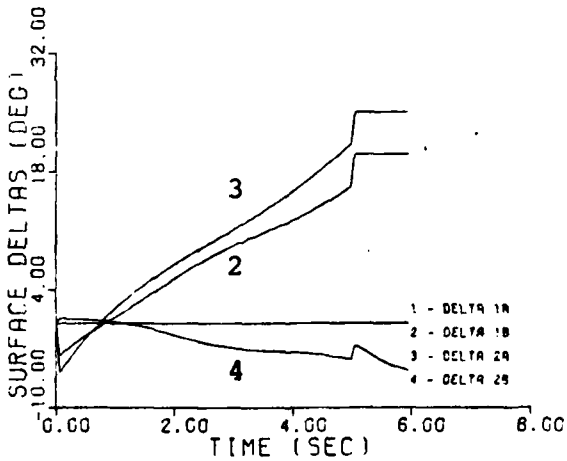

Fig. G-1(b). Control Surface Deflections for Pitch Rate Command, Flight Condition 2--CSC Mode 2

Appendix G: Control Surface Deflections

In this appendix the control surface deflections due to q and p commands are illustrated for flight conditions two, three, and four.

```
C
C         P12
C
      DATA VP12K/.2418,-.2118,-6.472,-5.85/
      DATA VP12Z1/0.,0.,0.,0/
      DATA VP12Z2/-.06537,-.006697,-.01254,-.03459/
      DATA VP12Z3/-.2589,-1.861,-1.646,-.6861/
C
C         P22C
      DATA VP22K/-4.478,-17.446,-51.06,-14.168/
      DATA VP22Z1/0.,0.,0.,0./
      DATA VP22Z2/(-.205,.853),(-.219,1.607),(-.3541,2.927),
     +(-.4083,4.916)/
      DATA VP22Z3/(-.205 - .853),(-.219,-1.607),
     +(-.3541,-2.927),(-.4083,-4.916)/
      DATA VP22P1/-.6835,-.8265,-.02719,-.03448/
      DATA VP22P2/-.1041,-.07795,-2.697,-2.171/
      DATA VP22P3/(-.2741,1.909),(-.211,1.953),(-.391,2.962),
     +(-.4996,3.129)/
      DATA VP22P4/(-.2741,-1.909),(-.211,-1.953),
     +(-.391,-2.962),(-.4996,-3.129)/
C
C         P21
C
      DATA VP21K/-4.284,-13.584,-51.72,-46.6/
      DATA VP21Z1/0.,0.,0.,0./
      DATA VP21Z2/(-.3017,1.562),(-.2442,2.101),
     +(-.3749,3.578),(-.3774,3.848)/
      DATA VP21Z3/(-.3017,-1.562),(-.2442,-2.101),
     +(-.3749,-3.578),(-.3774,-3.848)/
C
C
C
      U12 = .25
      U21 = .25
      R1 = 10.
      R2 = 50.
      RETURN
      END
```

Zdata

```
      SUBROUTINE ZDATA
C
C-----  DIMENSION  -----
C     DIMENSION VP11K(4),VP11Z1(4),VP11Z2(4),VP11Z3(4)
C
      DIMENSION VP12K(4),VP12Z1(4),VP12Z2(4),VP12Z3(4)
C
      COMPLEX VP11P1(4),VP11P2(4),VP11P3(4),VP11P4(4)
C
      DIMENSION VP21K(4),VP21Z1(4)
      COMPLEX VP21Z2(4),VP21Z3(4)
C
      DIMENSION VP22K(4),VP22Z1(4)
      COMPLEX VP22Z2(4),VP22Z3(4)
C
      DIMENSION VP22P1(4),VP22P2(4)
      COMPLEX VP22P3(4),VP22P4(4)

C
C-----  COMMON  -----
      COMMON /R/ R1,R2
      COMMON /U/ U12,U21
C
      COMMON /VP11Z/VP11K,VP11Z1,VP11Z2,VP11Z3
      COMMON /VP11P/VP11P1,VP11P2,VP11P3,VP11P4
C
      COMMON /VP12Z/VP12K,VP12Z1,VP12Z2,VP12Z3
C
      COMMON /VP21Z/VP21K,VP21Z1,VP21Z2,VP21Z3
C
      COMMON /VP22Z/VP22K,VP22Z1,VP22Z2,VP22Z3
      COMMON /VP22P/VP22P1,VP22P2,VP22P3,VP22P4
C
C
C     PLANT DATA
C
C        P11
      DATA VP11K/-2.236,-5.862,-24.06,-32.9/
      DATA VP11Z1/0.,0.,0.,0./
      DATA VP11Z2/-.01822,-.01004,-.01263,-.02996/
      DATA VP11Z3/-.4568,-.5502,-1.51,-1.097/
      DATA VP11P1/(-1.3,.0),(-2.028,0.),(-3.223,0.),
     +(-.01516,.02343)/
      DATA VP11P2/(.3633,0.),(1.167,0.),(.9645,0.),
     +(-.01516,-.02343)/
      DATA VP11P3/(-.07683,.2065),(-.006472,.07803),
     +(-.007553,.05384),(-.8012,6.592)/
      DATA VP11P4/(-.07683,-.2065),(-.006472,-.07803),
     +(-.007553,-.05384),(-.8012,-6.592)/
```

```
C
      D1A = G1 + G12
      D1B = G1 - G12
      D2A = G21 + G2
      D2B = G21 - G2
C
      IF(IS1A .EQ. 0) D1A = 0.
      IF(IS1B .EQ. 0) D1B = 0.
      IF(IS2A .EQ. 0) D2A = 0.
      IF(IS2B .EQ. 0) D2B = 0.
C
C-----  SATURATION  -----
C
      IF(D1A .GT. 25.) D1A = 25.
      IF(D1A .LT. -25.) D1A = -.25.
      IF(D1B .GT. 25.) D1B = 25.
      IF(D1B .LT. -25.) D1B = -25.
C
      IF(D2A .GT. 20.) D2A = 20.
      IF(D2A .LT. 20.) D2A = -20.
      IF(D2B .GT. 20.) D2B = 20.
      IF(D2B .LT. -20) D2B = -20.
C
      RETURN
      END
```

```
C-----  F(S)  -----
C
      YP(17) = R1 - F1P*Y(17)
      F1 = F1K*Y(17)
C
      YP(18) = R2 - F2P*Y(18)
      F2 = F2K*Y(18)
C
C
C-----  G1(S)  -----
      E1 = F1 - C1
C
      YP(19) = E1
      G1A = Y(19)
C
      YP(20) = G1A - G1P1*Y(20)
      1 = YP(20) + G1Z1*Y(20)
C
      YP(21) = G1B - G1P2*Y(21)
      G1C = YP(21) + G1Z2*Y(21)
      YP(22) = Y(23)
      YP(23) = G1C - G1P3*Y(23) - G1P4*Y(22)
      G1D = YP(23) + G1Z3*Y(23) + G1Z4*Y(22)
      G1 = G1K*G1D
C
C
C-----  G2(S)  -----
C
      E2 = F2 - C2
C
      YP(24) = E2
      G2A = Y(24)
C
      YP(25) = G2A - G2P1*Y(25)
      G2B = YP(25) + G2Z1*Y(25)
C
      YP(26) = G2B - G2P2*Y(26)
      G2C = YP(26) + G2Z2*Y2)
C
      YP(27) = Y(28)
      YP(28) = G2C - G2P3*Y(28) - G2P4*Y(27)
C
      G2D = YP(28) + G2Z3*Y(28) + G2Z4*Y(27)
C
      G2 = G2K*G2D
C
C
C-----  DELTA  -----
C
      G12 = U12*G2
      G21 = U21*G1
```

```
C
      C11 = P11K*D11B
C
C-----  P12(S)  -----
C
      D12 = D2A + D2B
C
      YP(5) = Y(6)
      YP(6) = D12 - P11P1*Y(6) - P11P2*Y(5)
      D12A = Y(6) + P12Z1*Y(5)
C
      YP(7) = Y(8)
      YP(8) = D12A - P11P3*Y(8) - P11P4*Y(7)
      D12B = YP(8) + P12Z2*Y(8) + P12Z3*Y(7)
C
      C12 = P12K*D12B
C
C-----  P21(S)  -----
C
      D21 = D1A - D1B
      YP(9) = Y(10)
      YP(10) = D21 - P22P1*Y(10) - P22P2*Y(9)
      D21A = Y(10) + P21Z1*Y(9)
C
      YP(11) = Y(12)
      YP(12) = D21A - P22P3*Y(12) - P22P4*Y(11)
      D21B = YP(12) + P21Z2*Y(12) + P21Z3*Y(11)
C
      C21 = P21K*D21B
C
C-----  P22(S)  -----
C
      D22 = D2A - D2B
C
      YP(13) = Y(14)
      YP(14) = D22 - P22P1*Y(14) - P22P2*Y(13)
      D22A = Y(14) + P22Z1*Y(13)
C
      YP(15) = Y(16)
      YP(16) = D22A - P22P3*Y(16) - P22P*(5)
      D22B = YP(16) + P22Z2*Y(16) + P22Z3*Y(15)
C
      C22 = P22K*D22B
C
C
C-----  C  -----
      C1 = C11 + C12
      C2 = C21 + C22
C
C
```

Derv

```
      SUBROUTINE DERV(T,Y,YP)
C
C   RECONFIGURATION SYSTEM
C
      DIMENSION Y(28),YP(28)
C**************  COMMON  **************
C
      COMMON /P11Z/ P11K,P11Z1,P11Z2,P11Z3
      COMMON /P11P/ P11P1,P11P2,P11P3,P11P4
C
      COMMON /P12Z/ P12K,P12Z1,P12Z2,P12Z3
C
      COMMON /P21Z/ P21K,P21Z1,P21Z2,P21Z3
      COMMON /P21P/ P21P1,P21P2,P21P3,P21P4
C
      COMMON /P22Z/ P22K,P22Z1,P22Z2,P22Z3
      COMMON /P22P/ P22P1,P22P2,P22P3,P22P4
C
      COMMON /F/ F1K,F1P,F2K,F2P
C
      COMMON /G1Z/G1K,G1Z1,G1Z2,G1Z3,G124
      COMMON /G1P/G1P1,G1P2,G1P3,G1P4
C
      COMMON /G2Z/G2K,G2Z1,G2Z2,G2Z3,G2Z4
      COMMON /G2P/G2P1,G2P2,G2P3,GP
C
      COMMON /R/ R1,R2
      COMMON /U/ U12,U21
      COMMON /C/ C1,C2
      COMMON /D/ D1A,D1B,D2A,D2B
      COMMON /IS/ IS1A,IS1B,IS2A,IS2B
      COMMON /M/ F1,F2,G1,G2,E1,E2,D11,D12,D21,D22,
         C11,C12,C21,C22
C
C
C-----  P11(S)  -----
C
      D11 = D1A + D1B
C
      YP(1) = Y(2)
      YP(2) = D11 - P11P1*Y(2) - P11P2*Y(1)
      D11A = Y(2) + P11Z1*Y(1)
C
      YP(3) = Y(4)
      YP(4) = D11A - P11P3*Y(4) - P11P4*Y(3)
      D11B = YP(4) + P11Z2*Y(4) + P11Z3*Y(3)
```

```
      DO 20 L = 1,NEQN
         YPOUT(L) = 0.0
 20      YOUT(L) = 0.0
      DO 30 J = 1,KI
         I = KIP1 - J
         TEMP2
= G(I)
         TEMP3 = RHO(I)
         DO 25 L = 1,NEQN
            YOUT(L) = YOUT(L) + TEMP2*PHI(L,I)
            YPOUT(L) = YPOUT(L) + TEMP3*PHI(L,I)
 30   CONTINUE
    DO 35 L = 1,NEQN
 35   YOUT(L) = Y(L) + HI*YOUT(L)
    RETURN
C
    END
```

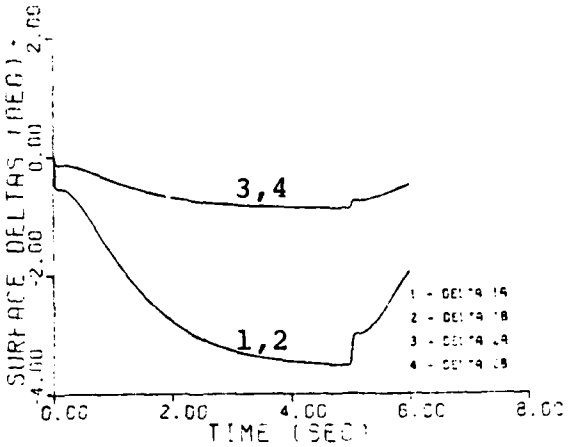

Fig. G-3(a). Control Surface Deflections for Pitch Rate Command, Flight Condition 4--CSC Mode 1

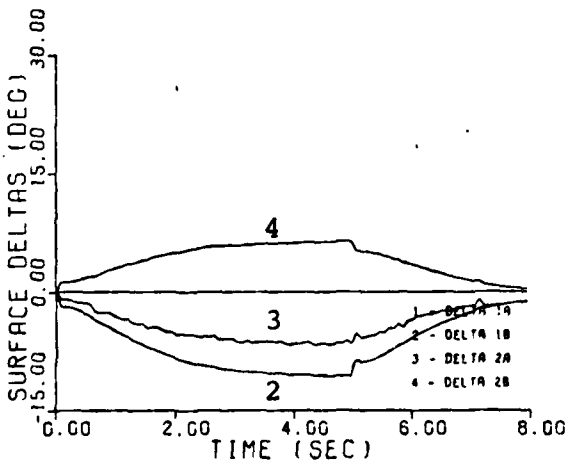

Fig. G-3(b). Control Surface Deflections for Pitch Rate Command, Flight Condition 4--CSC Mode 2

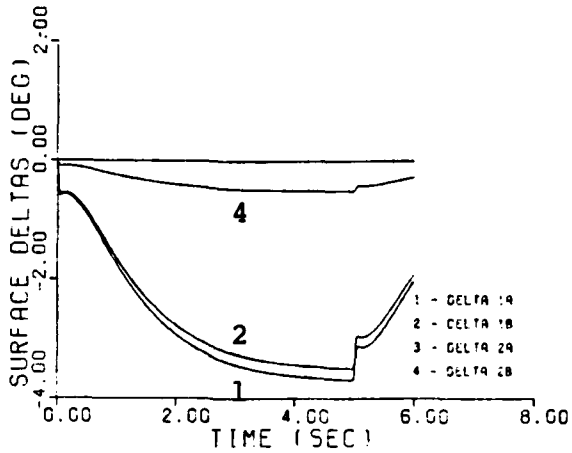

Fig. G-3(c). Control Surface Deflections for Pitch Rate Command, Flight Condition 4--CSC Mode 3

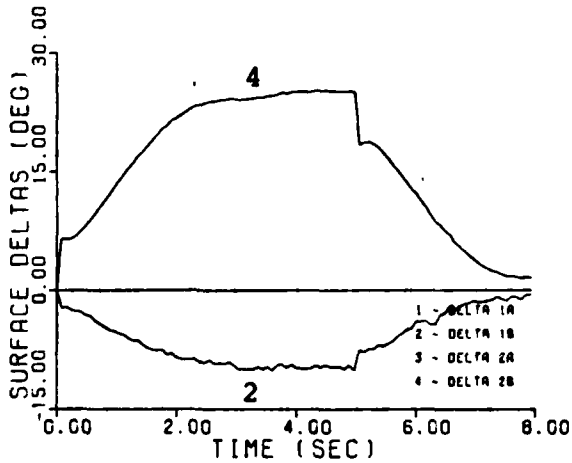

Fig. G-3(d). Control Surface Deflections for Pitch Rate Command, Flight Condition 4--CSC Mode 4

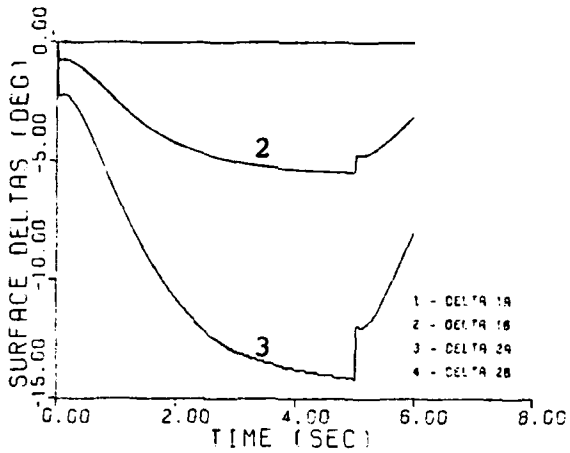

Fig. G-3(e). Control Surface Deflections for Pitch Rate Command, Flight Condition 4--CSC Mode 5

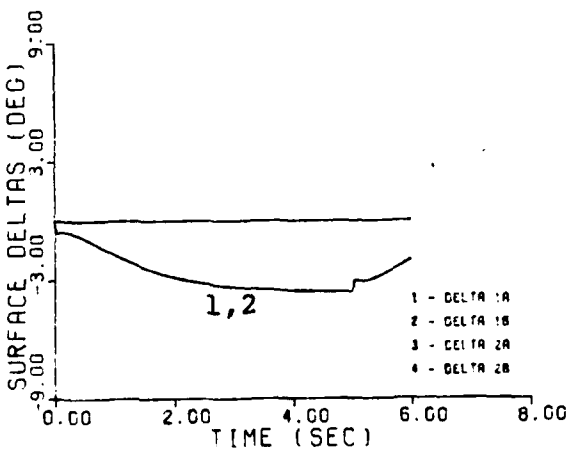

Fig. G-3(f). Control Surface Deflections for Pitch Rate Command, Flight Condition 4--CSC Mode 6

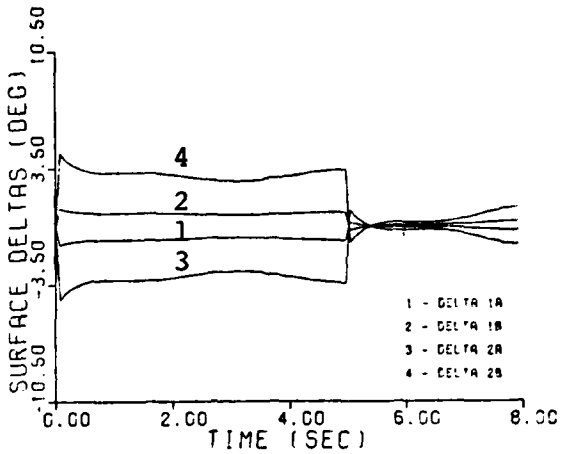

Fig. G-4(a). Control Surface Deflections for Roll Rate Command, Flight Condition 2--CSC Mode 1

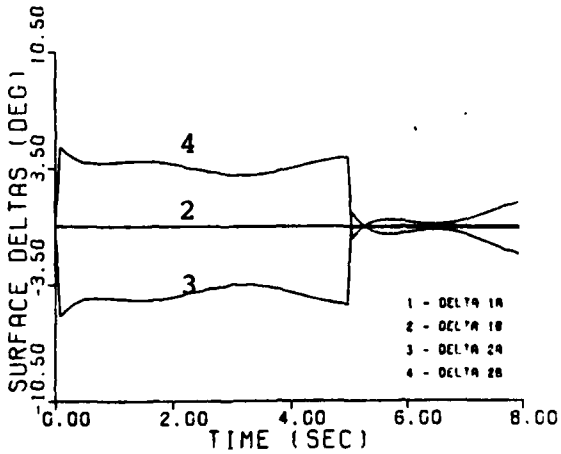

Fig. G-4(b). Control Surface Deflections for Roll Rate Command, Flight Condition 2--CSC Mode 2

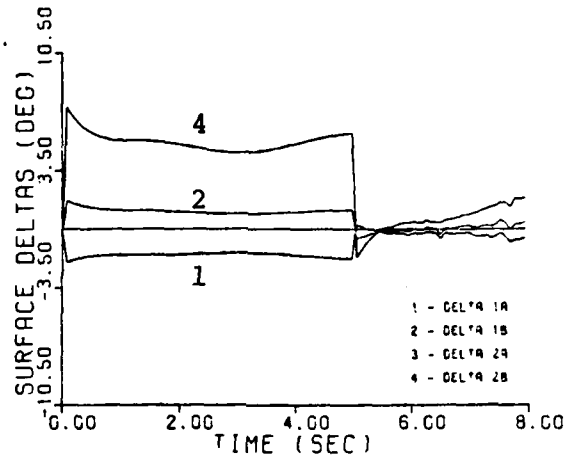

Fig. G-4(c). Control Surface Deflections for Roll Rate Command, Flight Condition 2--CSC Mode 3

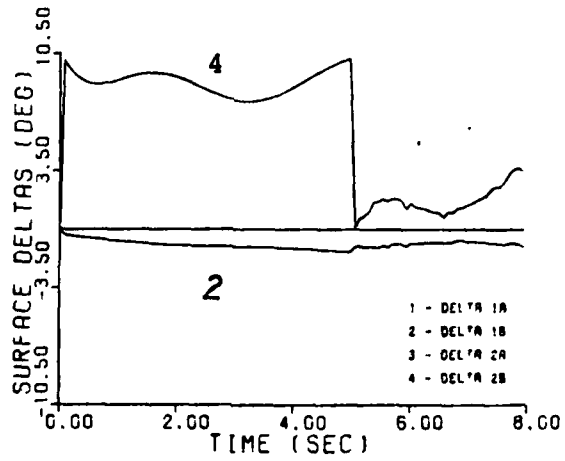

Fig. G-4(d). Control Surface Deflections for Roll Rate Command, Flight Condition 2--CSC Mode 4

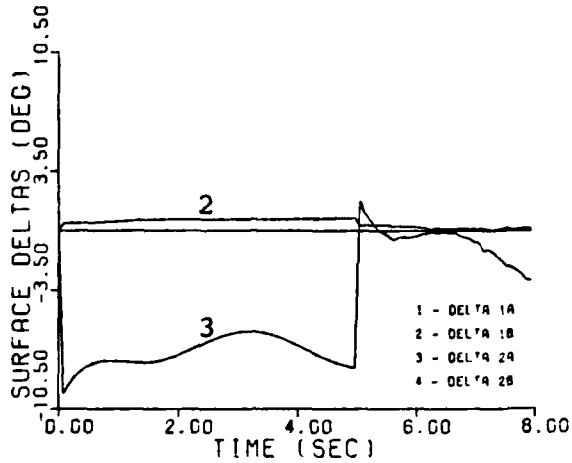

Fig. G-4(e). Control Surface Deflections for Roll Rate Command, Flight Condition 2--CSC Mode 5

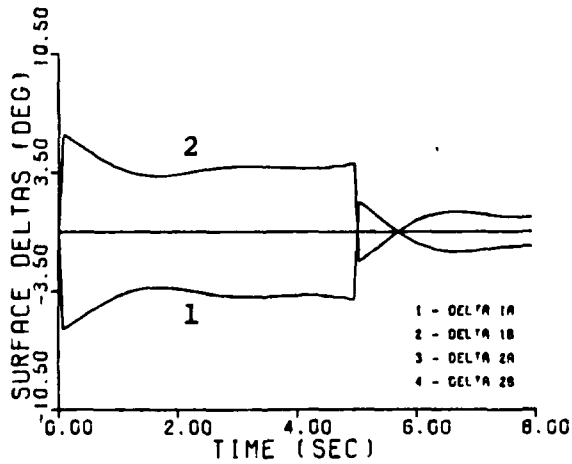

Fig. G-4(f). Control Surface Deflections for Roll Rate Command, Flight Condition 2--CSC Mode 6

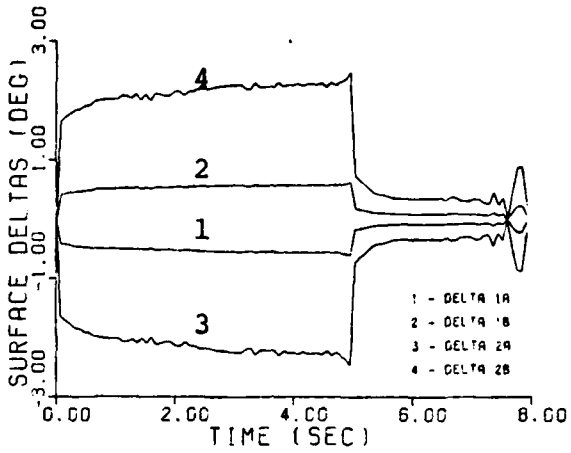

Fig. G-5(a). Control Surface Deflections for Roll Rate Command, Flight Condition 3--CSC Mode 1

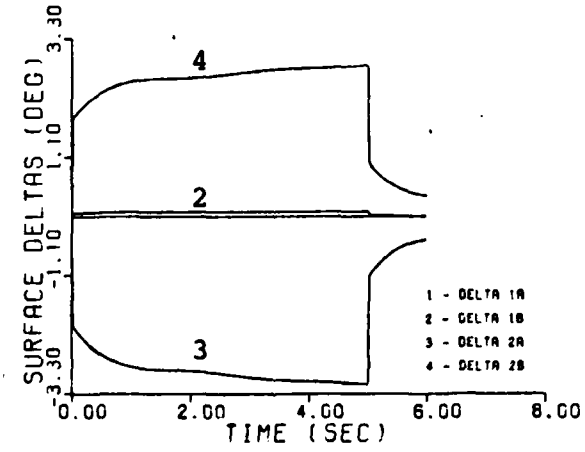

Fig. G-5(b). Control Surface Deflections for Roll Rate Command, Flight Condition 3--CSC Mode 2

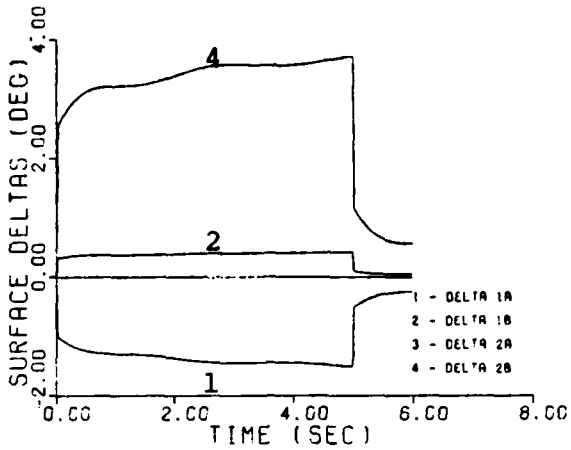

Fig. G-5(c). Control Surface Deflections for Roll Rate Command, Flight Condition 3--CSC Mode 3

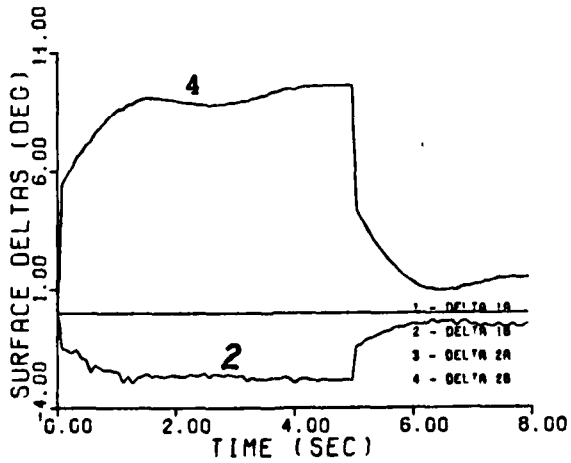

Fig. G-5(d). Control Surface Deflections for Roll Rate Command, Flight Condition 3--CSC Mode 4

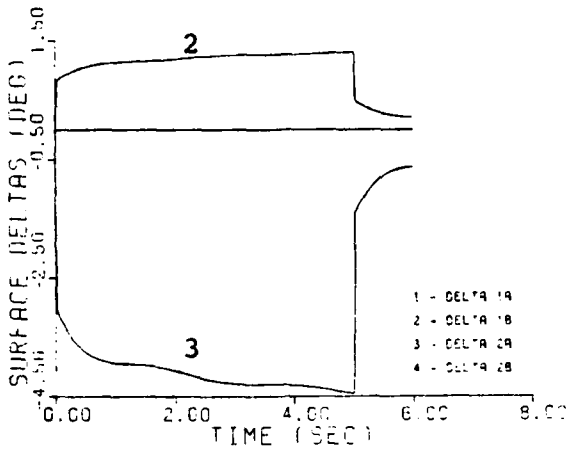

Fig. G-5(e). Control Surface Deflections for Roll Rate Command, Flight Condition 3--CSC Mode 5

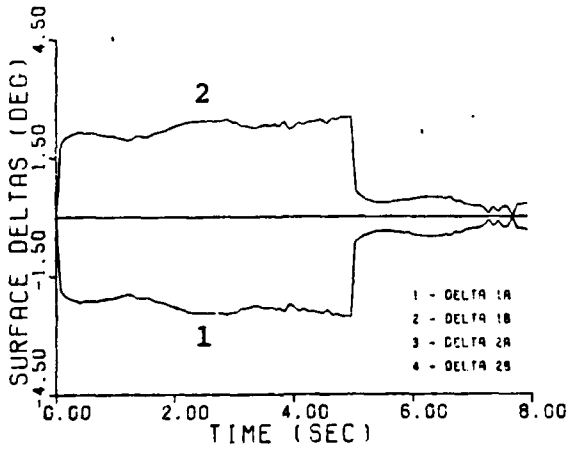

Fig. G-5(f). Control Surface Deflections for Roll Rate Command, Flight Condition 3--CSC Mode 6

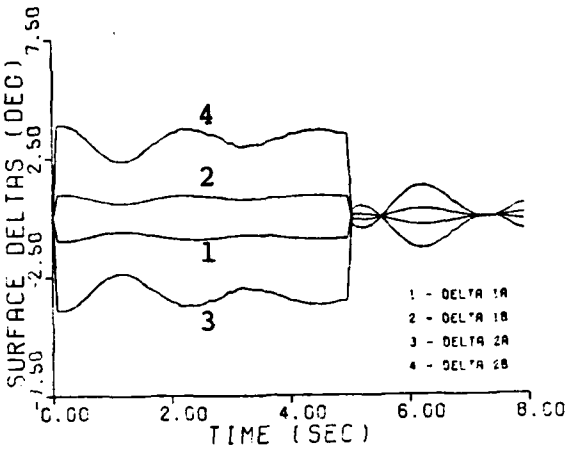

Fig. G-6(a). Control Surface Deflections for Roll Rate Command, Flight Condition 4--CSC Mode 1

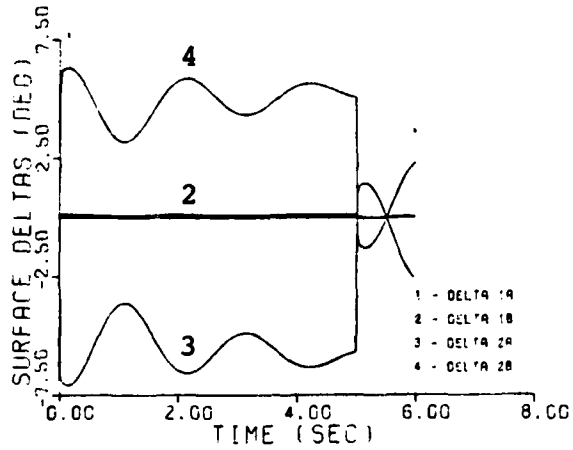

Fig. G-6(b). Control Surface Deflections for Roll Rate Command, Flight Condition 4--CSC Mode 2

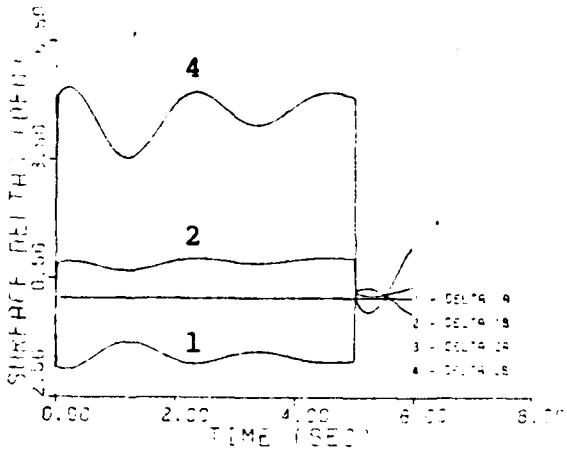

Fig. G-6(c). Control Surface Deflections for Roll Rate Command, Flight Condition 4--CSC Mode 3

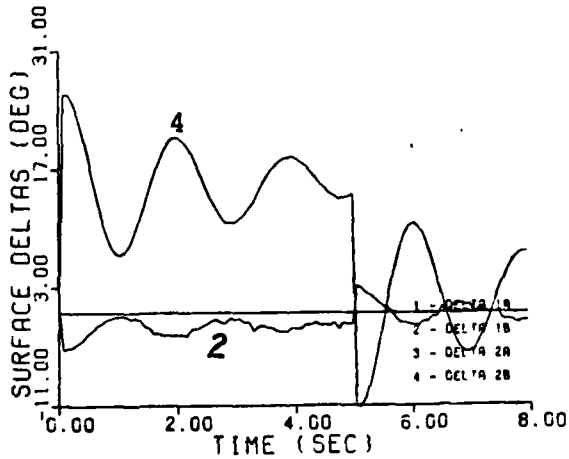

Fig. G-6(d). Control Surface Deflections for Roll Rate Command, Flight Condition 4--CSC Mode 4

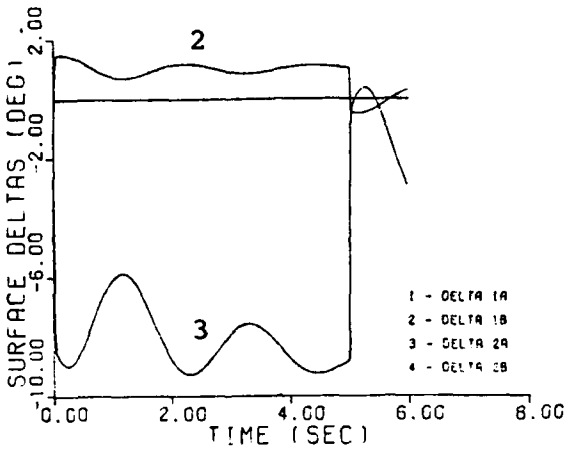

Fig. G-6(e). Control Surface Deflections for Roll Rate Command, Flight Condition 4--CSC Mode 5

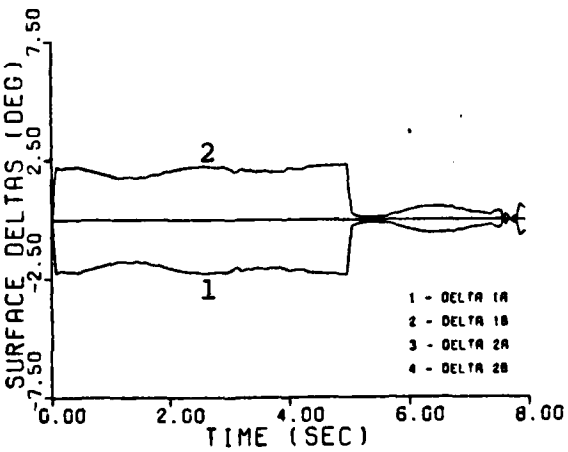

Fig. G-6(f). Control Surface Deflections for Roll Rate Command, Flight Condition 4--CSC Mode 6

Bibliography

1. Larimer, S. J. and Scott Maher. Continuously Reconfiguring Multi-Microprocessor Flight Control System. In-house study. AFWAL TR-81-3070. Air Force Wright Aeronautical Laboratory, WPAFB OH, May 1981.

2. Horowitz, Isaac and Marcel Sidi. "Synthesis of Feedback Systems with Large Plant Ignorance for Prescribed Time-Domain Tolerances," International Journal of Control, 16 (2): 287-309 (1972).

3. Horowitz, Isaac. "Quantitative Synthesis of Uncertain Multiple Input-Output Feedback Systems," International Journal of Control, 30 (1): 81-106 (1979).

4. Chandler, Phillip R. Self-Repairing Flight Control System Reliability and Maintainability. Program Plan. Air Force Wright Aeronautical Laboratories. Wright-Patterson AFB OH, February 1984.

5. Horowitz, Isaac. A Quantitative Inherent Reconfiguration Theory for a Class of Systems. Universal Energy Systems, Inc., Dayton OH, July 1984 (F33615-82-C-3000).

6. Barfield, A. Finley. Multivariable Control Laws for the AFTI/F-16. MS thesis. Air Force Institute of Technology, Wright-Patterson AFB OH, July 1983.

7. Larimer, S. J. An Interactive Computer-Aided Design Program for Digital and Continuous System Analysis and Synthesis (TOTAL). MS thesis GE/GGC/EE/78-2. School of Engineering, Air Force Institute of Technology (AU), Wright-Patterson AFB OH, 1978.

8. Horowitz, Isaac. "Improved Design Technique for Uncertain Multiple Input-Multiple Output Feedback Systems," International Journal of Control, 36 (6): 977-988 (1982).

9. Horowitz, Isaac and Marcel Sidi. "Optimum Synthesis of Nonminimum Phase Feedback Systems with Plant Uncertainty," International Journal of Control, 27 (3): 361-386 (1978).

10. D'Azzo, John J. and Constantine H. Houpis. Linear Control System Analysis and Design, Conventional and Modern (Second edition). New York: McGraw-Hill Book Company, 1981.

Vita

Major Phillip B. Arnold attended the University of Oklahoma from September 1965 until May 1970. He graduated with the degree of Bachelor of Science in Electrical Engineering, and received a reserve commission through the Air Force ROTC program in May 1970. In October 1971 he was awarded his pilot's wings, and the next six years were spent as an interceptor pilot in the Air Defense Command flying the F-106. From May 1977 until June 1980 he served as an exchange officer with the Canadian Armed Forces in British Columbia, Canada flying the CF-101. In June 1981 he graduated from the USAF Test Pilot School at Edwards AFB, California. The two years prior to coming to the Air Force Institute of Technology (AFIT) were spent in the Tactical Air Command at Tyndall AFB, Florida as a test pilot in an operational test and evaluation squadron.

Major Arnold has a senior pilot rating and more than 3000 hours of flying time. His assignment following graduation from AFIT is to the USAF Test Pilot School where he will be on the staff.

UNCLASSIFIED

SECURITY CLASSIFICATION OF THIS PAGE

REPORT DOCUMENTATION PAGE

1a. REPORT SECURITY CLASSIFICATION UNCLASSIFIED	1b. RESTRICTIVE MARKINGS
2a. SECURITY CLASSIFICATION AUTHORITY	3. DISTRIBUTION/AVAILABILITY OF REPORT Unclassified - Distribution unlimited As it appears on the report.
2b. DECLASSIFICATION/DOWNGRADING SCHEDULE	
4. PERFORMING ORGANIZATION REPORT NUMBER(S) AFIT/GE/ENG/84D-15	5. MONITORING ORGANIZATION REPORT NUMBER(S)
6a. NAME OF PERFORMING ORGANIZATION Air Force Institute of Technology 6b. OFFICE SYMBOL (If applicable) AFIT/EN	7a. NAME OF MONITORING ORGANIZATION
6c. ADDRESS (City, State and ZIP Code) Wright-Patterson AFB, OH 45433	7b. ADDRESS (City, State and ZIP Code)
8a. NAME OF FUNDING/SPONSORING ORGANIZATION Flight Dynamics Lab 8b. OFFICE SYMBOL (If applicable) AFWAL/FIGL	9. PROCUREMENT INSTRUMENT IDENTIFICATION NUMBER
8c. ADDRESS (City, State and ZIP Code) Wright-Patterson AFB, OH 45433	10. SOURCE OF FUNDING NOS. PROGRAM ELEMENT NO. / PROJECT NO. / TASK NO. / WORK UNIT NO.
11. TITLE (Include Security Classification) See Block 19	
12. PERSONAL AUTHOR(S) Phillip A. Arnold, Major, USAF	
13a. TYPE OF REPORT MS Thesis 13b. TIME COVERED FROM _____ TO _____	14. DATE OF REPORT (Yr., Mo., Day) 1984 December 15. PAGE COUNT 232
16. SUPPLEMENTARY NOTATION Approved for public release; IAW AFR 190-17	
17. COSATI CODES FIELD / GROUP / SUB. GR.	18. SUBJECT TERMS (Continue on reverse if necessary and identify by block number) Inherent Reconfiguration; Loop Transmission; Flight Control Systems; Quantitative Feedback Theory; Control Systems, Computer Programs, Theses

19. ABSTRACT (Continue on reverse if necessary and identify by block number)

Title: FLIGHT CONTROL SYSTEM RECONFIGURATION DESIGN USING QUANTITATIVE FEEDBACK THEORY

Thesis Chairman: Dr. Constantine H. Houpis

Approved for public release: IAW AFR 190-17.
LYNN E. WOLAVER
Dean for Research and Professional Development
Air Force Institute of Technology (ATC)
Wright-Patterson AFB OH 45433

20. DISTRIBUTION/AVAILABILITY OF ABSTRACT UNCLASSIFIED/UNLIMITED ☒ SAME AS RPT. ☒ DTIC USERS ☐	21. ABSTRACT SECURITY CLASSIFICATION UNCLASSIFIED
22a. NAME OF RESPONSIBLE INDIVIDUAL	22b. TELEPHONE NUMBER (Include Area Code) 22c. OFFICE SYMBOL

DD FORM 1473, 83 APR EDITION OF 1 JAN 73 IS OBSOLETE.

UNCLASSIFIED

SECURITY CLASSIFICATION OF THIS PAGE

Quantitative theory developed by Dr. Isaac Horowitz of the Weizmann Institute of Science, Israel is used to develop control laws for the AFTI/F-16 with a reconfigurable flight control system. Compensators are synthesized to control pitch rate and roll rate through individually controlled elevators and flaperons. Robust control of these variables is required over a large portion of the flight envelope despite flight control surface failures.

Linearized aerodynamic data are used to develop the aircraft model in state-variable format. The longitudinal and lateral-directional equations are coupled in the control matrix. Individual control of the elevators and flaperons is obtained by dividing the dimensionalized control derivatives for a control surface pair in half and assigning each surface of the pair one-half of the total derivative value. The system with individually controlled surfaces represents a four input-two output system which is transformed into an equivalent two input-two output system for each control surface configuration and flight condition. Quantitative feedback theory is then applied to the equivalent systems. Originator-supplied keywords included. → 1 cat p.

Fixed-compensators and prefilters are synthesized for the pitch rate and roll rate channels, and a digital simulation is conducted at four points in the flight envelope with up to two simultaneous surface failures, as well as, for the unimpaired aircraft. Results of the simulation show that the compensators provide robust control for each control surface configuration at each flight condition. Compensator designs are also synthesized to provide only stability when three of the four surfaces are failed.

The theory developed by Dr. Horowitz is found to be effective in designing for robustness despite large uncertainty arising from control surface failures, and plant parameter variation. Flight control research using quantitative feedback theory should be continued. The fixed-compensator design approach has potential to significantly reduce the complexity of a reconfigurable flight control system. A computer-aided design package for quantitative feedback theory should be developed to facilitate design work.

END

FILMED

4-85

DTIC